

AMERICAN UNIVERSITY OF BEIRUT

OXIDATIVE CAPACITY OF COARSE AND FINE
PARTICLES IN DIFFERENT ENVIRONMENTS

by
MALEK MOHAMMAD JAAFAR

A thesis
submitted in partial fulfillment of the requirements
for the degree of Master of Science
to the Department of Chemistry
of the Faculty of Arts and Sciences
at the American University of Beirut

Beirut, Lebanon
May 2014

AMERICAN UNIVERSITY OF BEIRUT

OXIDATIVE CAPACITY OF COARSE AND FINE
PARTICLES IN DIFFERENT ENVIRONMENTS

by
MALEK MOHAMMAD JAAFAR

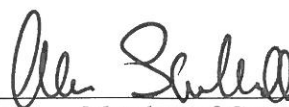
Approved by:

Dr. Najat A. Saliba, Professor
Chemistry



Advisor

Dr. Alan Louis Shihadeh, Professor
Mechanical Engineering



Member of Committee

Dr. Pierre Karam, Assistant Professor
Chemistry



Member of Committee

Date of thesis defense: May 7, 2014

AMERICAN UNIVERSITY OF BEIRUT

THESIS RELEASE FORM

Student Name: Jaafar Malek Mohammad
Last First Middle

Master's Thesis Master's Project Doctoral Dissertation

I authorize the American University of Beirut to: (a) reproduce hard or electronic copies of my thesis, dissertation, or project; (b) include such copies in the archives and digital repositories of the University; and (c) make freely available such copies to third parties for research or educational purposes.

I authorize the American University of Beirut, **three years after the date of submitting my thesis, dissertation, or project**, to: (a) reproduce hard or electronic copies of it; (b) include such copies in the archives and digital repositories of the University; and (c) make freely available such copies to third parties for research or educational purposes.

Malek Jaafar 13 MAY 2014
Signature Date

ACKNOWLEDGMENTS

I would like to thank, my advisor Dr. Najat A. Saliba, for her help and support throughout this journey, it wouldn't have been possible without her. I thank her for providing me with the invaluable opportunity of being part of her group

I would like to also thank my jury; Dr. Alan Louis Shihadeh and Dr. Pierre Karam for taking the time to review this thesis and for their valuable comments.

This research work is due to the collaboration of many people, I am thankful to Dr. Walid Saad, Dr. Costantinos Siotas and Dr. Nancy Daher for their insightful and constructive feedback and fruitful discussions.

Moreover I would like to thank the members of the AAL, especially Ms. Rima Baalbaki for her help in the sampling, analysis and discussions. It was a pleasure to work with you all; Rima Baalbaki, Rawad Massoud, Elizabeth Sepedtjian, Rita Tohme, Lamis Al Aaraj, Lubna Dada, Nour Nafaa, Johnny Nicolas. My thanks go as well for Mr. Issam Saliba, for his help with machine calibrations.

A special thanks to the Central Research Science Laboratory team for their help in the SEM optimization, the staff at Wisconsin State Laboratory of Hygiene for their assistance with the chemical measurements, the staff and faculty of the chemistry department here at AUB and the RYMCO Jal El-Dib office for giving us the premise to sample.

I would like to express my sincerest gratitude to my mom, dad and sister who have supported me on every single step.

AN ABSTRACT OF THE THESIS OF

Malek Mohammad Jaafar for Master of Science
Major: Chemistry

Title: Oxidative Capacity of Coarse and Fine Particles in Different Environments

Numerous epidemiological evidence indicates significant associations between exposure to particulate matter (PM) and increased risk of adverse health outcomes. Although the components of and the mechanism by which PM causes these health effects, is still unclear, and the majority of these studies state that they are due to cellular oxidative stress, caused by reactive oxygen species. Additionally, because the redox potential of PM is dependent on its composition, it is expected that variations in the sources affecting PM composition could cause a change in redox potential.

This study focuses on determining the chemical and oxidative properties of size-segregated PM in different environments; urban background, roadside and dusty. Gravimetric analysis, high-resolution magnetic sector Inductively Coupled Plasma Mass Spectrometry (HR-ICP-MS), ion chromatography, NIOSH Thermal Optical Transmission method, Scanning Electron Microscope, Total Organic Carbon Analyzer, macrophage-based ROS (m-ROS) assay and Dithiothreitol (DTT) assay were used to assess the mass concentration, ionic, elemental and organic composition of coarse and fine PM and obtain the chemical mass closure and oxidative potential. Additionally, results will be used to deduce relationships and correlations between different PM components and the oxidative capacity.

Considering the roadside site, particle mass levels were 1.3-2.6 times greater at than the urban background. A chemical mass closure showed that coarse PM was mostly composed of crustal material, contributing to 12-23% of its mass across sites. In fine (PM_{2.5-0.25}) and quasi-ultrafine (PM_{0.25}), organic matter was dominant (46-56%) at the roadside location, while secondary ions (SI, 54-68%) were more abundant at the background site. Measured ROS-activity, on a per m³ of air volume basis, was 1.4-2.6 times greater at the roadside than background location, indicating that exposure to redox-active PM species may be greatest near the freeway. Conversely, size-resolved PM intrinsic redox activity was generally comparable at both sites, possibly suggesting a similarity in the sources of ROS-active species.

For the dust episodes, the average PM mass concentrations of coarse and fine fractions increased over non-dusty by 48.5 and 14.6 %, respectively. Consequently, crustal materials, which are often associated with dust transport sources, were significantly enhanced for coarse and fine PM by 47 and 107%, respectively. Elemental carbon and trace element only differed in the coarse fraction while that of organic matter did not change in both the coarse and fine PM. The oxidative potential of PM showed an increase in the dust to non-dust percent difference for the coarse mode, and a decrease for the fine mode. Since crustal material, in the form of mineral oxides, is the dominant class during these episodes, the redox potential of some was tested on the DTT assay. Of these oxides, CuO showed the highest redox activity while Cr₂O₃ showed none.

Results of this work provide much needed information on the levels, variability, chemical composition and oxidative capacity of PM for Beirut and the region. In addition to the understanding of the correlation between different chemical components, deducing their sources and the mode of actions, of some of these components, on the redox assays.

CONTENTS

| | |
|---|------|
| ACKNOWLEDGMENTS | v |
| AN ABSTRACT OF THE THESIS OF | vi |
| ILLUSTRATIONS | xi |
| TABLES | xiii |
| INTRODUCTION..... | 1 |
| A. Particulate Matter | 1 |
| B. Thesis Layout | 2 |
| Chapter | |
| Chemical Composition of Size-Resolved Particulate Matter at Near-freeway and Urban Background Sites in the Greater Beirut Area..... | 5 |
| A. Introduction | 5 |
| B. Methodology | 6 |
| 1. Sampling Sites..... | 6 |
| 2. Sample Collection | 7 |
| 3. Sample Analysis | 8 |
| C. Results and Discussion | 9 |
| 1. Size-Resolved Particle Mass Concentrations | 9 |
| 2. Size-Resolved Particle Mass Composition..... | 10 |
| a. Carbonaceous Species..... | 13 |
| b. Secondary Ions..... | 15 |
| c. Sea Salts..... | 19 |
| d. Crustal Material and Trace Elements..... | 20 |
| e. Chemical Mass Closure | 21 |
| 3. Organic Compound Characterization | 21 |
| a. Polycyclic Aromatic Hydrocarbons (PAHs)..... | 22 |
| b. Hopanes and Steranes | 25 |
| c. N-Alkanes | 26 |
| D. Summary and Conclusion | 28 |

**Oxidative Potential and Chemical Speciation of Size-Resolved
Particulate Matter (PM) at Near-freeway and Urban
Background Sites in the Greater Beirut Area..... 30**

| | |
|---|-----------|
| A. Introduction..... | 30 |
| B. Methodology..... | 32 |
| 1. Sampling Site..... | 32 |
| 2. Sample Collection..... | 33 |
| 3. Sample Analysis..... | 33 |
| C. Results and Discussion..... | 35 |
| D. Metals and Trace Elements..... | 37 |
| 1. Size-Resolved Concentrations and Crustal Enrichment Factors..... | 37 |
| 2. Water Solubility..... | 42 |
| 3. Water-Soluble Elemental Composition..... | 44 |
| E. Size-Resolved Oxidative Potential..... | 45 |
| 1. Reactive Oxygen Species (ROS)-activity..... | 45 |
| 2. Association of ROS-activity with PM Components..... | 47 |
| 3. ROS Comparison to Other Urban Areas..... | 49 |
| F. Summary and Conclusion..... | 51 |

**Dust episodes and their effect on the redox activity of coarse and
fine particles in an east Mediterranean city 53**

| | |
|---|-----------|
| A. Introduction..... | 53 |
| B. Methodology..... | 55 |
| 1. Sample Collection..... | 55 |
| 2. Sample Analysis..... | 56 |
| 3. DTT and m-ROS Assays..... | 57 |
| 4. Chemical Mass Closure..... | 58 |
| 5. Particle Size Distribution..... | 59 |
| C. Results and Discussion..... | 59 |
| 1. Particle Size Distribution..... | 59 |
| 2. Chemical Mass Closure..... | 62 |
| 3. Dust Versus Non-Dust Chemical Composition..... | 64 |
| 4. DTT and m-ROS assays..... | 66 |
| 5. Correlation of Redox activity with PM chemical components..... | 67 |
| D. Summary and Conclusions..... | 70 |

**THE EFFECT OF METAL OXIDE NANOPARTICLES ON
THE DTT ASSAY 71**

| | |
|--|---------------|
| A. Introduction..... | 71 |
| B. Methodology..... | 73 |
| 1. Solution Preparation..... | 73 |
| 2. DTT Assay..... | 74 |
| 3. DLS Experiment..... | 75 |
| 4. SEM Imaging..... | 76 |
| C. Results and Discussion..... | 76 |
| 1. DTT Response for Metal Oxide Nanoparticles..... | 76 |
| D. Physicochemical Characteristics and Redox Activity..... | 79 |
| a. Metal Oxide DTT Redox Activity with Respect to Particle Size..... | 79 |
| b. Metal Oxide DTT Redox Activity with Respect to Surface Area..... | 80 |
| i. <u>Sample Calculation</u> | 80 |
| c. Metal Oxide DTT redox activity with respect to surface morphology:..... | 83 |
| E. Conclusion..... | 84 |
| CONCLUSION..... | 86 |
| Bibliography..... | 90 |

ILLUSTRATIONS

| | | |
|----|--|----|
| 1 | Figure 2.1 Map of the urban background (A) and near-freeway sites (B). | 7 |
| 2 | Figure 2.2a-b. Chemical composition and gravimetric mass concentration of PM _{10-2.5} , PM _{2.5-0.25} and PM _{0.25} at the a) near-freeway and b) background sites. Error bars correspond to one standard error. | 11 |
| 3 | Figure 2.3 a-b. Average concentration of water-soluble organic carbon (WSOC), organic carbon (OC) and elemental carbon (EC) in PM _{10-2.5} , PM _{2.5-0.25} and PM _{0.25} at the a) near-freeway and b) background sites. Error bars correspond to one standard error. | 13 |
| 4 | Figure 2.4a-b. Comparison of size-resolved a) organic carbon (OC) and b) elemental carbon (EC) concentrations (current study) with data from I-710 freeway and an urban background site in the Los Angeles (LA) area (Kam et al., 2012). | 15 |
| 5 | Figure 2.5a-b. Average concentration of nitrate, non-sea-salt sulfate and ammonium in PM _{10-2.5} , PM _{2.5-0.25} and PM _{0.25} at the a) near-freeway and b) background sites. Error bars correspond to one standard error. | 16 |
| 6 | Figure 2.6. Average charge balance ratios of (Na ⁺ + NH ₄ ⁺ + ssCa ²⁺ + ssMg ²⁺) to (Cl ⁻ + NO ₃ ⁻ + SO ₄ ²⁺). Error bars represent one standard error. | 18 |
| 7 | Figure 2.7. Backward air mass trajectories for the entire sampling campaign (July-August 2012), simulated using HYSPLIT model from NOAA. For each sampling day, four 48-hour trajectories were modeled every six hours at 500 m-agl using vertical wind velocity field from the meteorological data. | 19 |
| 8 | Figure 2.8a-c. Average n-alkanes concentration (C ₁₉ -C ₃₄) in a) PM _{10-2.5} , b) PM _{2.5-0.25} and c) PM _{0.25} at the near-freeway and background sites. Error bars correspond to one analytical or standard error. | 27 |
| 9 | Figure 3.1. DCFH-DA structure | 34 |
| 10 | Figure 3.2a-b. Average total concentration of metals and elements in PM _{10-2.5} , PM _{2.5-0.25} and PM _{0.25} at the a) near-freeway and b) urban background sites. Error bars represent one standard error. | 38 |
| 11 | Figure 3.3a-b. Average crustal enrichment factors (CEF) in PM _{10-2.5} and PM _{2.5} at the a) near-freeway and b) urban background sites. Error bars represent one standard error. | 40 |
| 12 | Figure 3.4. Water-solubility of metals and elements in PM _{10-2.5} , PM _{2.5-0.25} and PM _{0.25} , averaged across the sampling sites. Error bars represent one standard error. | 44 |
| 13 | Figure 3.5. Water-soluble elemental composition of PM _{10-2.5} , PM _{2.5-0.25} and PM _{0.25} , averaged across the sampling sites. Error bars represent one standard | 45 |

| | | |
|----|--|----|
| | error. | |
| 14 | Figure 3.6a-b. Average a) air volume-based (μg Zymosan/ m^3) and b) PM mass-based (intrinsic) (μg Zymosan/mg PM) reactive oxygen species (ROS)-activity of $\text{PM}_{10-2.5}$, $\text{PM}_{2.5-0.25}$ and $\text{PM}_{0.25}$ at the near-freeway and urban background sites. Error bars represent one standard error. | 46 |
| 15 | Figure 3.7. Comparison of average intrinsic reactive oxygen species (ROS)-activity (μg Zymosan/mg PM) of $\text{PM}_{10-2.5}$, $\text{PM}_{2.5}$ and $\text{PM}_{0.25}$ in Beirut (current study) with data from Los Angeles (LA), Milan and Lahore during July-August. Error bars represent one standard error. <i>*ROS-activity of ambient $\text{PM}_{2.5}$ in LA corresponds to that of samples collected in October-November 2007 during and after wildfires.</i> | 50 |
| 16 | Figure 4.1. Size-fractionated particle mass concentration during dust episodes (upper left). Associated error bars represent the standard deviation of the gravimetric analysis of the two parallel Teflon filters. Average particle mass concentration during dust episodes compared to non-dust episodes (upper right) Number (a) and volume size distribution (b) of particles with mean geometric diameter ranging between 0.265 and 15 μm during dust and non-dust episodes (bottom). | 61 |
| 17 | Figure 4.2. Average chemical composition of coarse and fine PM in comparison to the total gravimetric mass represented by * (upper graph), and % contribution of the different chemical components to the total mass of coarse and fine PM (lower graph) during dust and non-dust events. Please note that Oct 22-24 dust coarse PM filter was not included in the chemical analysis because it was overloaded. | 63 |
| 18 | Figure 4.3. Size-segregated dust to non-dust percent difference of different elements. | 65 |
| 19 | Figure 4.4a-b. Size-segregated dust-rich to normal ROS activity using: a) m-ROS and b) DTT assays. Error bars correspond to one standard error. | 66 |
| 20 | Figure 5.1. Controlled experiment, DTT rate loss for CuCl_2 on the New and Old DTT assay | 75 |
| 21 | Figure 5.2. DTT rate loss for metal oxide nanoparticles (normalized to mass). | 76 |
| 22 | Figure 5.3. Potential mechanisms of DTT stabilization through complexation with solubilized lead (A) or PM surfaces (B) (Uzu et al. 2011) | 78 |
| 23 | Figure 5.4. SEM images of different MO (Left to Right) Cr_2O_3 , CuO , MnO_2 , ZnO | 84 |

TABLES

| | | |
|---|---|----|
| 1 | Table 2.1. Average (\pm standard error) size-fractionated particle mass levels at the near-freeway and background sites. | 9 |
| 2 | Table 2.2. Average (\pm standard error) concentration of PAHs, hopanes and steranes in PM _{10-2.5} , PM _{2.5-0.25} and PM _{0.25} at the near-freeway and background sites. bdl indicates an undetected compound or a concentration below detection limit. *Error corresponds to analytical error. | 24 |
| 3 | Table 3.1. Average (\pm standard error) mass concentration and chemical composition of PM _{10-2.5} , PM _{2.5-0.25} and PM _{0.25} at the near-freeway and urban background sites. | 35 |
| 4 | Table 3.2. Spearman correlation coefficients (R) between ROS-activity (μ g Zymosan/mg PM) and select species (ng/ μ g PM) in PM _{10-2.5} , PM _{2.5-0.25} and PM _{0.25} . Bold indicates $R \geq 0.70$ and significant at a 0.05 level. | 49 |
| 5 | Table 4.1. Dust-rich sampling episodes dates | 56 |
| 6 | Table 4.2. Spearman correlation coefficient (R) for different components with redox activity from both assays ($p < 0.05$) | 69 |
| 7 | Table 5.1. MO Particle Size (nm) | 79 |

CHAPTER I

INTRODUCTION

A. Particulate Matter

Concerns over air pollution have been well documented and can be traced back many centuries. Air pollutants can be classified into two main categories; the gaseous pollutants and the particulate matter (PM). This study will focus on PM, their composition and oxidative potential. Particulate matter is a mixture of solid or liquid particles, of different sizes and shapes, suspended in a gas. The components of PM include organics, inorganics, metals, trace elements and crustal material. PM can be directly emitted by biogenic (Volcanic eruption, dust, sea spray) and anthropogenic (vehicular emissions, fossil fuel burning) sources (also known as Primary PM) or formed in the atmosphere (Secondary PM) ¹. As stated above, PM vary in sizes, they can range from a few nanometers to several micrometers. Those with a diameter less than 10 μm are of concern because they can enter our airways ². These PM can be classified into two general modes; coarse and these are PM with a diameter between 2.5 and 10 μm and fine with a diameter less than 2.5 μm . The fine mode can be further divided into accumulation (diameter between 2.5 and 0.25 μm) and quasi-ultrafine or ultrafine (diameter less than 0.25 μm). Each PM mode has its own sources, chemical composition, respiratory penetration and atmospheric lifetime. Due to their large size, coarse PM usually deposit within hours ³ and don't reach further than the upper

respiratory track. Fine PM can have an atmospheric lifetime in the order of days ⁴ and can penetrate deep into the pulmonary interstitial sites ^{5,6}.

A number of epidemiological evidence indicates significant associations between exposure to PM and increased risk of adverse health outcomes ^{7,8}. With many studies linking increase in respiratory and cardiovascular diseases as well mortality after exposure to atmospheric PM ⁹. Although the mechanism by which PM affects biological systems is still unclear, many studies link the pro-oxidative and pro-inflammatory effects of PM exposure to the increased PM- catalyzed formation of reactive oxygen species (ROS) within the cells ¹⁰⁻¹². ROS is a collective term comprising chemically reactive oxygen radicals or oxygen-derived species (e.g. hydroxyl radical and hydrogen peroxide) ¹³. They are formed normally in cells and are used for cellular activities ¹⁴, but at high levels they are associated with inflammation and apoptosis ¹⁵. Additionally, because the redox potential of PM is dependent on its composition, it is expected that variations in the sources affecting PM composition could cause a change in redox potential.

B. Thesis Layout

Chapter 2 outlines the analysis of size-resolved ambient PM (PM_{10-2.5}, PM_{2.5-0.25}, PM_{0.25}) in the Greater Beirut area, Lebanon. Sampling was concurrently conducted at near-freeway and urban background sites, with size-fractionated samples analyzed for their detailed chemical composition. The dependency of PM chemistry on particle-size and location is explored. Results are also evaluated in the context of metropolitans and

roadways worldwide. Findings provide insight on commuter exposure in the Beirut area.

Chapter 3 addresses the role of PM size and chemistry in inducing redox activity, for samples collected in Beirut-Lebanon (Chapter 2). The oxidative potential of PM_{10-2.5}, PM_{2.5-0.25} and PM_{0.25} samples, collected at near-freeway and urban background sites in the Greater Beirut area, was quantified using a macrophage-based ROS assay (m-ROS) and compared among PM modes to worldwide urban settings. The role of water-soluble metals and trace elements in PM-induced ROS-activity is also particularly investigated.

Chapter 4 outlines the analysis of coarse and fine for samples collected during dust episodes in an urban background site in Beirut. The redox potential of these PM samples is also analyzed using a cellular assay (m-ROS) and an acellular assay (Dithiothreitol (DTT) assay). The change in the redox potential is analyzed in light of the changes in the chemical components during dust episodes. The redox potential is compared to that of non-dust episodes sampled at the same location.

Chapter 5, in light of the changes in the chemical composition during dust episodes, specifically the increase in crustal material, the redox potential of some of these crustal material is analyzed on the DTT assay. The physicochemical characteristics, which include the surface area, size and morphology, are analyzed to check whether they are a key factor in controlling the redox potential.

Chapter 6 details the major findings of this thesis and highlights on its contribution to the scientific knowledge about urban air quality and its health

implications. The chapter concludes with recommendations for future atmospheric research directions

CHAPTER II

CHEMICAL COMPOSITION OF SIZE-RESOLVED PARTICULATE MATTER AT NEAR-FREEWAY AND URBAN BACKGROUND SITES IN THE GREATER BEIRUT AREA

The following Chapter is based on the following study:

*Daher, N., N. A. Saliba, A. L. Shihadeh, M. Jaafar, R. Baalbaki and C. Sioutas (2013). "Chemical composition of size-resolved particulate matter at near-freeway and urban background sites in the Greater Beirut Area." Atmospheric Environment **80**: 96-106.*

A. Introduction

In urban areas, motor vehicles are the primary source of PM^{16,17}, with populations in close proximity to trafficked-roadways being most susceptible to particle-induced health effects¹⁸. Accordingly, chemical characterization of PM in urban and roadways settings has been the focus of many research fronts, especially for areas in the U.S.¹⁹⁻²¹. PM vehicular emissions, derived from both exhaust and abrasion¹⁶, are composed of potentially toxic air pollutants, such as organic carbon (OC), polycyclic aromatic hydrocarbons (PAHs) and transition metals^{10,22,23}. Some of these components (OC, PAHs) also dominate the ultrafine particle-mode (aerodynamic diameter, $dp < 0.1-0.2 \mu\text{m}$) because of its increased number and surface area relative to larger coarse (PM_{10-2.5}, $10 \mu\text{m} < dp < 2.5 \mu\text{m}$) and fine (PM_{2.5}, $dp < 2.5 \mu\text{m}$) PM^{24,25}.

Lebanon, a developing country in the eastern Mediterranean basin, is afflicted with high PM levels, often exceeding the World Health Organization (WHO) guidelines²⁶. Its elevated particle levels, particularly in urban areas, can be largely related to road-traffic emissions given the absence of an efficient mass transportation system²⁷. The

rate of car ownership is estimated as 3 persons/car and is expected to further increase ²⁷. Accurate characterization of traffic-associated PM emissions in Lebanon is thus essential.

Investigation of PM in Lebanon has been generally restricted to urban areas and focused on determining the ionic and elemental content of coarse or fine PM ^{26,28,29}. Very few studies examined PM-organic matter ³⁰, smaller particle-size modes or PM composition at roadways. To determine chemically-specified and size-resolved properties of traffic-related particle emissions in Lebanon, coarse, accumulation (PM_{2.5-0.25}, 2.5 μm < dp < 0.25 μm) and quasi-ultrafine (PM_{0.25}, dp < 0.25 μm) PM samples were collected at two contrasting locations in the summer of 2012. Sampling sites included near-freeway and background locations in the greater Beirut area. Results are also evaluated in the context of metropolitans and roadways worldwide. Findings of this work provide the much-needed information on road-traffic emissions in Lebanon and could ultimately aid in establishing air pollution control strategies, currently very limited, in this region.

B. Methodology

1. *Sampling Sites*

The sampling campaign was conducted in the greater Beirut area at two contrasting sites, including urban background and near-freeway locations, as shown in Figure 2.1.

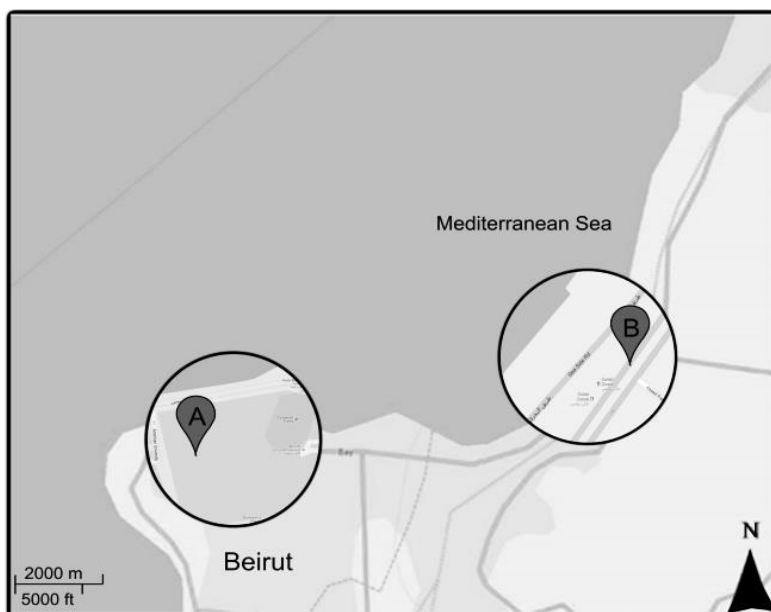


Figure 2.1 Map of the urban background (A) and near-freeway sites (B).

The background site was situated at the American University of Beirut (AUB), in a location overlooking AUB campus from the east and the Mediterranean coast from the west. It is surrounded by dense vegetation covers and mostly pedestrian roads, with the nearest street located about 150 m west of the site²⁸. This coastal roadway separates the site from the Mediterranean Sea and experiences fairly high traffic activity throughout the day, particularly during rush hours (7-9 a.m. and 4-7 p.m.). The sampling site is also within 1.5 and 2.5 km of a leisure yacht club and the commercial port of Beirut, respectively. Particle levels at this coastal site are commonly

2. Sample Collection

Sampling was conducted from 7:00 a.m. to 5 p.m. on weekdays during July-August 2012, with samples concurrently collected at the two sites on a weekly basis. Three parallel Sioutas Personal Cascade Impactor Samplers (Sioutas PCIS, SKC Inc.,

Eighty Four, PA, USA, ³¹), preceded by PM₁₀ inlets (Chemcomb 3500 speciation sampling cartridge, Rupprecht & Patashnick CO, Inc, Albany, USA) and operating at 9 lpm, were deployed at each site to collect size-fractionated particles in the size ranges: 10-2.5 μm (coarse PM), 2.5-0.25 μm (accumulation PM) and <0.25 μm (quasi-ultrafine PM). For the purpose of chemical speciation, one PCIS was loaded with quartz microfiber filters (Whatman International Ltd, Maidstone, England) while the other two PCISs were loaded with Teflon filters (Pall Life Sciences, Ann Arbor, MI). 25 mm filters were used as impaction substrates for PM_{10-2.5} and PM_{2.5-0.25} while 37 mm filters were used as collection media for PM_{0.25}. The collected particle mass was determined by pre- and post-weighing the Teflon filters using a UMX2 microbalance (Mettler Toledo GmbH, CH-8606 Greifensee, Switzerland), following equilibration under controlled temperature and relative humidity conditions (22–24°C and 40–50%, respectively).

3. *Sample Analysis*

To conduct chemical analyses of the samples, the collected Teflon and quartz filters were sectioned into portions. Quantification of carbonaceous species and organic compounds was conducted on the quartz substrates, while all other measurements were performed on the Teflon filters. Elemental and organic carbon (EC and OC, respectively) measurements were determined using the NIOSH Thermal Optical Transmission method ³². The ionic and water-soluble organic carbon (WSOC) contents of the filters were respectively quantified by ion chromatography and a Sievers 900 Total Organic Carbon Analyzer, following water-extraction and filtration of the samples ³³. The total

elemental mass of the filter substrates was measured using a high resolution magnetic sector Inductively Coupled Plasma Mass Spectrometry (Thermo-Finnigan Element 2). A microwave-aided Teflon bomb digestion protocol using a mixture of 1 mL of 16 M nitric acid, 0.25 mL of 12 M hydrochloric acid, and 0.10 mL of hydrofluoric acid was used for extraction of total metals and elements³⁴. Organic speciation was conducted using gas chromatography mass spectrometry (GC-6980, quadrupole MS-5973, Agilent Technologies). The filter substrates were spiked with isotopically-labeled standard solutions prior to extraction. Samples were then extracted in a 50/50 dichloromethane/acetone solution using Soxhlets, followed by rotary evaporation and volume reduction under high-purity nitrogen. Extracts were analyzed twice by GC/MS after derivitization of carboxylic acids with diazomethane and after silylation of hydroxyl groups. Additional details can be found in Sheesley et al.³⁵.

C. Results and Discussion

1. *Size-Resolved Particle Mass Concentrations*

Size-resolved PM mass concentrations (average \pm standard error) are presented in Table 2.1 for each location.

Table 2.1. Average (\pm standard error) size-fractionated particle mass levels at the near-freeway and background sites.

| Size range (μm) | Concentration ($\mu\text{g}/\text{m}^3$) | |
|------------------------------|--|----------------|
| | Near-freeway | Background |
| 10-2.5 | 34.0 \pm 1.5 | 15.8 \pm 0.9 |
| 2.5-0.25 | 13.8 \pm 0.9 | 8.6 \pm 1.0 |
| <0.25 | 36.1 \pm 0.9 | 14.0 \pm 0.4 |

Overall PM (PM₁₀) mass composition was relatively consistent across the two sites, with PM_{0.25} and PM_{10-2.5} prevailing (36-43% of PM₁₀). However, despite this comparability, PM concentrations were significantly higher (1.6-2.6 times) at the near-freeway than background site for all particle-size ranges. At the roadside location, PM mass levels varied from a low of 13.8 µg/m³ in PM_{2.5-0.25} to a high of 34.0 and 36.1 µg/m³ in PM_{10-2.5} and PM_{0.25}, respectively. Particle concentrations at the background site ranged from 8.6 µg/m³ in the accumulation mode to 15.8 and 14.03 µg/m³ in the coarse and quasi-ultrafine fractions, respectively. The persistently higher levels at the roadside suggest substantial contributions from vehicular emissions as well as traffic-induced re-suspension to PM levels at the freeway. Compared to other Mediterranean areas, while coarse particle levels at the background site are lower (0.55-0.60 times) than those reported at urban background locations in Athens-Greece (June-July) and Barcelona-Spain (March-May), PM_{2.5} concentrations are comparable (0.90-1.13 times)³⁶. Conversely, coarse and fine PM levels are 2.4-2.9 times greater than those measured at I-710; a major freeway with the highest ratio (up to 25%) of heavy-duty diesel vehicles (HDDVs) in Los Angeles (LA)-California highway network³⁷.

2. Size-Resolved Particle Mass Composition

To determine the bulk composition of the PM samples, a chemical mass reconstruction was conducted for each particle mode and sampling site, as displayed in Figure 2.2a-b.

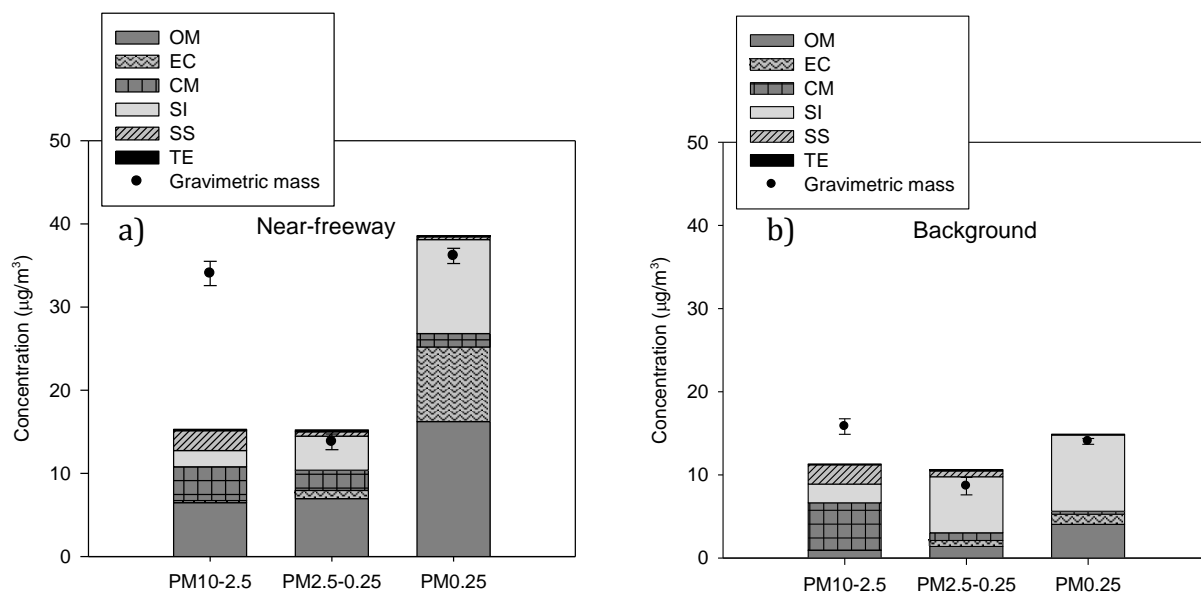


Figure 2.2a-b. Chemical composition and gravimetric mass concentration of PM_{10-2.5}, PM_{2.5-0.25} and PM_{0.25} at the a) near-freeway and b) background sites. Error bars correspond to one standard error.

PM chemical species were classified into organic matter (OM), EC, sea-salt (SS), secondary ions (SI), crustal material (CM) and trace elements (TE). To account for the contributions of non-carbon atoms (e.g. oxygen, hydrogen) to the total mass of OM, a factor of 1.6 ± 0.2 and 2.1 ± 0.2 is recommended for urban and non-urban aerosols, respectively³⁸. A factor of 1.6 is used to convert OC to OM in this study. SS contribution was estimated as the sum of Na⁺ concentration and sea-salt fractions of Cl⁻, Mg²⁺, K⁺, Ca²⁺, and SO₄²⁻ concentrations, assuming standard sea-water composition³⁹ and using soluble Na⁺ as a tracer for sea-salt. SI includes ammonium, nitrate and non-sea-salt sulfate (nss-sulfate), where nss-sulfate is obtained by subtracting the sea-salt fraction of sulfate from total measured sulfate. The proportion of CM in the PM samples

was determined by summing the oxides of crustal metals, Al, K, Fe, Ca, Mg, Ti and Si, using the following equation ⁴⁰⁻⁴²:

$$CM = 1.89Al + 1.21K + 1.43Fe + 1.4Ca + 1.66Mg + 1.7Ti + 2.14Si \quad (2.1)$$

Ca and Mg correspond to their non-sea-salt portions and Si concentration, which was not measured in this study, was estimated as $3.41 \times Al$ ⁴¹.

We should note that multiplying Ca and Mg by their respective factors could lead to an overestimation of their oxides, if Ca and Mg were associated with nitrate or sulfate ions, which are directly measured and included in the mass closure. However, a sensitivity analysis showed that using this approach would only result in a $2 \pm 0.38\%$ (arithmetic mean \pm standard error) overestimation in the reconstructed mass across sites and particle-size fractions. Its impact on the overall mass balance is thus minimal. Lastly, TE consists of the remaining measured elements such as Cu, Zn and Cr.

In the coarse fraction, CM was the predominant component at the background site ($22.9 \pm 8.1\%$), while the second most abundant compound ($12.2 \pm 3\%$), closely following OM ($19.4 \pm 3.4\%$), at the freeway site. These rather low CM fractions will be discussed in a subsequent section. On the other hand, accumulation and quasi-ultrafine PM modes were dominated by OM (46-56%) at the near-freeway site while SI (54-68%) at the background location. This variability in particle composition between sites, mainly for $PM_{0.25}$ and $PM_{2.5-0.25}$, confirms that these modes are strongly dependent on sources in their microenvironment.

a. Carbonaceous Species

In PM_{2.5-0.25} and PM_{0.25}, OM was the most prevalent component at the near-freeway location (45.7-55.8%) while the next most prominent species at the background site (15.2-29.3%). Its contribution to the coarse fraction was moderate at both locations, averaging less than 19.4% and 6.5 µg/m³.

To evaluate the extent of primary and secondary contributions to the organic mass, the variation in size-resolved OC, WSOC and EC concentrations is shown in Figure 2.2 for each site.

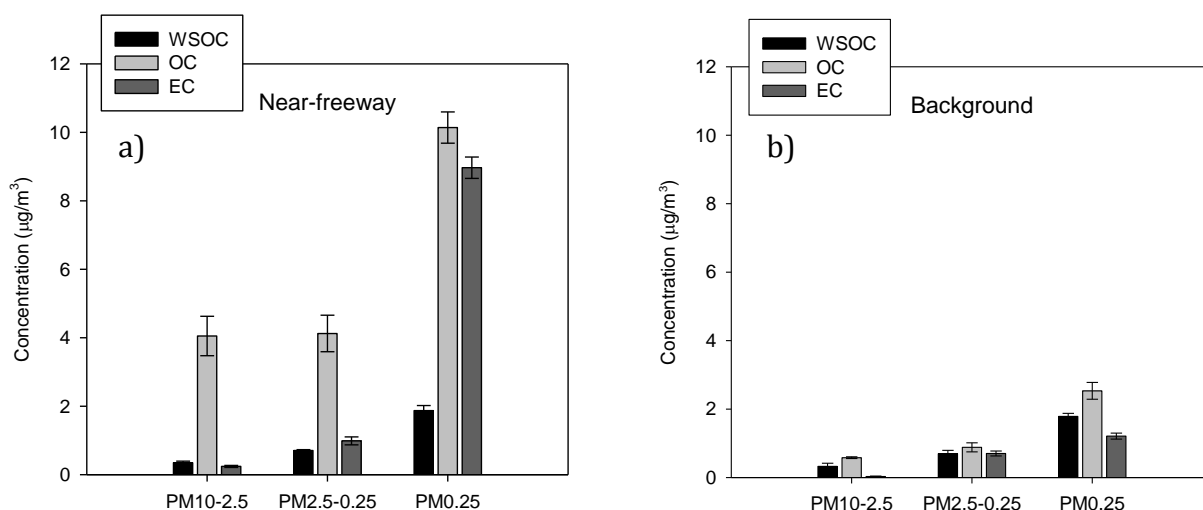


Figure 2.3 a-b. Average concentration of water-soluble organic carbon (WSOC), organic carbon (OC) and elemental carbon (EC) in PM_{10-2.5}, PM_{2.5-0.25} and PM_{0.25} at the a) near-freeway and b) background sites. Error bars correspond to one standard error.

As can be inferred, the majority of these carbonaceous species (55-88%) is confined in the quasi-ultrafine mode. OC in the fine fraction can be directly emitted from primary sources, such as fossil fuel combustion, or produced via secondary organic aerosol (SOA) formation processes; whereas OC in the coarse fraction may also include biological debris^{43,44}. OC was mostly water-insoluble at the freeway site, corroborating

its predominantly primary origin. Its concentration ranged from a low of $4 \mu\text{g}/\text{m}^3$ in $\text{PM}_{10-2.5}$ to a high of $10.1 \mu\text{g}/\text{m}^3$ in $\text{PM}_{0.25}$ and was 4-7—fold greater than levels at the background site. This trend indicates substantial contributions from vehicular sources at the highly trafficked-freeway site. Although OC concentration significantly varied between locations, mass levels of $\text{PM}_{2.5-0.25}$ - and $\text{PM}_{0.25}$ -WSOC, indicators of SOA formation processes ⁴⁵, were comparable ($p>0.05$) across the two sites, likely suggesting their regional secondary nature. Moreover, OC was largely water-soluble at the background site, particularly in the quasi-ultrafine ($71.7\pm 0.1\%$) and accumulation ($79.2\pm 0.1\%$) size ranges, indicating its mainly secondary origin. Its water-soluble fraction varied from $0.69 \mu\text{g}/\text{m}^3$ in $\text{PM}_{2.5-0.25}$ to $1.79 \mu\text{g}/\text{m}^3$ in $\text{PM}_{0.25}$. Lastly, it is noteworthy that OC levels are 2-4 times levels at I-710 in Los Angeles, CA ⁴⁶, as can be inferred from Figure 2.4a. I-710 is characterized by a HDDV composition of 11-25% and a total vehicular traffic flow of 4247 vehicles/hour ^{37,46}, roughly half of that estimated for the freeway in this study. In contrast, levels at the background site are comparable to those measured at an urban background location in LA ⁴⁶, Figure 2.4a. EC, a key tracer for diesel exhaust ⁴⁷, minimally contributed to coarse PM at both sites, accounting for less than 0.7% and $0.24 \mu\text{g}/\text{m}^3$ of its mass. Its contribution to fine PM was more significant, with EC dominating the quasi-ultrafine mode and comprising 25.3 ± 0.9 and $8.9\pm 0.9\%$ of $\text{PM}_{0.25}$ at the near-freeway and background sites, respectively. Its $\text{PM}_{0.25}$ -levels varied from $9.0 \mu\text{g}/\text{m}^3$ at the roadside location to $1.2 \mu\text{g}/\text{m}^3$ at the background site, spanning a 7.4-fold increase, which indicates a considerable impact from HDDVs on particle levels at the freeway. At the coastal background site, EC could partly originate from non-road sources such as diesel

generators, largely used due to regular power outages, or also fuel oil combustion given the site's proximity to nearby ports (1.5-2.5 km). Finally, it is worth noting that $PM_{0.25}$ -EC levels at the freeway site greatly exceed (5-fold) those measured at the I-710 in LA, which is characterized by a high truck flow of 470/hour⁴⁶, Figure 2.4b. This is likely due to lack of diesel particulate filters and higher prevalence of smoking vehicles (vehicles emitting atypically large amounts of lubricating oil) in Lebanon than LA. Mobile sources in Lebanon are characterized by a large, old (average age exceeds 13 years) and poorly maintained vehicular fleet^{27,48}.

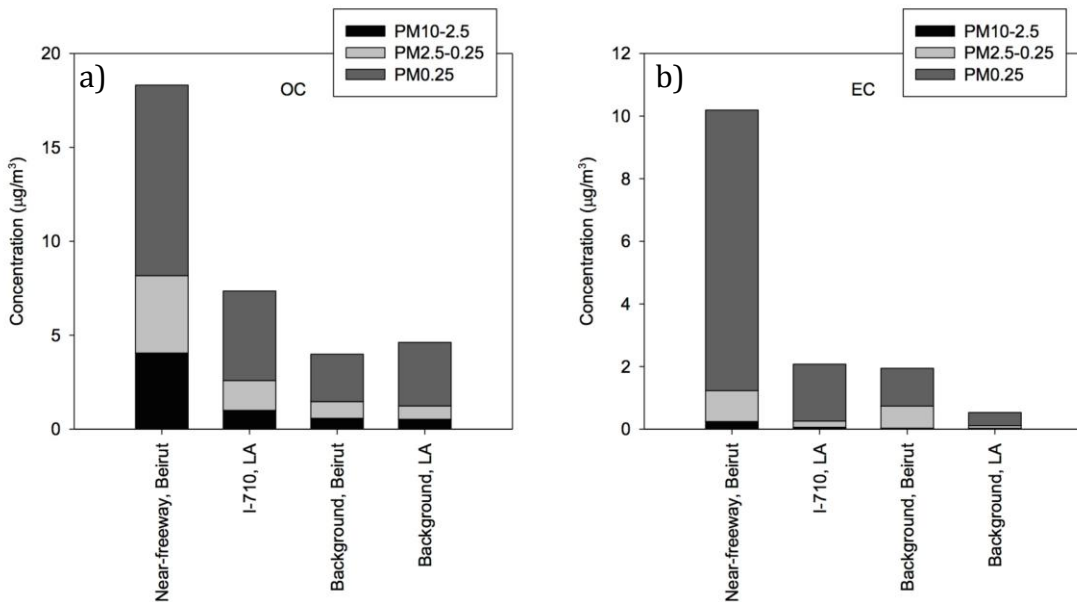


Figure 2.4a-b. Comparison of size-resolved a) organic carbon (OC) and b) elemental carbon (EC) concentrations (current study) with data from I-710 freeway and an urban background site in the Los Angeles (LA) area (Kam et al., 2012).

b. Secondary Ions

Coarse mode-SI contributed only marginally to $PM_{10-2.5}$ ($< 14\%$ and $2.25 \mu\text{g}/\text{m}^3$), with nitrate dominating its mass ($77-93\%$), followed by nss-sulfate ($7-23\%$), as shown in Figure 2.5a-b. Ammonium was undetected in this mode, consistent with several studies which documented that ammonium particles mostly exist in the fine mode ^{49,50}. Coarse nitrate and nss-sulfate are likely formed from the respective reactions of nitric and sulfuric acids with soil dust ^{51,52}, promoted by the calcium-carbonate-rich soil in Lebanon, as demonstrated by a previous study conducted in the Beirut area ⁵³. A significant fraction of these anions could also originate from the reaction of nitric and sulfuric acids with sea salt ⁵¹, given the proximity of the sites to the Mediterranean Sea (150-380 m).

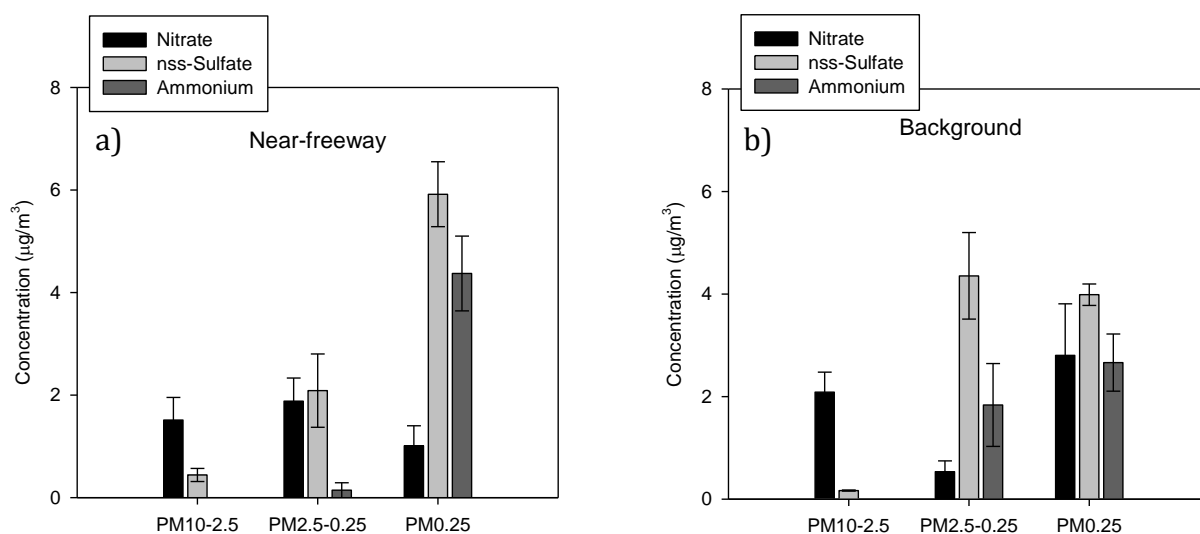


Figure 2.5a-b. Average concentration of nitrate, non-sea-salt sulfate and ammonium in $PM_{10-2.5}$, $PM_{2.5-0.25}$ and $PM_{0.25}$ at the a) near-freeway and b) background sites. Error bars correspond to one standard error.

These observations are further supported by a charge balance, estimated as the ratio of $(\text{Na}^+ + \text{NH}_4^+ + \text{ssCa}^{2+} + \text{ssMg}^{2+})$ to $(\text{Cl}^- + \text{NO}_3^- + \text{SO}_4^{2-})$ in equivalent units. This balance revealed a non-neutralized aerosol in the coarse fraction, indicating that the excess nitrate and sulfate are possibly in the form of soil-associated calcium nitrate and sulfate (Figure 2.6).

In the quasi-ultrafine and accumulation PM, SI was the major component at the background location while the next most abundant species at the freeway site, with average mass fractions of 54-68% and 29-31%, respectively. Nss-sulfate was mostly prevalent among secondary ions, accounting for 2.09-5.92 $\mu\text{g}/\text{m}^3$ and 42-65% of their collective mass. Ammonium and nitrate were less abundant, with ammonium contributing to 0.14/4.4 and 1.8/2.7 $\mu\text{g}/\text{m}^3$ in PM_{2.5}-0.25/PM_{0.25} at the near-freeway and background sites, respectively. Nitrate, averaging 1.01 and 2.8 $\mu\text{g}/\text{m}^3$ in PM_{2.5}-0.25 and PM_{0.25}, respectively, at the background location, is potentially in the form of ammonium nitrate formed from the photochemical reaction of nitric acid with ammonia⁵⁴. Nss-sulfate, on the other hand, is likely present as ammonium sulfate, formed from photochemical reactions of ammonia with sulfuric acid⁵⁴, as suggested by its strong correlation with ammonium at both sites ($R=0.74-0.95$ and $p<0.05$). This observation is in agreement with a previous study conducted in this region⁵³.

Additionally, it is noteworthy that sulfate and ammonium display fairly uniform concentrations in PM_{2.5} across the two sites ($p>0.05$), suggesting their predominantly regional secondary nature due to the long-range transport of their precursor gases. SO₂ levels in the eastern Mediterranean basin and Lebanon, in particular, are highly

influenced by air masses originating from Eastern and Central Europe^{55,56}. This was further confirmed by a backward air mass trajectory analysis, using HYSPLIT model⁵⁷, which showed predominantly N-NW winds during the sampling campaign (Figure 2.7). Local primary sources such as diesel-operating buses and ship emissions may also contribute to SO₂ emissions and sulfate formation, to some extent. PM_{0.25}-sulfate could originate from bunker fuel combustion from marine vessels⁵⁸, particularly at the background site given its close proximity (ca. 2.5 km) to the commercial port of Beirut.

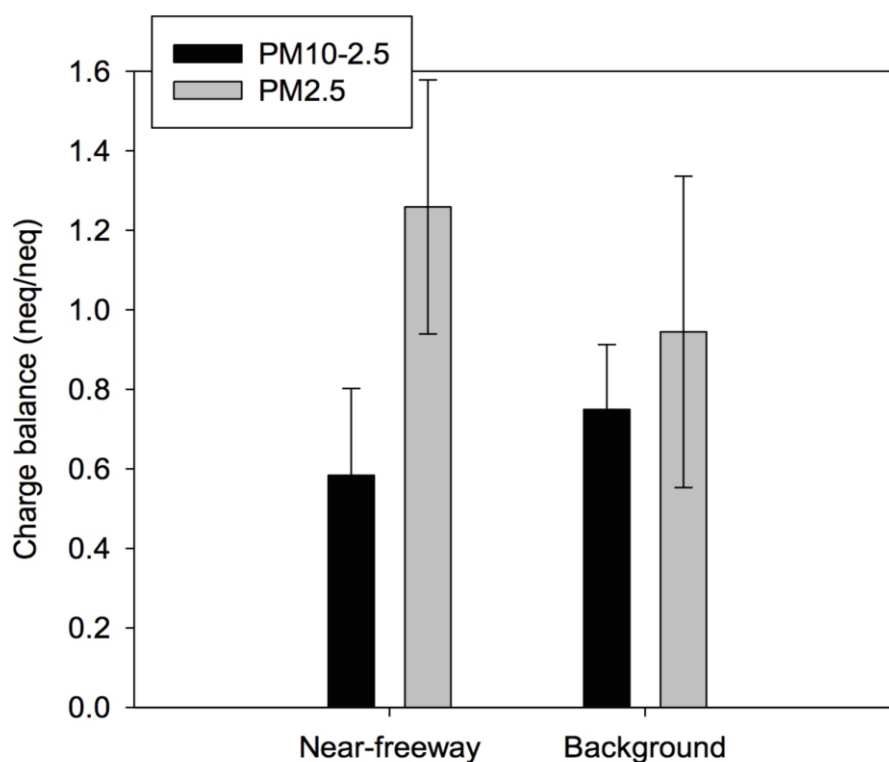


Figure 2.6. Average charge balance ratios of ($\text{Na}^+ + \text{NH}_4^+ + \text{ssCa}^{2+} + \text{ssMg}^{2+}$) to ($\text{Cl}^- + \text{NO}_3^- + \text{SO}_4^{2+}$). Error bars represent one standard error.

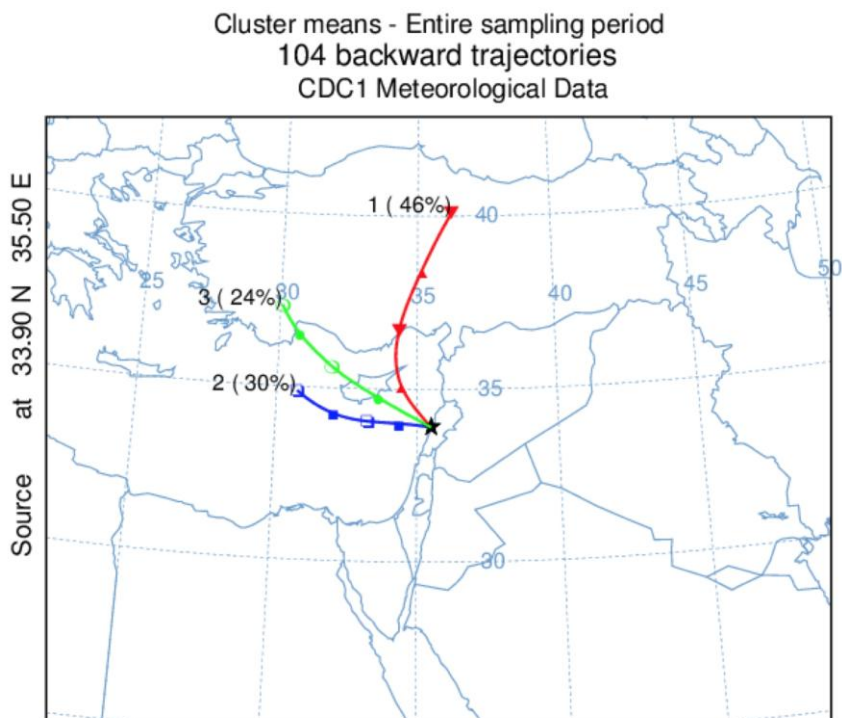


Figure 2.7. Backward air mass trajectories for the entire sampling campaign (July-August 2012), simulated using HYSPLIT model from NOAA. For each sampling day, four 48-hour trajectories were modeled every six hours at 500 m-agl using vertical wind velocity field from the meteorological data.

c. Sea Salts

Sea-salt mass concentration was considerably higher in $PM_{10-2.5}$ relative to the other two size fractions, with about 75% of sea-spray accounted for in the coarse mode at both sampling locations, consistent with expectations. Furthermore, although $PM_{10-2.5-SS}$ existed in similar amounts at both sites (2.37 ± 0.91 and $2.31 \pm 0.46 \mu\text{g}/\text{m}^3$, on average), sea-salt was a more significant component of coarse PM at the coastal background site than the traffic-impacted freeway location, accounting for 14.7 ± 3.1 and $7.3 \pm 2.8\%$ of its mass, respectively.

d. Crustal Material and Trace Elements

At both sites, CM was more prevalent in the coarse mode than accumulation and ultrafine particle-size fractions. It accounted for 12.2 ± 3.0 and $22.9\pm 8.1\%$ of $PM_{10-2.5}$ at the near-freeway and background locations, respectively. These proportions are, however, low compared to other Mediterranean areas, where 36% (Barcelona) to 65% (Athens) CM mass fractions were reported during spring and summer⁵⁰. CM may be under-represented using the sum of oxides method since this technique does not include all components known to contribute to dust. Moreover, soil in Lebanon is rich in calcite and limestone rocks^{53,59}. Its mineral content may therefore be underestimated using a factor of 1.4 to account for Ca oxides. Andrews et al.⁶⁰ reported that, depending on the soil composition, the crustal mass may be underestimated by as much as 50% using the sum of oxides approach. Furthermore, although vehicular-induced resuspension is expected to promote CM concentration at the freeway site, $PM_{10-2.5}$ -CM levels were comparable at the background and near-freeway locations, averaging 3.84 ± 1.6 and $4.08\pm 0.95 \mu\text{g}/\text{m}^3$, respectively. Soil dust re-suspension at the background site may be enhanced by local sea breeze or also construction activities and vehicular traffic nearby the site. The site is about 150 m away from a coastal road, where the driving mode involves intermittent acceleration and deceleration of vehicles at intersections and street shops, which could increase dust re-suspension.

Trace metals' contribution was consistently low at 0.5-1.8% for all size fractions and sites.

e. Chemical Mass Closure

Chemical mass balance results show an overall good agreement between the reconstructed and gravimetric PM mass. Percent mass apportioned varied between 45-123% across size fractions and sites, with lesser agreement observed for the coarse mode. The fraction of unknown mass for PM_{10-2.5} is nonetheless consistent with other studies, which reported a 28-50% range of unaccounted coarse PM mass^{41,43}. The unidentified mass could be related to uncertainties in the gravimetric and chemical measurements as well as multiplication factors used to convert OC to OM. Unmeasured crustal components and uncertainties in the correction factors used to account for oxides of metals could also lead to some inconsistency, particularly for the coarse fraction.

3. *Organic Compound Characterization*

To further investigate PM-organic composition, size-resolved mass concentrations (arithmetic mean \pm standard error) of PAHs, hopanes, steranes and n-alkanes were determined at each sampling site as summarized in Table 2.2 and Figures 2.8a-c. Undetected compounds or compounds with a concentration below the limit of detection (LOD) are reported as bdl. These values were also treated as zero in the reported sums. LOD for a given species is estimated as two times its uncertainty measurement in the limit as the concentration of the compound approaches zero. The LODs for speciated organics are listed in Table 2.2.

a. Polycyclic Aromatic Hydrocarbons (PAHs)

Polycyclic aromatic hydrocarbons (PAHs), many of which have been identified as potent human carcinogens⁶¹, are common products of incomplete combustion⁶². Because of their semi-volatile nature, these species can partition between the gaseous and particulate phase, depending on ambient temperature and atmospheric dilution conditions^{63,64}. Levels at the background site were below detection limit for all size-fractionated PAHs, as shown in Table 2.2. This site is surrounded by mostly pedestrian roads and dense vegetation covers, with the nearest street located at about 150 m away. PAH emissions from this adjacent road are likely shifted to the gaseous phase during their advection from the roadway to the sampling site. The high summertime temperatures coupled with frequent daytime on-shore winds and increased atmospheric dilution at this non-enclosed coastal site likely favor the volatilization, photodegradation and dispersion of PAHs. In contrast, levels of PAHs reached a cumulative concentration of $11.5 \pm 0.6 \text{ ng/m}^3$ at the near-freeway site, with the majority distributed in the quasi-ultrafine size range. Most of the measured compounds displayed concentrations that are about an order of magnitude higher in $\text{PM}_{0.25}$ than $\text{PM}_{2.5-0.25}$. Moreover, while high and medium molecular weight (MW) ($\text{MW} \geq 276$ amu and $\text{MW} = 252$ amu, respectively) benzo(ghi)perylene, coronene, benzo(e)pyrene and benzo(b)fluoranthene were the predominant PAHs in $\text{PM}_{0.25}$ and $\text{PM}_{2.5-0.25}$, low MW PAHs (≤ 228 amu) were also detected in the quasi-ultrafine mode. These results indicate significant contributions from LDVs as well as HDVs to PAH levels at the roadway. Previous works showed that both gasoline- and diesel-powered motor vehicles contribute to high MW PAHs, whereas HDVs are the major source of low MW PAHs

^{65,66}. Benzo(a)pyrene, commonly used as an index for PAH carcinogenicity ⁶⁷, exhibited a cumulative concentration of 0.69 ng/m³, exceeding that reported at I-710-freeway in LA by about 7 times ⁶⁸. Size-segregated overall PAH concentrations were also 1.3-3.9 fold greater relative to those measured at I-710 ⁶⁸, indicating substantial vehicular combustion emissions at the near-freeway site.

Table 2.2. Average (\pm standard error) concentration of PAHs, hopanes and steranes in PM_{10-2.5}, PM_{2.5-0.25} and PM_{0.25} at the near-freeway and background sites. bdl indicates an undetected compound or a concentration below detection limit. *Error corresponds to analytical error.

| | PM10-2.5 | | PM2.5-0.25 | | PM0.25 | | |
|--|---|---------------------|----------------|-----------------|-----------------|-----------------|-----------------|
| | JED | AUB | JED* | AUB | JED | AUB | |
| PAHs (ng/m³) | Pyrene | bdl | bdl | bdl | bdl | 0.4 \pm 0.01 | bdl |
| | Benzo(ghi)fluoranthene | bdl | bdl | bdl | bdl | 0.8 \pm 0.39 | bdl |
| | Benz(a)anthracene | bdl | bdl | bdl | bdl | 0.4 \pm 0.02 | bdl |
| | Chrysene | bdl | bdl | bdl | bdl | 0.7 \pm 0.03 | bdl |
| | Benzo(b)fluoranthene | bdl | bdl | 0.11 \pm 0.04 | bdl | 1.3 \pm 0.04 | bdl |
| | Benzo(k)fluoranthene | bdl | bdl | 0.05 \pm 0.01 | bdl | 0.64 \pm 0.04 | bdl |
| | Benzo(e)pyrene | bdl | bdl | 0.1 \pm 0.03 | bdl | 1.4 \pm 0.02 | bdl |
| | Benzo(a)pyrene | bdl | bdl | 0.06 \pm 0.02 | bdl | 0.63 \pm 0.03 | bdl |
| | Indeno(1,2,3-cd)pyrene | bdl | bdl | 0.1 \pm 0.03 | bdl | 1.1 \pm 0.06 | bdl |
| | Benzo(ghi)perylene | bdl | bdl | 0.17 \pm 0.02 | bdl | 2.6 \pm 0.12 | bdl |
| | Coronene | bdl | bdl | 0.1 \pm 0.03 | bdl | 1.6 \pm 0.03 | bdl |
| Total | - | - | 0.7 \pm 0.07 | - | 11.5 \pm 0.59 | - | |
| Hopanes and steranes (ng/m³) | 17 α (H)-22,29,30-Trisnorhopane | bdl | bdl | 0.22 \pm 0.02 | bdl | 0.32 \pm 0.05 | bdl |
| | 17 α (H)-21 β (H)-30-Norhopane | 0.2 \pm 0.02 | bdl | 0.78 \pm 0.08 | bdl | 2.4 \pm 0.13 | 0 \pm 0.05 |
| | 17 α (H)-21 β (H)-Hopane | 0.15 \pm 0.03 | bdl | 0.62 \pm 0.12 | bdl | 3.3 \pm 0.12 | 0.1 \pm 0.09 |
| | 22S-Homohopane | 0.15 \pm 0.02 | bdl | 0.54 \pm 0.04 | bdl | 4.1 \pm 0.25 | 0.1 \pm 0.09 |
| | 22R-Homohopane | 0.09 \pm 0.02 | bdl | 0.4 \pm 0.03 | bdl | 3.3 \pm 0.14 | 0.1 \pm 0.07 |
| | 22S-Bishomohopane | 0.13 \pm 0.02 | bdl | 0.32 \pm 0.02 | bdl | 2.9 \pm 0.22 | bdl |
| | 22R-Bishomohopane | 0.1 \pm 0.0000804 | bdl | 0.2 \pm 0.02 | bdl | 2.2 \pm 0.15 | bdl |
| | 22S-Trishomohopane | bdl | bdl | 0.2 \pm 0.02 | bdl | 2.3 \pm 0.08 | bdl |
| | 22R-Trishomohopane | bdl | bdl | 0.14 \pm 0.01 | bdl | 1.3 \pm 0.06 | bdl |
| | $\alpha\alpha\alpha$ -20S-C27-Cholestane | bdl | bdl | 0.13 \pm 0.02 | bdl | 0.38 \pm 0.06 | bdl |
| | $\alpha\beta\beta$ -20R-C27-Cholestane | bdl | bdl | 0.13 \pm 0.01 | bdl | 0.24 \pm 0.01 | bdl |
| | $\alpha\alpha\alpha$ -20R-C27-Cholestane | bdl | bdl | 0.14 \pm 0.02 | bdl | 0.37 \pm 0.04 | bdl |
| | Total | 0.82 \pm 0.09 | - | 3.8 \pm 0.16 | - | 23.1 \pm 0.89 | 0.29 \pm 0.28 |

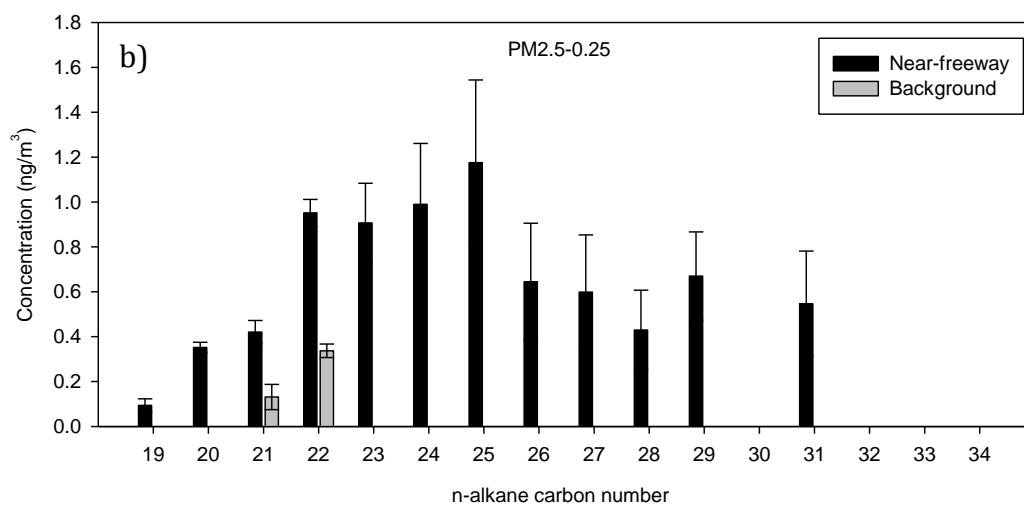
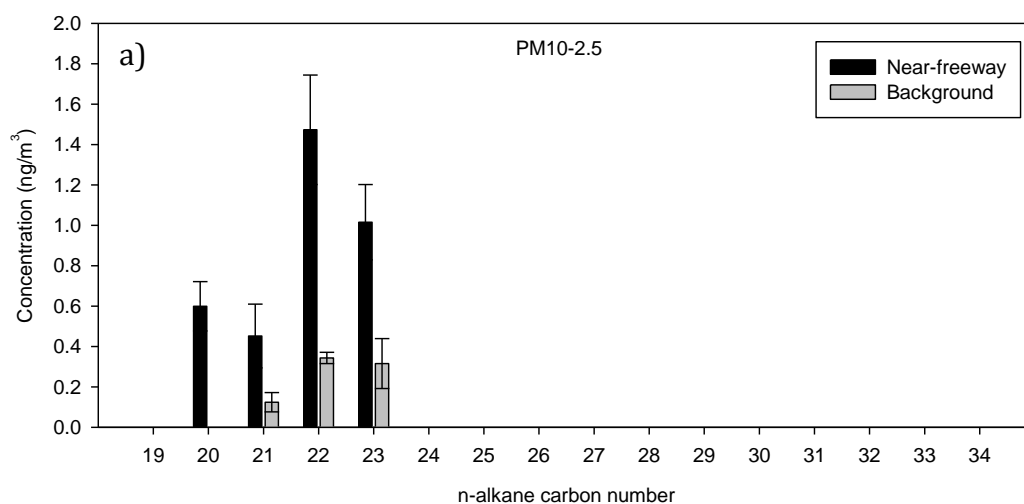
b. Hopanes and Steranes

Hopanes and steranes, which are derived from fuel oil and automotive lubricating oil ^{65,69}, were several folds greater at the near-freeway site than background location, confirming a strong impact from vehicular exhaust on PM levels at the roadway (Table 2.2). Similarly to PAHs, hopanes and steranes were mostly confined in the quasi-ultrafine mode, with 17 α (H)-21 β (H)-hopane, 22S-homohopane and 22R-homohopane prevailing at both sites. In proximity of the freeway, hopanes and steranes displayed a collective concentration ranging from a low of 0.82 ng m⁻³ in PM_{10-2.5} to a high of 23.1 ng m⁻³ in PM_{0.25}. These levels were 2.1-17.4 times those measured at diesel-impacted I-710 freeway in California ⁶⁸. Additionally, these organic compounds exhibited high hopanes plus steranes to total carbon (TC=OC+EC) ratios (0.16-1.1 ng/ μ g) compared to those recorded at I-710 (0.20-0.35 ng/ μ g) ⁶⁸, which is likely related to different engine operating conditions and configurations (e.g. after-treatment control technologies) or also lubricating oil formulation. The Lebanese vehicular fleet is characterized by a high percentage of non-catalyst equipped vehicles ⁷⁰. At the coastal background site, unlike PAHs which were below detection limit, PM_{0.25}-hopanes exhibited a cumulative mean concentration of 0.29 \pm 0.28 ng/m³. Because of their lower vapor pressure, hopanes are more atmospherically stable than PAHs ⁷¹, and may thus be less sensitive to meteorological conditions at this site. The large error associated with the measured levels suggests a change in source strength or an impact from multiple sources, such as vehicular emissions and nearby harbor activities. Marine vessels may contribute to urban concentrations of hopanes ⁷².

c. N-Alkanes

To assess the influence of anthropogenic and biogenic emissions at the sampling sites, size-resolved particle-phase n-alkanes (C₁₉-C₃₄) were quantified, as illustrated in Figure 2.8a-c. The origin of the selected n-alkanes was investigated by estimating their carbon preference index (CPI), defined as the concentration ratio of their odd-to-even numbered homologues⁷³. A CPI about 1 indicates a dominance of anthropogenic sources, whereas a CPI greater than 2 suggests a prevalence of biogenic sources^{73,74}. In both coarse and accumulation modes, overall levels of n-alkanes were several folds greater (4.5-16.6 times) at the near-freeway compared to the background site. While PM_{2.5-0.25}-bound n-alkanes at the roadside displayed notable peaks at C₂₉ and C₃₁, a signature of biogenic sources⁷⁵, these compounds were characterized by a predominance of homologues <C₂₅ and a CPI approaching 1 (1.31). Coarse mode n-alkanes showed a similar distribution, with a CPI close to 1 (0.70±0.03) and maxima at C₂₂ and C₂₃. These profiles confirm a strong impact from vehicular combustion emissions at the freeway site. Rogge et al.⁶⁹ found that fine particulate n-alkanes emitted from diesel and gasoline exhaust emissions show no carbon number preference but rather high levels of n-alkanes in C₁₉-C₂₅. In PM_{0.25}, C₁₉-C₃₄ at the near-freeway site, which accounted for most of total n-alkanes mass (86%), averaged 74.6±3.4 ng/m³, with n-alkanes enriched across the entire range of carbon numbers and a CPI of 1.03±0.08. This distribution indicates both road dust and vehicular exhaust emissions as major sources of n-alkanes in proximity of the freeway. N-alkanes derived from fine particulate road dust exhibit no carbon number preference, but greater concentrations for high MW homologues⁷⁶. At the background site, PM_{0.25}-n-alkanes were consistently lower than those at the freeway location, reaching a total concentration of 18.7±4.3

ng/m³ with a CPI of 1.2±0.06. These compounds were also dominated by high MW congeners, spanning homologues up to C₃₄, which suggests road dust as a dominant source of n-alkanes at this site.



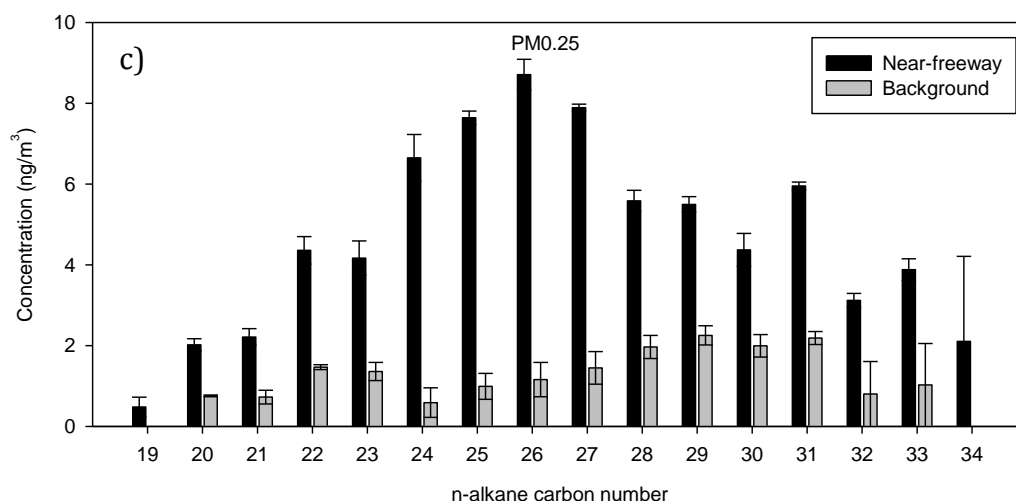


Figure 2.8a-c. Average n-alkanes concentration (C₁₉-C₃₄) in a) PM_{10-2.5}, b) PM_{2.5-0.25} and c) PM_{0.25} at the near-freeway and background sites. Error bars correspond to one analytical or standard error.

D. Summary and Conclusion

To investigate road-traffic emissions in the greater Beirut area, PM_{10-2.5}, PM_{2.5-0.25} and PM_{0.25} samples were concurrently collected at near-freeway and background sites. Particle mass levels at the background location were significantly lower than those at the roadway for all size modes. PM at the background site was mainly influenced by secondary sources as evidenced by SI contribution to the overall particle mass (~50%). The prevalence of secondary emissions was further confirmed by OM, which accounted for 17% of PM₁₀ and was mostly water-soluble (70.4%) at this location. Contrarily, particle levels at the near-freeway location were dominated by vehicular emissions from both road dust and tailpipe. OM, which accounted for 46-56% of PM_{2.5-0.25} and PM_{0.25}, was mainly water-insoluble at this location, indicating its predominantly primary origin. Moreover, PM_{0.25}-EC varied from 1.21 µg/m³ at the background site to 8.97 µg/m³ in proximity of the freeway, highlighting a strong impact from HDDVs on roadway emissions. The influence of HDDVs in addition to LDVs was further supported by

PAHs molecular composition. Both high and low MW PAHs were detected in significant levels near the freeway. Moreover, relatively to other roadways, speciated organics exhibited high hopanes plus steranes-to-total carbon ratios (0.16-1.1 ng/ μ g), indicating dissimilar engine configurations or also lubricating oil formulation. Lastly, CM, indicative of soil dust resuspension, was a significant component of coarse particles at both sites. Road-dust contribution to PM at both locations was also corroborated by PM_{0.25}-bound n-alkanes which were enriched in high MW congeners and showed no carbon number preference. The redox potential of these sites is discussed in Chapter 3.

CHAPTER III

OXIDATIVE POTENTIAL AND CHEMICAL SPECIATION OF SIZE-RESOLVED PARTICULATE MATTER (PM) AT NEAR-FREEWAY AND URBAN BACKGROUND SITES IN THE GREATER BEIRUT AREA

The following chapter is based on the following study:

Daher, N., N. A. Saliba, A. L. Shihadeh, M. Jaafar, R. Baalbaki, M. M. Shafer, J. J. Schauer and C. Sioutas (2014). "Oxidative potential and chemical speciation of size-resolved particulate matter (PM) at near-freeway and urban background sites in the greater Beirut area." Sci Total Environ 470-471: 417-426.

A. Introduction

An increasing body of epidemiological and toxicological evidence indicates robust associations between adverse health effects and exposure to particulate matter (PM)^{7,8}. Many of the observed health endpoints may result, at least in part, from oxidative stress initiated by the formation of reactive oxygen species (ROS) upon the interaction of PM with epithelial cells and macrophages^{11,77}. ROS is a collective term comprising chemically reactive oxygen radicals or oxygen-derived species (e.g. hydroxyl radical and hydrogen peroxide)¹³. However, while particle mass has been proven useful in demonstrating the associations between PM exposure and acute health responses, aerosol mass is probably only a surrogate for causal particle components⁷⁸. Specific PM species contributing to aerosol toxicity remain to be identified. Particle compounds implicated in ROS formation include organic carbon, polycyclic aromatic hydrocarbons and quinones^{10,79,80}. PM oxidative potential may also be largely related to the PM content of soluble species, particularly transition metals^{81,82}. Metals such as iron, copper and vanadium, can initiate ROS formation both directly and indirectly through redox-mediated mechanisms^{83,84}. Particle-size could also be critical in

mediating PM toxicity. Because of their increased number, large surface area and high pulmonary deposition efficiency⁸⁵⁻⁸⁷, ultrafine particles (aerodynamic diameter, $d_p < 0.1-0.2 \mu\text{m}$) may be more potent than larger coarse ($\text{PM}_{10-2.5}$, $10 \mu\text{m} < d_p < 2.5 \mu\text{m}$) or fine ($\text{PM}_{2.5}$, $d_p < 2.5 \mu\text{m}$) particles^{10,88}.

Lebanon, with a growing population and limited air pollution controls, is afflicted with elevated PM levels, particularly in its urban areas²⁶. Lacking an efficient public transportation system⁸⁹, its high particle levels can be mainly related to vehicular emissions. Regional sources could also contribute to its PM concentrations. Being located in the eastern Mediterranean basin, aerosol emissions from industrialized areas of northern and north-eastern Europe are significant particle sources in Lebanon^{26,90}. Accurate characterization of PM-associated redox activity at urban and roadside settings in Lebanon is thus vital.

The chemical composition of PM in Lebanon has been previously investigated (Chapter II)^{26,28,90}, but its oxidative potential is yet to be explored. To date, there is a significant dearth of information on particle toxicity in this region. To determine PM redox activity in Lebanon, coarse, accumulation ($\text{PM}_{2.5-0.25}$, $2.5 \mu\text{m} < d_p < 0.25 \mu\text{m}$) and quasi-ultrafine ($\text{PM}_{0.25}$, $d_p < 0.25 \mu\text{m}$) particle samples were collected at near-freeway and urban background sites in the greater Beirut area. Samples were analyzed for their ability to induce oxidative stress on rat alveolar macrophages based on their reactive oxygen species (ROS) content. Their chemical composition was also determined, with particular focus on the effect of metals and trace elements. To the best of the authors' knowledge, this is the first study to evaluate particle-induced toxicity in Lebanon. The intrinsic redox activity of PM in Beirut —representative of developing areas lacking air

quality regulations— is also compared to that of aerosols from other worldwide urban settings for which similar ROS data, using the same assay, are available.

B. Methodology

1. *Sampling Site*

The sampling campaign was conducted in the greater Beirut area at urban background and near-freeway sites, as shown in Figure 2.1. The background site was situated at the American University of Beirut (AUB). This monitoring site, which overlooks the Mediterranean coast from the north/west and AUB campus from the south/east, is mostly surrounded by dense vegetation covers and pedestrian roads. The nearest street is located about 150 m west of the site. This coastal roadway, which separates the site from the Mediterranean Sea, experiences relatively high traffic activity throughout the day, especially during peak hours (7-9 a.m. and 4-7 p.m.). Moreover, the sampling site is about 1.5 and 2.5 km away from a leisure yacht club and the commercial port of Beirut, respectively. The second sampling site consisted of 5-lane Jal El Dib freeway, along its southbound segment. The sampling point was directly adjacent to the freeway at about 1 m from its edge and 1.5 m above ground level. The site is therefore heavily influenced by vehicular emissions from the roadway. This freeway, which serves as a main conduit for vehicles traveling from Mount/North Lebanon to the capital Beirut, experiences heavy traffic throughout the day, with increased congestion during rush hours (7-11 a.m. and 4-7 p.m.). Additionally, the site is within 0.4 and 3.3 km of the Mediterranean coast and a yacht port/club, respectively.

2. Sample Collection

Sampling was conducted on weekdays during July-August 2012 from 7:00 a.m. to 5 p.m. Samples were concurrently collected at both sites on a weekly basis. Three parallel Sioutas Personal Cascade Impactor Samplers (Sioutas PCIS, SKC Inc., Eighty Four, PA, USA³¹), operating at 9 lpm and fitted with PM₁₀ inlets (Chemcomb 3500 speciation sampling cartridge, Thermoelectron Corp., Ohio, USA) were deployed at each location to collect size-resolved particles in the following size ranges: 10-2.5 μm (coarse PM), 2.5-0.25 μm (accumulation PM) and <0.25 μm (quasi-ultrafine PM). For chemical analyses purposes, two PCISs were loaded with Teflon filters (Pall Life Sciences, Ann Arbor, MI) while one PCIS was loaded with quartz microfiber filters (Whatman International Ltd, Maidstone, England). 25 mm filters were used as impaction substrates for PM_{10-2.5} and PM_{2.5-0.25} while 37 mm filters were used as collection media for PM_{0.25}. The collected particle mass was determined by pre- and post-weighing the Teflon filters using a UMX2 microbalance (Mettler Toledo GmbH, CH-8606 Greifensee, Switzerland), following equilibration under controlled temperature and relative humidity conditions (22–24°C and 40–50%, respectively).

3. Sample Analysis

To perform chemical and oxidative analyses of the samples, each of the collected Teflon and quartz filters was sectioned into two equal portions. Measurements of carbonaceous species and organic compounds were conducted on the quartz substrates, while all other analyses were performed on the Teflon filters. Depending on the analytical mass requirements, measurements were conducted on either individual

weekly samples (carbonaceous species, ions, ROS-activity, metals and elements) or composites of the weekly samples (water-soluble organic carbon).

Elemental and organic carbon (EC and OC, respectively) contents of the filters were determined using the NIOSH Thermal Optical Transmission method³². The total elemental composition of the filter substrates was measured using a high resolution (magnetic sector) Inductively Coupled Plasma Mass Spectrometry (HR-ICP-MS Thermo-Finnigan Element 2). A mixed acid (1 mL of 16 M nitric acid, 0.25 mL of 12 M hydrochloric acid and 0.1 mL of hydrofluoric acid) microwave-assisted digestion was applied for extraction of total metals and elements³⁴. The water-soluble elemental content of the filters was also quantified using HR-ICP-MS, but following water-extraction and filtration of the samples. Ions and water-soluble organic carbon (WSOC) were respectively determined by ion chromatography and a Sievers 900 Total Organic Carbon Analyzer, after extraction of the samples with high purity water^{91,92}.

The redox activity of the samples was measured using a macrophage-based reactive oxygen species (ROS) assay. This assay is a fluorogenic cell-based method that uses 2',7'-dichlorodihydrofluorescein diacetate (DCFH-DA) as the fluorescent probe, Figure 3.1.

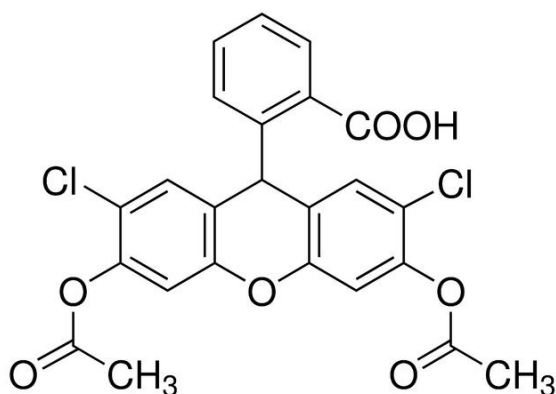


Figure 3.1. DCFH-DA Structure

Prior to the assay, substrates were extracted with high purity water and filtered. The aqueous PM suspensions were then mixed with DCFH-DA and added to rat alveolar macrophage cells (cell line NR8383, American Type Culture Collection). DCFH-DA, a membrane permeable compound, is de-acetylated upon entering a cell, yielding 2',7'-dichlorodihydrofluorescein (DCFH). Non-fluorescent DCFH is then converted by ROS species produced within the cell cytoplasm into the highly fluorescent 2,7-dichlorofluorescein (DCH), which is monitored using a microplate reader. Further details can be found in Landreman et al.⁹³.

C. Results and Discussion

To investigate PM chemical composition, size-resolved particle mass concentrations and mass fractions of bulk PM components (average \pm standard error) were determined, as presented in Table 3.1 for each site and particle mode. PM samples were classified into water-insoluble organic matter (WIOM), water-soluble organic matter (WSOM), EC, secondary ions (SI), sea-salt (SS), crustal material (CM) and trace elements (TE).

Table 3.1. Average (\pm standard error) mass concentration and chemical composition of PM_{10-2.5}, PM_{2.5-0.25} and PM_{0.25} at the near-freeway and urban background sites.

| | Particle size (μm) | Mass ($\mu\text{g}/\text{m}^3$) | WIOM (%) | WSOM (%) | EC (%) | SI (%) | SS (%) | CM (%) | TE (%) |
|--------------|---------------------------------|-----------------------------------|----------------|----------------|----------------|-----------------|----------------|----------------|----------------|
| Near-freeway | 10-2.5 | 34.0 \pm 1.5 | 17.5 \pm 3.6 | 1.6 \pm 0.3 | 0.7 \pm 0.1 | 6.0 \pm 1.8 | 7.3 \pm 2.8 | 12.2 \pm 3.0 | 0.5 \pm 0.2 |
| | 2.5-0.25 | 13.8 \pm 0.9 | 41.7 \pm 8.9 | 8.8 \pm 0.7 | 7.7 \pm 1.0 | 31.3 \pm 7.2 | 4.1 \pm 2.9 | 18.6 \pm 2.7 | 1.8 \pm 0.5 |
| | < 0.25 | 36.1 \pm 0.9 | 36.7 \pm 1.2 | 8.4 \pm 0.9 | 25.3 \pm 0.9 | 28.7 \pm 2.3 | 1.1 \pm 0.8 | 4.7 \pm 0.6 | 0.4 \pm 0.05 |
| Background | 10-2.5 | 15.8 \pm 0.9 | 2.6 \pm 0.7 | 3.2 \pm 0.7 | 0.2 \pm 0.1 | 14.0 \pm 1.9 | 14.7 \pm 3.1 | 22.9 \pm 8.1 | 0.6 \pm 0.3 |
| | 2.5-0.25 | 8.6 \pm 1.0 | 2.8 \pm 1.3 | 12.2 \pm 3.0 | 7.5 \pm 1.2 | 67.5 \pm 6.2 | 7.3 \pm 5.2 | 9.9 \pm 3.6 | 1.6 \pm 0.4 |
| | < 0.25 | 14.0 \pm 0.4 | 8.4 \pm 2.6 | 21 \pm 1.9 | 8.9 \pm 0.9 | 53.5 \pm 11.8 | 0 \pm 0 | 2.8 \pm 0.6 | 0.7 \pm 0.2 |

WSOM and OM (WSOM+WIOM) were determined by multiplying measured WSOC and OC by a factor of 1.6, respectively³⁸. WIOM was then estimated as the difference between OM and WSOM. SS contribution was determined as the sum of Na⁺ concentration and sea-salt fractions of chloride, magnesium, potassium, calcium and sulfate concentrations, assuming standard sea-water composition³⁹ and using Na⁺ as a tracer for sea-salt. SI comprises ammonium, nitrate and non-sea-salt sulfate (nss-sulfate), with nss-sulfate estimated by subtracting the sea-salt fraction of sulfate from measured sulfate. The fraction of CM in the PM samples was determined by summing the oxides of crustal metals, Al, K, Fe, Ca, Mg, Ti and Si⁴⁰⁻⁴², with Ca and Mg representing their non-sea-salt portions. TE includes other measured elements such as Cu, Zn and Ba.

Total PM (PM₁₀) mass composition was predominated by PM_{0.25} and PM_{10-2.5} (36-43% of PM₁₀) at both sampling locations. However, particle concentrations were 1.6-2.6 times greater at the near-freeway than background site for all particle-size modes. PM mass levels ranged from 13.8-36.1 and 8.6-15.8 µg/m³ at the roadside and background locations, respectively. The consistently lower concentrations at the background site illustrate the significant contributions from vehicular emissions and traffic-induced re-suspension to PM levels at the freeway location. Size-resolved PM composition also varied between sites. In PM_{0.25} and PM_{2.5-0.25}, WIOM was the most dominant component at the near-freeway site (37-42%), with primary vehicular emissions as the most likely sources. On the other hand, SI prevailed at the background site in both the accumulation and quasi-ultrafine modes, contributing to 54-68% of their mass. PM_{2.5-0.25}- and PM_{0.25}-WSOM, mainly derived from secondary organic aerosol (SOA) formation processes⁴⁵, were the next most abundant components at the

background site (12-21%), indicating considerable contributions from secondary sources at this urban site. In $PM_{10-2.5}$, CM was the major PM constituent at the background site ($22.9 \pm 8.1\%$), while the next most prominent component at the near-freeway location ($12.2 \pm 3\%$). WIOM, with a comparable mass fraction to CM ($17.5 \pm 3.6\%$), was predominant in the coarse mode at the roadside location. EC, a key tracer for diesel exhaust⁴⁷, significantly contributed to $PM_{0.25}$, particularly at the near-freeway site. It accounted for $25 \pm 0.9\%$ of the quasi-ultrafine mass at the roadside site, suggesting an influence from diesel vehicles on road-traffic emissions. Its contribution to the larger particle-size fractions was less substantial, averaging less than 9%. SS mostly contributed to $PM_{10-2.5}$, consistent with expectations, accounting for 7-15% of its mass across sites. TE were the least abundant species, contributing to less than 2% of PM mass across sites and particle-modes. Nonetheless, several of these trace metals (e.g. Co, Mn, Ni) are toxicologically-relevant⁸⁴, with only few of them listed by the U.S. Environmental Protection Agency (EPA) as air toxics⁹⁴.

D. Metals and Trace Elements

1. *Size-Resolved Concentrations and Crustal Enrichment Factors*

The toxicological relevance of several transition metals (e.g. Cu, Cr, Fe) warranted a thorough examination of metals and elements in the PM samples. Average (\pm standard error) mass concentration and crustal enrichment factor (CEF) of select total metals and elements were determined for each particle-mode and sampling site, as displayed in Figures 3.2 a-b and 3.3 a-b. CEFs were estimated in order to assess the relative contributions of anthropogenic and natural sources to the elemental components. For a given element, CEF was estimated as the ratio of its abundance in a

PM sample to its average abundance in the upper continental crust (UCC) after normalization to Al. Al was selected as a reference element and UCC composition was obtained from Taylor and McLennan⁹⁵. Typically, elements with a CEF approaching 1 are of crustal origin whereas elements with a CEF exceeding 10 are considered anthropogenic⁹⁶. We should note that the selection of Al as a reference element could lead to an underestimation of the CEFs if Al was enriched in the samples. To minimize this potential bias, PM_{2.5-0.25} and PM_{0.25} elemental data was combined into PM_{2.5} data in this analysis.

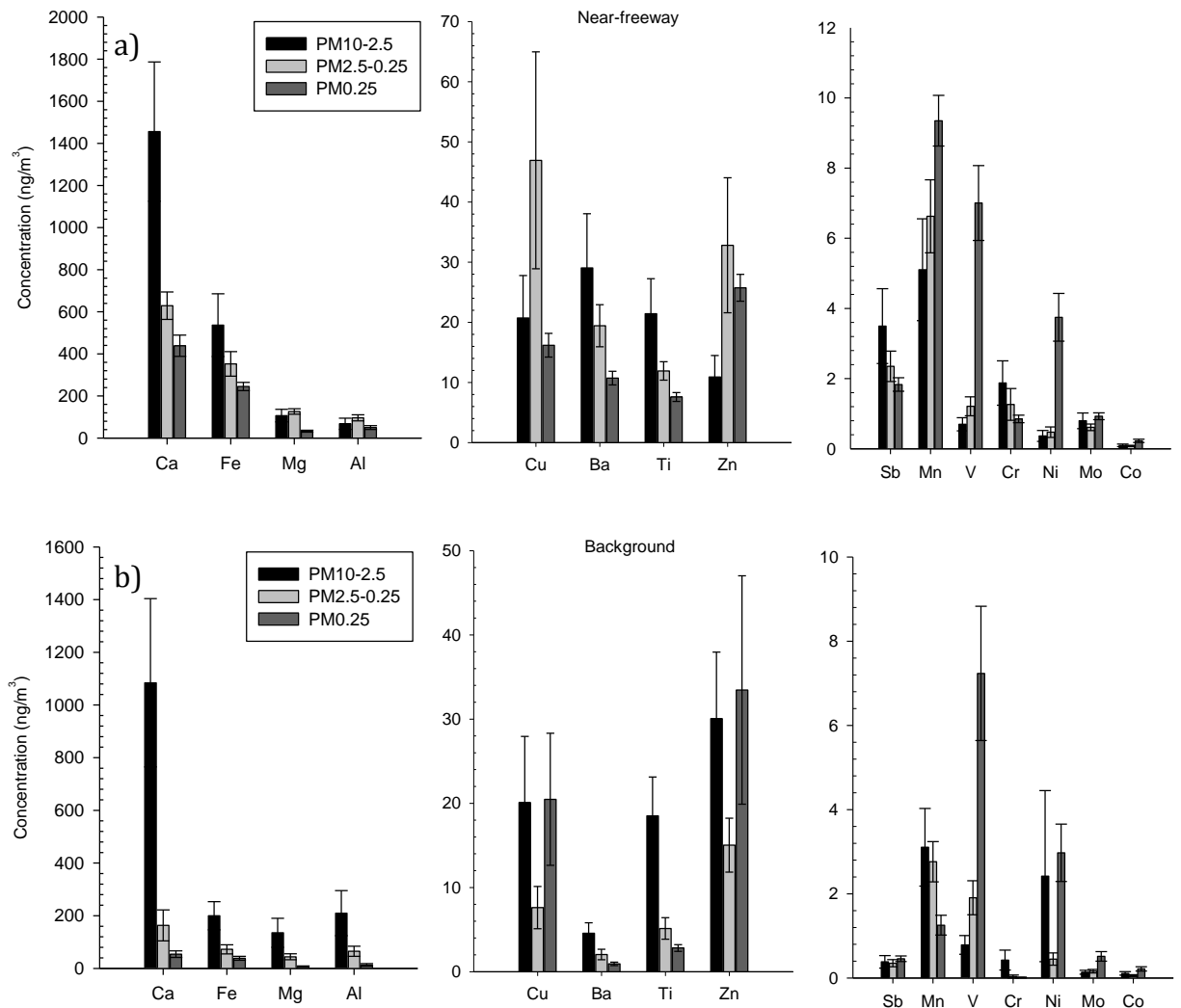


Figure 3.2 a-b. Average total concentration of metals and elements in PM_{10-2.5}, PM_{2.5-0.25} and PM_{0.25} at the a) near-freeway and b) urban background sites. Error bars represent one standard error.

Size-resolved Ca, Mg, Fe, Al and Ti generally displayed comparable levels and CEFs < 10 at both locations, confirming their soil dust origin. These PM components also showed a gradual increase in concentration with particle-size, reaching a peak in the coarse mode, in accordance with their geochemical origin. Ca was mostly abundant among these elements at both sampling sites and in all three particle-size fractions, peaking at 1084.2 ± 319.3 and 1455.9 ± 330.5 ng/m³ in PM_{10-2.5} at the background and near-freeway locations, respectively. A modest enrichment was also notable for Ca (CEF=15-22) at the roadway site. However, while lube oil emissions contribute to Ca levels²⁰ to some extent, the increased enrichment observed for Ca at the roadside could be mainly related to the abundance of calcite and limestone rocks in Lebanon^{53,59}. Ca crustal fraction may not be adequately represented using the UCC composition from Taylor and McLennan⁹⁵. Furthermore, the strong correlations of Ca with Mg and Ti at the near-freeway site further corroborate its origin in soil dust ($R^2=0.82-0.90$). In contrast, an indication of anthropogenic contamination was generally noted for transition and trace metals. Sb and Ba were overall mostly confined to the coarse fraction and displayed CEFs exceeding 10, which suggests that their sources are anthropogenic, likely brake and tire wear⁹⁷.

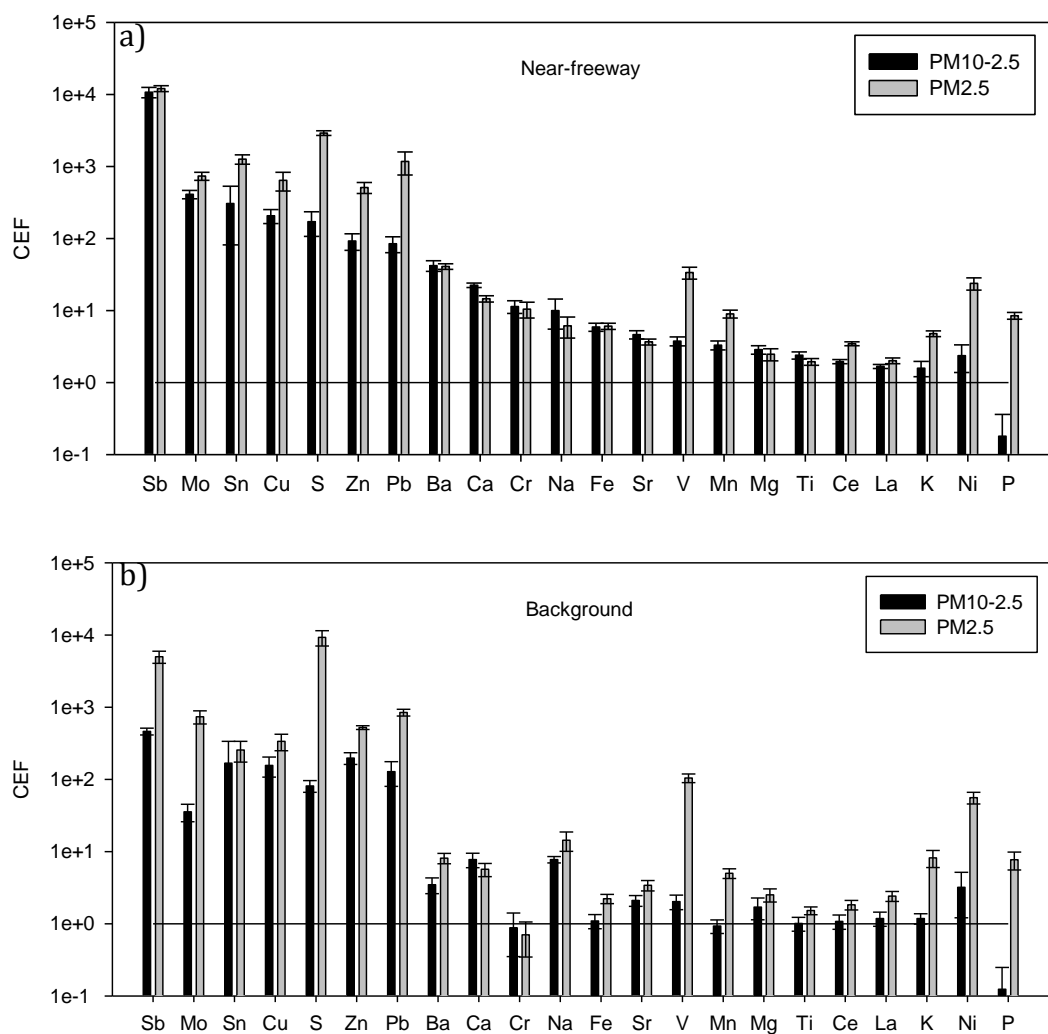


Figure 3.3a-b. Average crustal enrichment factors (CEF) in PM_{10-2.5} and PM_{2.5} at the a) near-freeway and b) urban background sites. Error bars represent one standard error.

These elements also presented greater concentrations (4-11.6 times) and a markedly stronger enrichment at the roadside location, further supporting their traffic-related sources. While both Cu and Zn exhibited a strong enrichment (CEF > 90), indicative of their anthropogenic origin, these elements displayed different partitioning at the sampling sites, suggesting distinct or mixed sources, each producing PM in different size ranges. At the near-freeway location, Cu and Zn were mostly distributed in PM_{2.5-0.25} (47-56% by mass), similarly to the findings of Lin et al.⁹⁸ near a heavily-trafficked

road. Lin et al.⁹⁸ reported that Zn and Cu have respective mass median diameters of 1.21 and 1.56 μm , with Zn possibly derived from tire friction or also brake wear in fine PM. In the accumulation mode, Zn strongly correlated with Cu ($R^2=0.92$), but moderately with brake-wear tracer Sb ($R^2=0.61$), implying that Zn and Cu originate from tire wear and brake wear to a lesser extent⁹⁹. On the other hand, at the background location, Cu and Zn were mostly distributed in $\text{PM}_{0.25}$ and $\text{PM}_{10-2.5}$, accounting for 38-43% of their respective mass, with brake wear as a potential source. While the majority of particles produced by abrasion are in the coarse mode, brake attrition could also contribute to ultrafine particles¹⁰⁰. Cu and Zn have been associated with brake wear in both the coarse and ultrafine PM modes^{98,101}. We should, however, note that the rather even distribution of Cu and Zn between the coarse and quasi-ultrafine size ranges could also indicate a multiplicity of sources. Combustion sources, possibly exhaust emissions, may contribute to these elements in $\text{PM}_{0.25}$. Ultrafine mode-Zn and $\text{PM}_{0.1}$ -Cu have been associated with diesel and gasoline emissions, respectively⁹⁸. Similarly to Cu and Zn, Mn showed a dissimilar particle-size distribution at the sampling sites. In proximity of the freeway, Mn presented a CEF approaching 10 (9 ± 1.1), with most of its mass (45%) associated with $\text{PM}_{0.25}$, thereby suggesting road dust enriched with exhaust combustion emissions, as a possible source for this metal⁹⁸. At the background location, Mn was less enriched ($\text{CEF} < 5$) and displayed lower levels (0.13-0.61 times) with 82% of its mass distributed relatively evenly between $\text{PM}_{2.5-0.25}$ and $\text{PM}_{10-2.5}$, which indicates that Mn mainly originates from soil and/or road dust¹⁰². V and Ni were generally more enriched in the fine fraction ($\text{CEF} = 24-105$), with greater partitioning in the quasi-ultrafine mode. These elements, which presented similar $\text{PM}_{0.25}$ concentrations at both sampling sites ($p>0.05$), likely originate from fuel oil combustion^{103,104}, given the location of the

sites nearby ports (2.5-3.3 km). PM_{2.5}- and PM_{10-2.5}-bound Mo displayed a CEF exceeding 10 at both locations. This element, which was mostly confined to the quasi-ultrafine mode (40-63%), exhibited a stronger enrichment and higher concentrations in proximity of the freeway, confirming its traffic-related source, possibly lube oil combustion²⁰. Cr peaked in the coarse mode and was more enriched at the roadway than background location. This element also displayed a CEF approaching 10 in PM_{10-2.5} at the near-freeway location, suggesting its road dust source¹⁰². Co existed in similar amounts at both sites, ranging from a low in PM_{2.5-0.25} (0.06-0.08 ng/m³) to a high in PM_{0.25} (0.22-0.23 ng/m³). A similar trend was also reported by Song et al.¹⁰⁵. Despite its trace levels, this element is particularly toxic⁸⁴ with road dust re-suspension and fuel combustion as possible sources in the coarse and ultrafine modes, respectively^{106,107}.

2. Water Solubility

The water solubility of PM is an important physico-chemical property governing its toxicological behavior¹⁰⁸. Soluble species exhibit enhanced bioavailability, and may thus be more toxicologically-relevant. Water-soluble metals, in particular, have been implicated as potent initiators of particle-mediated oxidative stress^{81,109}. Figure 3.4 shows size-resolved percent water-solubility of select metals and elements, averaged across sites. The solubility of a given PM species was determined as the ratio of its water-soluble to total elemental concentration. Few elements exhibited fractions exceeding 1, which can be attributed to the analytical uncertainties associated with the chemical measurements. Water-solubility of measured metals and trace elements varied considerably with particle-size and element. It is overall highest in PM_{0.25} and PM_{2.5-0.25} while lowest in PM_{10-2.5}. A stronger size-dependency was also

observed for Cu, Pb and Cr, with water-solubility peaking in the quasi-ultrafine fraction then decreasing with increasing particle-size. Soil- or road dust-related elements, Al, Ti, Fe and Cr, displayed low water-solubility ($\leq 31\%$), consistent with their geochemical origin. Unlike other crustal elements, Ca was highly water-soluble ($>70\%$) despite its mainly soil origin. Ca, which was mostly confined to the coarse mode, is likely present as calcium-carbonate with a significant fraction in the form of calcium nitrate and sulfate, as demonstrated by a previous study conducted in the Beirut area⁵³. Calcium carbonate is moderately water-soluble while calcium nitrate and sulfate, formed from the reactions of nitric and sulfuric acids with sea-salt or mineral dust¹¹⁰, are both highly water-soluble¹¹¹. Sea-salt component, Na, displayed a high solubility in all three size fractions, exceeding 78%. S, mainly in the form of soil-associated sulfate in PM_{10-2.5} and ammonium sulfate in PM_{0.25} and PM_{2.5-0.25}, was highly water-soluble in all three size fractions ($>81\%$). Anthropogenic-related elements, such as Zn, Cd, Co, Mn, V, Cu, Ni, Mo, Pb and Sb, displayed peak solubility in the accumulation or quasi-ultrafine modes and were moderately-to-strongly water-soluble in these fractions ($>43\%$). These elements are mainly associated with high-temperature combustion processes, such as vehicular exhaust emissions and fuel oil combustion^{98,103}. The water-solubility of these metals was lowest in the coarse mode, ranging between 2 and 59%, which can be attributed to a difference in their geochemical origin and sources across modes. In PM_{10-2.5}, these elements are mostly associated with vehicular abrasion or re-suspended road dust^{102,52}. These results generally agree with those reported for size-fractionated PM in urban areas in the Los Angeles (LA) basin¹¹².

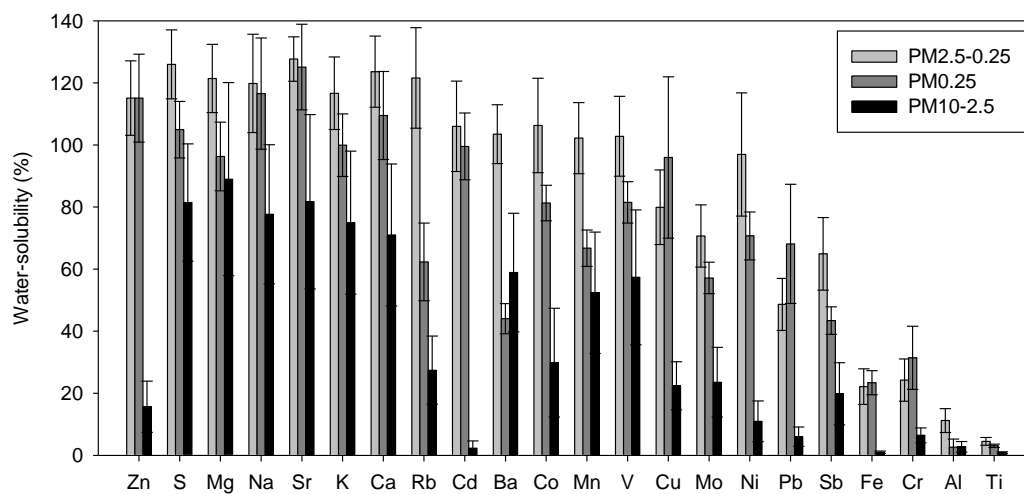


Figure 3.4. Water-solubility of metals and elements in PM_{10-2.5}, PM_{2.5-0.25} and PM_{0.25}, averaged across the sampling sites. Error bars represent one standard error.

3. Water-Soluble Elemental Composition

The water-soluble elemental composition ($\mu\text{g/g PM}$) of the size-resolved PM samples is shown in Figure 3.5, with mass fractions averaged across sites. The overall species' distribution in either PM fractions is generally consistent with expectations. Soil-related elements, such as Ti, Ca, Mg, Sr and Al, were least abundant in PM_{0.25}, while mostly prevalent in PM_{10-2.5} or PM_{2.5-0.25}. On the other hand, anthropogenic-related elements, including Cu, Zn, Mn, V, Ni, Sb, Cr, Mo, As, Co and Cd, were generally largely enriched in the accumulation or quasi-ultrafine modes. These elements are mostly derived from high-temperature combustion processes, which emit a large fraction of water-soluble components⁹⁶. Moreover, potentially toxic or ROS-active species generally rank high among the considered array of elements. In the accumulation mode, water-soluble Zn and Cu were mostly dominant among the anthropogenic-elements, accounting for 0.19-0.25% of PM_{2.5-0.25}. Their mass fractions

also approached those of bulk particle components, Ca, K and Mg, which indicates a significant PM anthropogenic contamination. Additionally, despite their very low mass fractions (0.01-0.028%), soluble PM_{10-2.5}-Mn as well as PM_{0.25}-V and -Ni are significant contributors to particle mass relative to other trace elements.

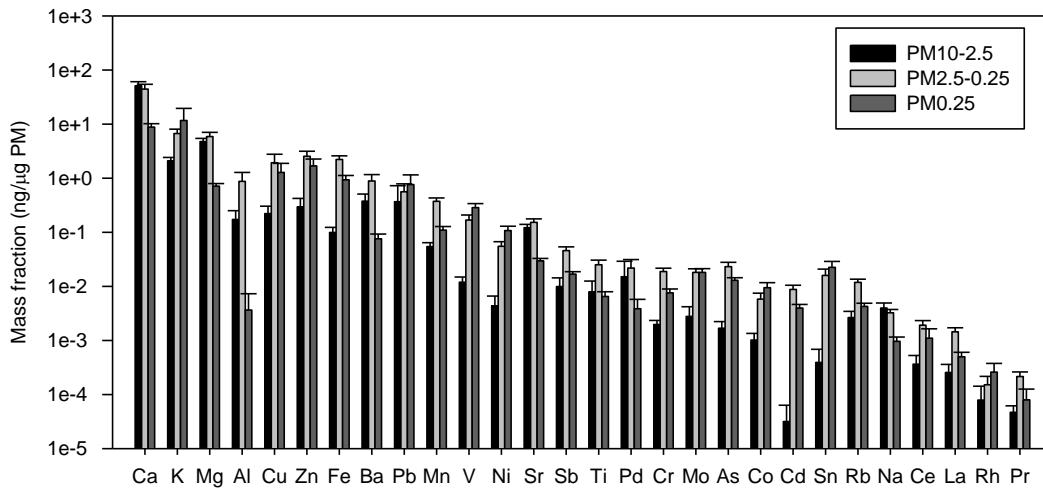


Figure 3.5. Water-soluble elemental composition of PM_{10-2.5}, PM_{2.5-0.25} and PM_{0.25}, averaged across the sampling sites. Error bars represent one standard error.

E. Size-Resolved Oxidative Potential

1. Reactive Oxygen Species (ROS)-activity

Measured ROS-activity of the size-resolved PM samples is shown in Figure 3.6 a-b on both per air volume (μg Zymosan equivalents m^{-3} air) and per PM mass (μg Zymosan equivalents mg^{-1} PM) bases. The air volume-based ROS-activity reflects the redox activity associated with PM exposure, while the PM mass-based ROS-activity is a measure of the intrinsic potency of PM.

The air volume-based ROS-activity was greater (1.5-2.8—fold) at the near-freeway site than background location for all particle-size ranges. This trend, which coincides with higher PM concentrations at the near-freeway site, suggests that

exposure to redox-active PM species is greatest at the roadway. The measured ROS-activity also exhibited a particle-size dependency, with lowest activity associated with coarse mode particles at both sampling sites. At the background location, although PM levels reached a minimum in the accumulation mode, the redox activity varied from a low of 11.7 μg Zymosan/ m^3 in $\text{PM}_{10-2.5}$ to a high of 440.0 μg Zymosan/ m^3 in $\text{PM}_{2.5-0.25}$. This peak occurrence in the accumulation mode likely reflects the influence of specific and highly redox active PM components. At the roadway site, ROS-activity ranged from a minimum in $\text{PM}_{10-2.5}$ (17.4 μg Zymosan/ m^3) to relatively comparable magnitudes in $\text{PM}_{2.5-0.25}$ and $\text{PM}_{0.25}$ (645.6 and 654.9 μg Zymosan/ m^3 , respectively).

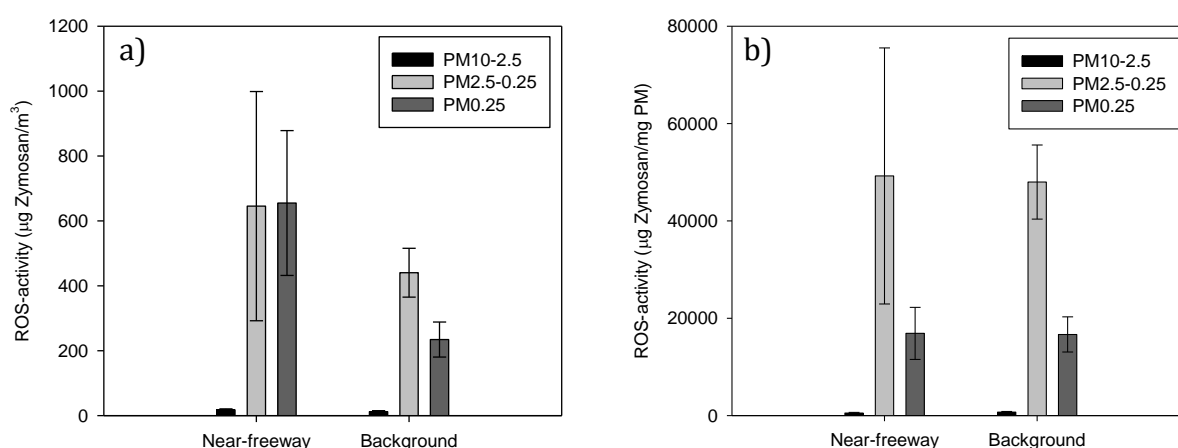


Figure 3.6 a-b. Average a) air volume-based (μg Zymosan/ m^3) and b) PM mass-based (intrinsic) (μg Zymosan/mg PM) reactive oxygen species (ROS)-activity of $\text{PM}_{10-2.5}$, $\text{PM}_{2.5-0.25}$ and $\text{PM}_{0.25}$ at the near-freeway and urban background sites. Error bars represent one standard error.

On a per PM mass basis, the ROS-activity also exhibited a size-dependent relationship at both sites, ranging from a maximum (49229.6 and 47975.6 μg Zymosan/mg PM) in the accumulation mode to a minimum (528.9 and 698 μg Zymosan/mg PM) in the coarse fraction. This rather large variability (a 69- and 93-fold range) in size-resolved redox activity suggests that ROS-active species have a distinct size-specific distribution,

with greater potency associated with PM_{2.5-0.25} and PM_{0.25} than the larger PM_{10-2.5} mode. A strong dependence of ROS on particle size was also documented by Hu et al. for PM in Long Beach/LA¹¹². However, contrary to the volume-based ROS-activity, the size-resolved intrinsic activity (i.e. normalized to PM mass) was generally comparable at both sampling locations, possibly suggesting a similarity in the sources of presumed PM ROS-active species.

2. Association of ROS-activity with PM Components

To identify PM chemical species (or source tracers) associated with ROS formation in the ambient air of the greater Beirut area, Spearman correlation coefficients (R) were determined between ROS-activity (μg Zymosan/mg PM) and select PM species (water-soluble metals, EC and OC in $\mu\text{g/g}$ PM), as summarized in Table 3.2 for each particle mode. To increase statistical significance, data points from all sites were pooled in this analysis. This was possible given the comparable mass-based ROS activity between sampling locations.

In PM_{10-2.5}, ROS-activity strongly correlated with Mn (R=0.79, $p < 0.05$), a component of road dust¹⁰² with moderate water-solubility (52%, one of the highest among all species in coarse PM). A relatively high association was also found between PM_{10-2.5}-based ROS-activity and Co (R=0.76, $p < 0.05$), in agreement with previous findings. Shafer et al.¹¹³ documented a strong association between water-soluble Mn/Co and ROS-activity in both PM₁₀ and PM_{2.5}. In PM_{2.5-0.25}, ROS-activity was strongly correlated with vehicular-abrasion element Cu (R=0.76, $p < 0.05$), which was more enriched in the accumulation mode (Figure 3.4) and almost entirely water-soluble (Figure 3.3). Cu can act directly to catalyze the formation of ROS via Fenton

chemistry⁸⁴ and has been implicated in ROS formation in PM_{2.5} in Milan, Italy^{56,114}. A moderate correlation ($R= 0.66-0.70$, $p<0.05$) was also noted between PM_{2.5-0.25} ROS-activity and combustion elements, Ni and Co, consistent with other studies^{112,113}. Both of these metals are associated with redox-cycling or -mediated mechanisms⁸⁴. In the quasi-ultrafine mode, ROS-activity was robustly associated with V and Ni ($R=0.79$ and 0.73), both elements of residual oil combustion¹⁰³ with greater abundance in PM_{0.25} and high water-solubility (>60%) (Figures 3.4 and 3.5). We should note that these findings are in agreement with several other studies^{112,115,116}, which highlight the impact of heavy fuel oil combustion on particle redox activity. Furthermore, ROS-activity was not correlated with EC in any PM size fraction—a finding that is not unexpected—as EC in isolation does not mechanistically participate in ROS formation. This result is also consistent with earlier investigations^{114,117}.

Lastly, we should emphasize that the lack of an association between ROS-activity and OC does not necessarily imply that OC is not a redox-active agent or does not participate in ROS induction. Studies conducted in the LA basin, Denver and Milan documented a moderate association between ROS-activity and WSOC ($R=0.69$ and 0.75)^{112,114,118}. The relationship between ROS-activity and OC in this study, where data from all sites was combined in the regression analysis, could be obscured by the distinct OC chemical composition between the sampling locations. As can be inferred from Table 3.1, OC was mostly water-insoluble at the near-freeway site, while it was predominately water-soluble at the background location. An investigation of size-resolved associations between ROS-activity and WSOC in this study was precluded by the limited number of data points for WSOC ($N<6$). However, a combination of data points for all PM size fractions and sites revealed a significant correlation between

ROS-activity and WSOC (R=0.77), which implies a potential role for secondary organic compounds in ROS generation.

Table 3.2. Spearman correlation coefficients (R) between ROS-activity (μg Zymosan/mg PM) and select species (ng/ μg PM) in PM_{10-2.5}, PM_{2.5-0.25} and PM_{0.25}. Bold indicates R \geq 0.70 and significant at a 0.05 level.

| | | PM _{10-2.5} | PM _{2.5-0.25} | PM _{0.25} |
|--|-----------|----------------------|------------------------|--------------------|
| Carbonaceous species | OC | -0.52 | -0.52 | -0.41 |
| | EC | 0.05 | -0.12 | -0.65 |
| Water-soluble metals and elements | V | 0.02 | 0.58 | 0.79 |
| | Cr | -0.24 | 0.33 | -0.17 |
| | Mn | 0.79 | 0.59 | 0.13 |
| | Fe | 0.50 | 0.60 | 0.17 |
| | Co | 0.76 | 0.70 | 0.08 |
| | Ni | 0.29 | 0.66 | 0.73 |
| | Cu | 0.29 | 0.76 | -0.20 |
| | Zn | -0.04 | 0.50 | -0.30 |
| | As | -0.33 | 0.59 | 0.10 |
| | Rb | -0.31 | 0.50 | 0.22 |
| | Mo | -0.26 | 0.49 | 0.23 |
| | Rh | 0.29 | 0.08 | -0.02 |
| | Pd | 0.66 | -0.28 | 0.06 |
| | Sb | -0.05 | 0.29 | 0.04 |
| | Ba | 0.05 | 0.57 | -0.04 |
| | Pb | -0.21 | -0.22 | 0.05 |
| | Cd | - | 0.60 | 0.11 |

3. ROS Comparison to Other Urban Areas

To put the intrinsic toxicity of ambient PM in Beirut in perspective, the mass-normalized ROS-activity of PM at the urban background site was compared to that of PM collected from a variety of worldwide urban settings, as shown in Figure 3.7. This comparison was possible because the same macrophage-ROS bioassay was applied to PM samples collected in these studies^{111,113,114,117}. For consistency with the current work, the comparison was based on average intrinsic ROS-activity of samples (i.e. PM mass-normalized) collected during the same sampling period (July-August). The mass-based ROS-activity measured in ambient PM_{10-2.5} in Beirut is comparable (0.7 times) to

the activity of coarse particles in the LA basin¹¹¹. On the other hand, the intrinsic PM_{0.25}-associated ROS-activity at the background location in Beirut is 2.3-fold greater than that measured at an urban site in LA. While organic matter could play a key role in ROS generation/regulation¹¹⁹, the observed contrast in ROS-activity is generally consistent with the differences in concentrations and mix of transition metals and trace elements among the two sites⁶². The very strong correlation of ROS-activity with Ni in this study was not evident at the urban background site in LA. The greater average levels and mass fraction of water-soluble Ni (2.4- and 1.4-fold, respectively) in urban Beirut likely contribute to the observed correlation. In PM_{2.5}, the intrinsic ROS-activity measured for ambient particles in Beirut is comparable to that reported for PM in Milan, Italy (1.2 times) and, impressively, 3.6-fold greater than the activity of PM in Lahore, Pakistan, one of the most heavily polluted cities globally¹¹³. The difference in ROS values with Lahore is likely due to the dissimilarity in PM sources. PM_{2.5}-induced ROS-activity was related to tracers of re-suspended soil (Ce, Mn) and industrial metallurgical processes (Cd) in Lahore¹²⁰.

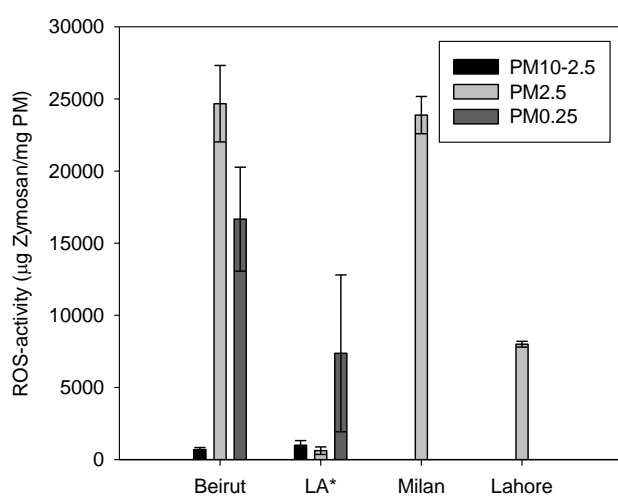


Figure 3.7. Comparison of average intrinsic reactive oxygen species (ROS)-activity (μg Zymosan/mg PM) of PM_{10-2.5}, PM_{2.5} and PM_{0.25} in Beirut (current study) with data from

Los Angeles (LA), Milan and Lahore during July-August. Error bars represent one standard error. **ROS-activity of ambient PM_{2.5} in LA corresponds to that of samples collected in October-November 2007 during and after wildfires.*

F. Summary and Conclusion

To determine the oxidative potential of ambient PM in the greater Beirut area, size-resolved PM_{10-2.5}, PM_{2.5-0.25} and PM_{0.25} samples were collected at near-freeway and urban background sites. At both locations, crustal elements, Ca, Mg, Fe, Al and Ti, generally displayed CEFs < 10, indicating their mainly soil dust origin. Conversely, transition metals and trace elements, comprising Mn, Cr, Cu, Zn, Ba, Mo, V, Ni and Sb, exhibited a stronger enrichment, particularly at the roadway, confirming their anthropogenic sources, such as combustion emissions and vehicular abrasion. These elements as well as Co, many of which are air toxics, were overall largely partitioned in PM_{2.5-0.25} and PM_{0.25}, with moderate-to-high water-solubility in these modes (> 30%). These physico-chemical characteristics may lead to increased adverse biological effects. Notably, road dust tracers, Mn and Co, were highly associated with PM_{10-2.5}-based ROS-activity. On the other hand, in PM_{2.5-0.25}, vehicular-abrasion element Cu and road dust tracer Co were potential ROS-active species. In PM_{0.25}, fuel combustion elements, V and Ni, had the highest correlation with ROS generation. At both sampling sites, ROS-activity reached a minimum in the coarse mode. While size-resolved PM intrinsic ROS-activity was overall comparable at both locations, volume-based ROS-activity was 1.4-2.6 fold greater at the roadway than background location. This trend indicates that exposure to redox-active PM species is greatest near the freeway. In comparison to other worldwide settings, although the intrinsic redox activity of PM_{10-2.5} in Beirut is comparable to that measured at an urban site in LA, its PM_{0.25}-induced ROS-activity is

roughly 2.5-times greater. In addition, the intrinsic ROS-activity of PM_{2.5} in Beirut is fairly comparable to that in Milan, but 3.6-fold greater than that in the heavily polluted city of Lahore.

CHAPTER IV

DUST EPISODES AND THEIR EFFECT ON THE REDOX ACTIVITY OF COARSE AND FINE PARTICLES IN AN EAST MEDITERRANEAN CITY

The following chapter is based on the following study:

Malek Jaafar, Rima Baalbaki, Nancy Daher, Alan Shihadeh, Constantinos Sioutas, Najat A. Saliba, 2014. Dust Episodes in Beirut and their effect on the chemical composition of size-resolved particulate matter. Under Review.

Introduction

Several studies have been published over the years concerning the adverse health effects of airborne particulate matter (PM) ^{9,121-123}. Although the mechanism by which PM affects biological systems is not completely understood, many studies link the pro-oxidative and pro-inflammatory effects of PM exposure to the increased PM-catalyzed formation of reactive oxygen species (ROS) within affected cells ^{10-12,124}. Reactive oxygen species are a collective term that includes oxygen radicals and some non-radical oxidizing agents such as hydrogen peroxide ¹²⁵. They are formed normally in cells and are used for cellular activities ¹⁴, but at high levels they are associated with inflammation and apoptosis ¹⁵.

Various cell-based and cell-free methods are used to quantify the oxidative potential of PM. The macrophage-based ROS (m-ROS) assay is one of the cell-based method while Dithiothreitol (DTT) is the commonly used cell-free method (i.e. ^{10,126,127}) mainly because DTT shares a similar structure to glutathione, an anti-oxidant present in cells ¹²⁸ and can therefore mimic cell-like activity towards certain ROS ¹²⁹. Additionally,

because the redox potential of PM is dependent on its composition, it is expected that variations in the sources affecting PM composition could cause a change in redox potential. Dusty days are events where PM composition changes¹³⁰ and therefore are prime candidate to study the effect of this change on the PM oxidative capacity. Many epidemiological and biological studies have associated morbidity to dust exposure (i.e. ¹³¹⁻¹³⁶). Of the PM components that vary substantially during dust episodes are organics, transition metals and mineral oxides^{137,138}, all of which have been shown to play a role in increasing PM redox activity^{10,139-143}. Yet, in a recent study conducted by Reche et al. (2012), it was shown that the redox activity of PM was not only associated to specific transition metals but rather it is linked to bioavailability and oxidation state¹⁴⁴ of the chemical components. The findings also indicated that the particle size is the main controlling factor of the aerosols toxicity in the city of Barcelona with urban sources being responsible for PM health effect variations.

In this study, the mass concentrations, chemical composition and particle toxicity are determined for coarse and fine PM collected during both dust and non-dust episodes in Beirut, Lebanon. Beirut is an east Mediterranean city, periodically subjected to dust storms originating from North Africa and the Arabian Peninsula^{137,138,145}. It provides an opportunity to observe the effects of compositional differences on PM oxidative capacity. The redox potential for PM was quantified using a cell-based assay (m-ROS) and a cell-free assay (DTT assay). The differences between the two episodes are analyzed.

G. Methodology

1. Sample Collection

Size-segregated PM samples were collected at the rooftop of the Chemistry department at the American University of Beirut (AUB), an urban background site located 33°90'N, 35°50'E at an elevation of 20 m above ground and 50 m above sea level. From the south this site is surrounded by a green area with the nearest street located about 150 m away¹³⁷. From the north, it overlooks the Mediterranean Sea, separated by a two-lane road which is congested during morning and afternoon rush hours. From the Eastern side resides the Beirut harbor within a distance of 2.5 km away. Particle levels at the site are commonly influenced by sea and land breeze circulation^{26,146}.

The sampling campaign was conducted on dust and non-dust episodes during summer and fall of 2012. Dust episodes were identified based on forecasting air mass trajectories using daily forecast-trajectories calculated by the HYSPLIT model¹⁴⁷ and relying on visual visibility limits and sky color. Those episodes were further confirmed using BSC-/DREAM dust maps (<http://www.bsc.es/projects/earthscience/DREAM/>). However, the residence time of transported dust particles is dependent upon the removal mechanism, with residence times varying from few hours to 10 days^{130,148,149}.

Moreover, if dust air masses are transported at high altitudes, they may affect ground level PM concentrations up to 2 days after an episode ends¹⁵⁰. Therefore, in this study, dust episodes include days during which air mass trajectories were coming from the desert, and subsequent days where transported dust remnants possibly remain. During the campaign, four dust episodes were identified, for which six samples were collected (Table 4.1).

Table 4.1. Dust-rich sampling episodes dates

| Dust episodes | 1 | 2 | 3 | 4 | | |
|----------------|--------------------|----------------------|------------------------------|-----------|-------------------|-------------|
| Sampling dates | Oct 3 - 4 | Oct 22 - 24 | Oct 31 - Nov 2 | Nov 2 - 4 | Nov 19 - 21 | Nov 21 - 23 |
| Episode Type | Arabian Remnant | Saharan - Arabian | Arabian + Saharan Remnant | | Saharan - Arabian | |

Coarse ($PM_{10-2.5}$), accumulation ($PM_{2.5-0.25}$) and quasi-Ultrafine ($PM_{0.25}$) size-fractionated particles were collected using three parallel Sioutas Personal Cascade Impactor Samplers (Sioutas PCIS, SKC Inc., Eighty Four, PA, USA, ³¹ preceded by PM_{10} inlets (Chemcomb Model 3500 Speciation Sampling Cartridge) and operating at a flow rate of $9 \text{ L}\cdot\text{min}^{-1}$. For the chemical analysis, two PCISs were loaded with Teflon filters (Pall Life Sciences, Ann Arbor, MI) and the third PCIS was loaded with quartz microfiber filters (Whatman International Ltd, Maidstone, England).

2. Sample Analysis

To determine PM mass concentration, Teflon filters were pre and post-weighed using a UMX2 microbalance (Mettler Toledo GmbH, CH-8606 Greifensee, Switzerland), following 24 h equilibration under controlled temperature and relative humidity conditions ($22\text{--}24^\circ\text{C}$ and $40\text{--}50\%$, respectively). The first set of Teflon filters was cut into 3 equal sections. The first section was analyzed for total elemental mass by means of a high resolution magnetic sector Inductively Coupled Plasma Mass Spectrometry (HR-ICP-MS Thermo-Finnigan Element 2) ¹⁵¹. The second section was extracted with high purity water and used to quantify PM concentrations of water soluble inorganic ions using ion chromatography (Model 2020i, Dionex Corp.). The

third section was also extracted with high purity water and analyzed for PM oxidative potential via the cell-based macrophage-ROS assay. The other set of Teflon filters was used to evaluate PM oxidative potential via the cell-free DTT assay.

Quartz filters, analyzed for Elemental Carbon, Organic Carbon and Water-Soluble Organic Carbon (EC, OC and WSOC, respectively), were prebaked at 550 °C for 12 h and stored in baked aluminum foil prior to sampling. Elemental and organic carbon contents of the filters were determined using the NIOSH Thermal Optical Transmission method¹⁵². Water-soluble organic carbon content was quantified using a Sievers 900 Total Organic Carbon Analyzer, following water-extraction and filtration of the samples¹⁵³.

3. *DTT and m-ROS Assays*

The DTT assay adopted in this study is the optimized procedure reported by Li et al. (2009). Yet, reports showed that methanol has a higher extraction efficiency than water^{154,155} and therefore was used as the solvent of extraction. Details about this assay's mode of action can be found in Kumagai et al.¹⁵⁶. Samples were extracted by sonication for 30 minutes, using 5-10 ml of methanol, depending on the mass loadings. Subsequently, a 200 µl aliquot of the solution was mixed with 1 ml phosphate buffer. Then 50 µl of 0.5 mM DTT was added, and the samples were incubated at 37°C. At the optimized designated times (0, 8, 12, 16 minutes) 50 µl of 1 mM 5,5'-dithiobis-(2-nitrobenzoic acid) (DTNB) was added to each vial. The yellow 2-nitro-5-thiobenzoate (TNB) solution was then measured, within 1 hour of the experiment completion, using a UV/VIS spectrophotometer (JASCO V-570 UV/VIS/NIR Spectrophotometer).

For the m-ROS assay, filters were extracted in 900 μL of water by agitation for 16 h. The extract was centrifuged at 6600 RPM for approximately 1 min; the supernatant was then passed through 0.22 μm polypropylene filters. The PM suspension was mixed with 2',7'-dichlorodihydrofluorescein diacetate (DCFH-DA) and added to rat alveolar macrophage cells. DCFH-DA, produces the non-fluorescent 2',7'-dichlorodihydrofluorescein (DCFH) upon entering the cells. DCFH is then converted by ROS into the fluorescent 2,7-dichlorofluorescein.⁹³

4. Chemical Mass Closure

For the purpose of chemical speciation, chemical components were classified into six categories: organic matter (OM), elemental carbon (EC), sea salt (SS), crustal material (CM), trace elements (TE) and secondary ions (SI). Organic matter was calculated by multiplying organic carbon (OC) by a factor of 2.1 in order to account for aged particles as recommended by several earlier studies¹⁵⁷⁻¹⁶⁰. Sea salt was estimated as the sum of Na^+ concentration and sea-salt fractions of Cl^- , Mg^{2+} , K^+ , Ca^{2+} , and SO_4^{2-} concentrations, assuming standard sea-water composition¹⁶¹. Crustal material includes typical crustal material elements (Al, K, Fe, Ca, Mg, Ti and Si) and was determined by summing the oxides of these metals using equation (4.1) with Ca and Mg representing their non-sea-salt fractions.⁴⁰⁻⁴² Calcium was multiplied by a factor of 1.95 to account for both CaO and CaCO_3 ¹⁶². Silicon, which was not measured in this study, it was calculated by multiplying Al by a factor of 3.41⁴¹. Trace Elements containing other measured elements such as Cu, Zn, V, Mn, Cr, Sb...were determined by multiplying the concentrations of these elements by appropriate factors to convert them to their mineral oxides.

$$CM = 1.89Al + 1.4K + 1.43Fe + 1.95Ca + 1.66Mg + 1.67Ti + 2.14Si \quad (4.1)$$

5. Particle Size Distribution

Particle number concentrations were measured using the Grimm EDM 365 system (GRIMM Aerosol Technik GmbH & Co. KG) deployed at the same site but at ground level. The system operates based on laser light scattering in 31 size channels ranging between 0.265 and 34 μm . Measurements are made every 6 s at a diode laser wavelength of 655 nm and particle count data were logged every 1 min.

H. Results and Discussion

Concerning the dust samples coarse and fine (accumulation and quasi-ultrafine filters) size fractions were considered for analysis. Results were compared to those of non-dust episodes sampled during July and August, 2012^{143,163}. Because the fine fraction consisted of the sum of the accumulation and quasi-ultrafine filters, only the non-dust days that were not composited during analysis were considered.

1. Particle Size Distribution

PM mass concentrations for the dust episodes ranged between 10 and 53 $\mu\text{g}\cdot\text{m}^{-3}$ for the coarse mode and between 21 and 39 $\mu\text{g}\cdot\text{m}^{-3}$ for the fine fraction. In comparison to the non-dust episodes, the coarse PM mass concentration increased by 48.5% while that of the fine increased only by 14.6%, on average (Figure 4.1). This is in agreement with other studies showing that desert dust intrusion has a larger effect on the increase of the mass concentration of the coarse mode^{137,164-166}.

Particle number and volume distributions for both dust and non-dust days are shown in Figure 4.1. Similar particle number distribution patterns were observed during both dust and non-dust days. Nevertheless, particle number concentrations for dust days display an increase over non-dust days for all particle size bins averaging at a 146% increase in particle total counts. It is important to note that the particle volume distribution showed an increase in all particle size bins between dust and non-dust episodes. This increase was mostly noticed for particles ranging in sizes between 2.25 and 5 μm .

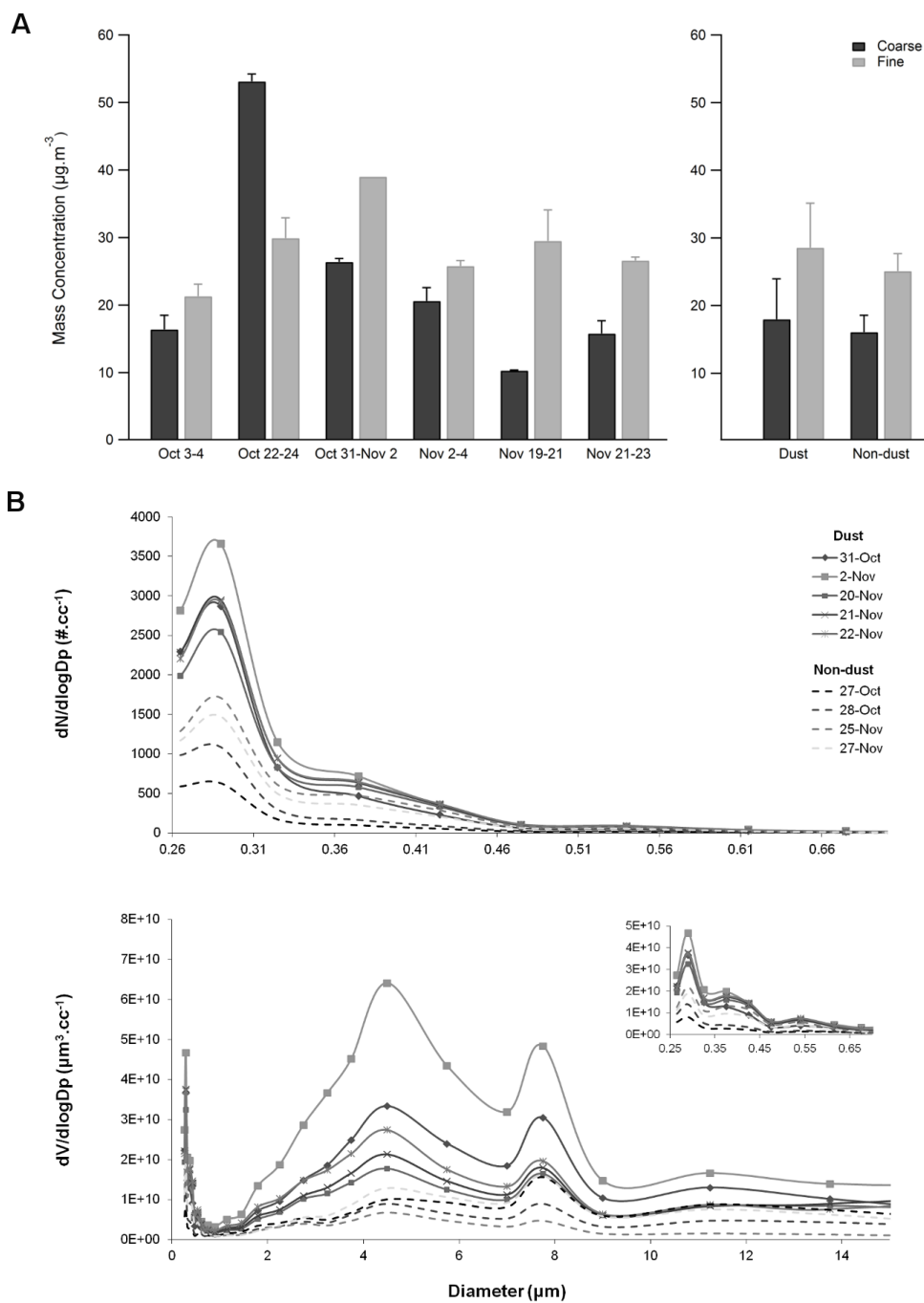


Figure 4.1. Size-fractionated particle mass concentration during dust episodes (upper left). Associated error bars represent the standard deviation of the gravimetric analysis of the two parallel Teflon filters. Average particle mass concentration during dust episodes compared to non-dust episodes (upper right) Number (a) and volume size distribution (b) of particles with mean geometric diameter ranging between 0.265 and 15 μm during dust and non-dust episodes (bottom).

2. *Chemical Mass Closure*

Almost full chemical mass closure is attained for fine PM of both dust (94%) and non-dust episodes (102%) whereas identified coarse aerosol components accounted for 70 and 72 % of the mass during dust and non-dust episodes, respectively. Unidentified PM mass is usually attributed to PM water content, where water is reported to constitute up to 35 % of PM₁₀ mass¹⁶⁷⁻¹⁶⁹ and/or to an underestimation in the factor used for the calculation of CM or OM (Figure 4.2). Relative to mass contribution, CM dominated the dust and non-dust coarse PM fraction with 47 % increase in PM composition of CM during dust events (39 ± 15 % and 26 ± 16 % contribution to the total mass, respectively). Coarse CM measured at six European cities contributed between 28 and 65 % of PM mass⁵⁰. Sea salt and secondary ions were the second most abundant elements.

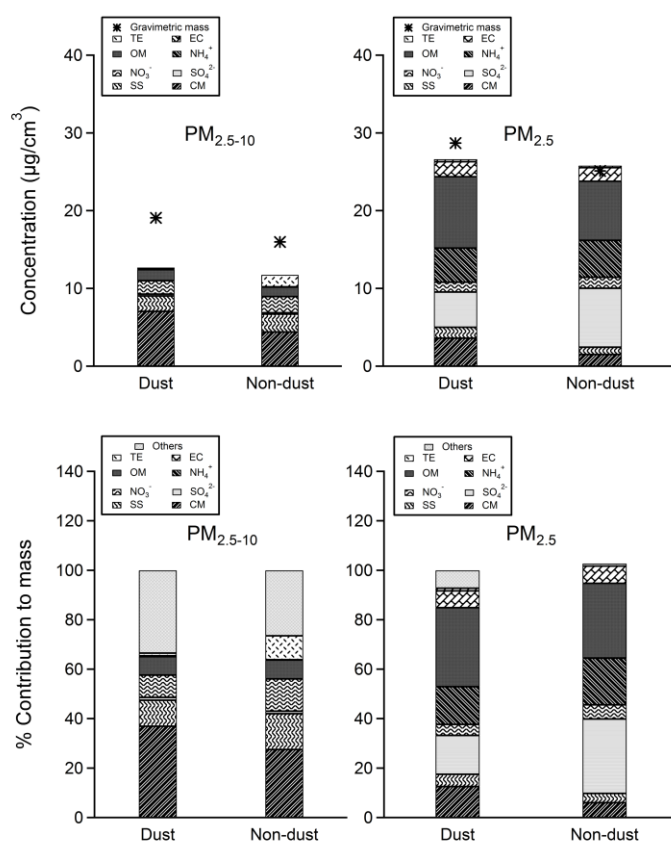


Figure 4.2. Average chemical composition of coarse and fine PM in comparison to the total gravimetric mass represented by * (upper graph), and % contribution of the different chemical components to the total mass of coarse and fine PM (lower graph) during dust and non-dust events. Please note that Oct 22-24 dust coarse PM filter was not included in the chemical analysis because it was overloaded.

Sea Salt accounted for 11 ± 10 % of the dust coarse fraction and 15 ± 6 % of the non-dust coarse fraction, while SI accounted for 11 ± 7 % and 14 ± 4 % of the dust and non-dust coarse fractions, respectively. This calculates almost a 20% decrease in both SS and SI. The coarse PM percent composition of OM was similar during both dust (8 ± 1 %) and non-dust (8 ± 1 %) episodes. Notably and despite the small contribution of TE to the total mass of the coarse fraction, the difference between dust and non-dust episodes was substantial with 1 ± 1 % in coarse dust versus 10 ± 18 % in the non-dust samples. Finally, EC was the least abundant element in both dust and non-

dust coarse samples accounting for 0.3 ± 0.2 and 0.2 ± 0.1 %, respectively. Elemental carbon contribution to coarse PM in this study is substantially lower than that measured in European cities where EC accounts between 0.96 and 5.5% of the PM mass⁵⁰

In the fine fraction, SI contribution to the total mass was substantially higher during non-dust episodes (53 ± 14 %) when compared to the dust episodes (36 ± 14 %) accounting for a 33 % decrease in SI contribution to fine PM mass. Nevertheless, SI was the most abundant PM constituent during both episodes. The second most abundant species is OM contributing 33 ± 7 % and 31 ± 12 % in the dust and non-dust fine mode, respectively. These results are in good agreement with other studies showing SI and OM as the main components of fine PM^{50,162}. Crustal material constituted 13 ± 2 % and 6 ± 4 % of fine PM mass during dust and non-dust episodes, respectively, implying a 107 % increase in CM contribution to fine PM mass during dust episodes. Elemental carbon had similar percentages during both episodes (7 ± 2). TE constituted around 1% of the fine PM mass during both events, while SS constituted 5 and 4 % of the dust and non-dust fine PM, respectively%.

3. Dust Versus Non-Dust Chemical Composition

As shown in Figure 4.2, dust episodes were accompanied by 60% and 107 % increase in CM concentrations in coarse and fine fractions, respectively. Enrichment of fine particles with crustal materials is highly characteristic of dust episodes and has been the subject of several studies^{170,171}. The water soluble nitrates were more abundant in non-dust coarse and fine PMs indicating the predominance of sodium and potassium nitrates due to the reaction of sea salt with nitric acid. Furthermore, higher soluble

fractions of sulfur in non-dust episodes reflected by the Sulfate/Sulfur ratios ($SO_4/total\ S = 2.5$ in dust and 3.1 in non-dust coarse and 2.8 and 3.5 in dust and non-dust fine, respectively) eluted to the association of sulfate with soluble cations in coarse and ammonium in fine particles. As for the variation in trace elements (Figure 4.3), the increase of Mn and P in the coarse fraction has been related to the chemical composition of African mineral dust¹⁷²⁻¹⁷⁴. Elements like Ni, Zn, Pb and Cu, which are mainly of anthropogenic sources, show higher concentrations in coarse mode during non-dust events than those observed for dust events. On the other hand, Cr and V are due to mixed biogenic and anthropogenic origins. Therefore, their enhancement in the coarse fraction is attributed to crustal material whereas, in the fine mode, it is due to dust transport episodes¹⁷⁴.

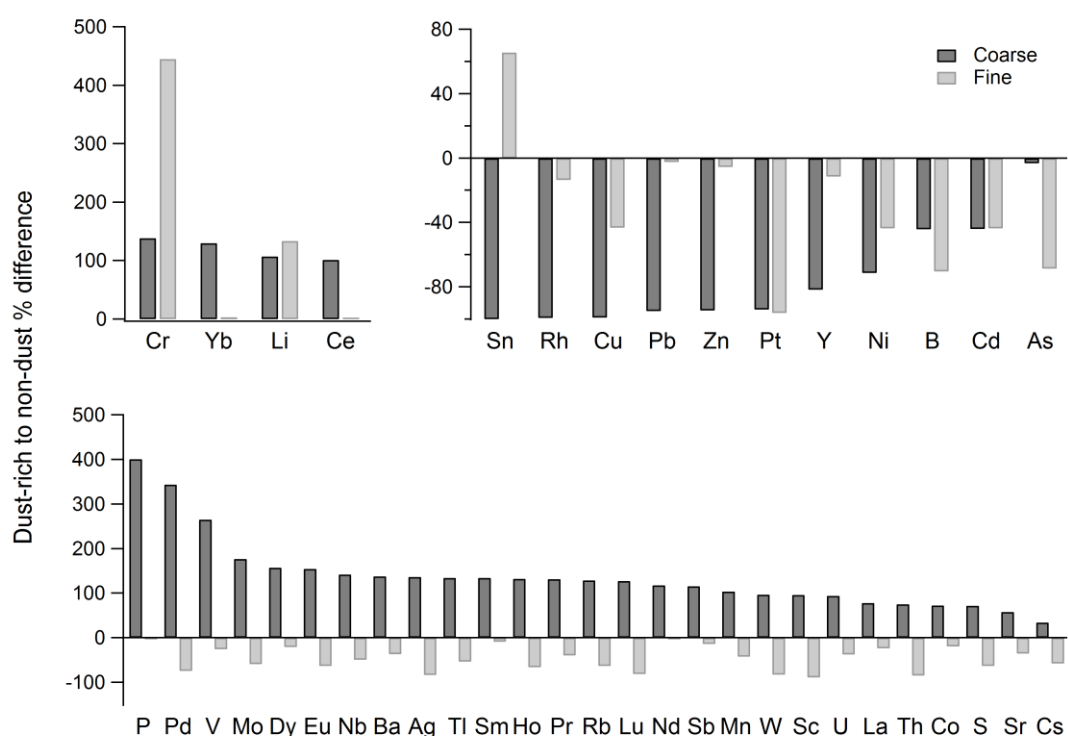


Figure 4.3. Size-segregated dust to non-dust percent difference of different elements.

4. DTT and m-ROS assays

DTT and m-ROS assays, both display a higher redox activity in the fine mode, when compared to the coarse mode during non-dust episodes (Fig. 4.4a-b)^{10,11,175,176}.

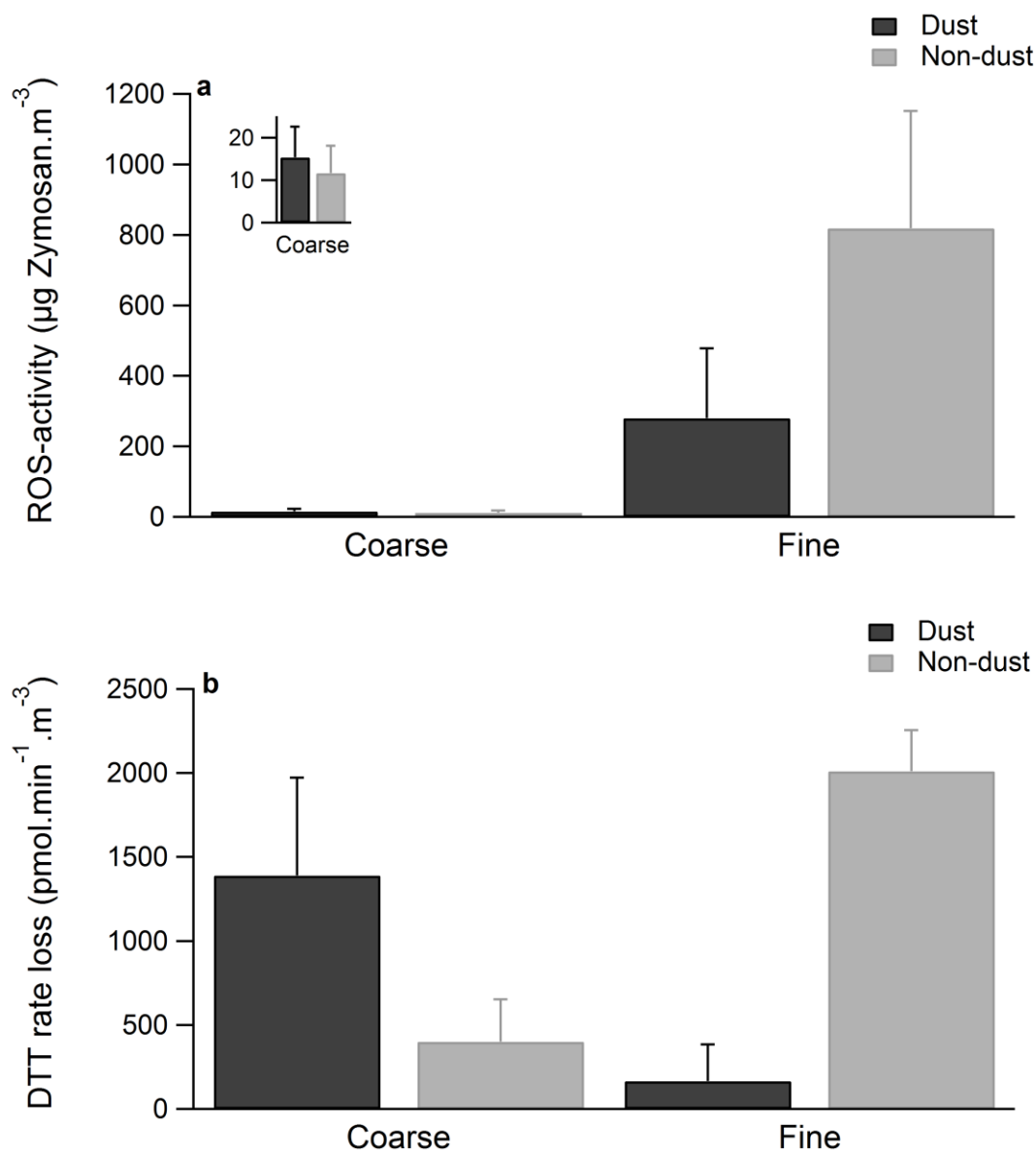


Figure 4.4a-b. Size-segregated dust-rich to normal ROS activity using: a) m-ROS and b) DTT assays. Error bars correspond to one standard error.

When considering dust episodes, the m-ROS assay shows lower activity in the coarse mode compared to the fine mode, while the DTT assay shows higher activity. This discrepancy could be attributed to the extraction solvent, considering that water was used for the m-ROS assay whereas methanol was used for the DTT assay. Reports state that methanol-extracted samples show generally higher redox activity, mainly because methanol extracts more effectively both water-soluble and water-insoluble species^{155 143}. Another reason could be the increase in the coarse mass loadings in the dust samples since the sensitivity of DTT assay may be mass-dependent¹²⁹. Nonetheless, both methods show an increase in the dust to non-dust percent difference for the coarse mode, and a decrease for the fine PM mode. Despite this, the overall PM₁₀ redox potential between dust and non-dust episodes decreased by 64.4 and 35.6% for the m-ROS and DTT assays respectively. This indicates that local pollutants during non-dust episodes are of more significance to ROS generation than long range transported particles. This is in line with the finding of Reche et al¹⁷⁷ showing that local pollutant sources are the main contributor to PM health effects.

5. Correlation of Redox activity with PM chemical components

In order to correlate the chemical components to both assays, statistical analysis between the ROS assays and different chemical components was conducted (Table 4.2). In the coarse fraction, the high correlations between m-ROS-activity and OC (R=0.88, p < 0.05) on one hand and m-ROS and different trace elements (Table 4.2) on the other are in agreement with the reported studies^{115,175,178,179}. Elements like V, Co, and Ni are known to participate in the Fenton chemistry and are able to produce ROS when in contacts with biological cells¹⁸⁰. In the Fine fraction, the correlation of the m-

ROS assay with OC ($R=0.72$, $p < 0.05$) can be attributed to the high correlation of these components with WSOC¹⁰. WSOC which are shown to have a good correlation with the m-ROS assay¹⁸¹, are thought to contribute to OH radical formation through secondary organic compound¹¹⁵.

Similarly, DTT rate loss was found to correlate with WSOC in the coarse fraction ($R=0.65$, $p < 0.05$) in conformity with other studies^{115,175,179,182}. It is suggested that the solubility of organic compounds is directly related to free radical generation¹¹⁵.

Furthermore, high correlation between DTT assay and trace elements in both size fractions is also observed^{115,139}. In particular, the correlation with some rare earth metals like (Eu, Dy, Ho...) could be ascribed to the presence of monazites which can be found in Sarahan sand¹⁸³. The fine fraction, CM also correlates ($R=0.82$, $p < 0.05$). Up to the authors' knowledge, there are no recent studies about the redox activity of biogenic mineral oxides which warrants further investigation.

Table 4.2. Spearman correlation coefficient (R) for different components with redox activity from both assays ($p < 0.05$)

| | m-ROS | | DTT | |
|------------------------------|-------------|-------------|-------------|-------------|
| | Coarse | Fine | Coarse | Fine |
| Mass | 0.97 | -0.08 | 0.22 | 0.89 |
| OC | 0.88 | 0.72 | -0.36 | -0.92 |
| EC | 0.86 | 0.04 | -0.28 | -0.62 |
| WSOC | 0.31 | 0.58 | 0.65 | -0.98 |
| Cl ⁻ | -0.10 | -0.07 | 0.94 | 0.10 |
| Nitrate | -0.34 | 0.09 | 0.69 | -0.65 |
| Phosphate | - | 0.77 | - | -0.30 |
| Sulfate | -0.07 | -0.38 | 0.82 | 0.05 |
| Na ⁺ | -0.43 | 0.24 | 0.76 | -0.04 |
| K ⁺ | -0.59 | 0.68 | 0.98 | -0.75 |
| NH ₄ ⁺ | -0.75 | 0.54 | -0.58 | -0.74 |
| Sea Salt | -0.43 | -0.21 | 0.76 | 0.05 |
| nss sulfate | 0.12 | -0.41 | 0.58 | 0.05 |
| Si | -0.26 | -0.09 | 0.67 | -0.37 |
| Li | 0.18 | 0.03 | 0.88 | 0.52 |
| B | -0.57 | 0.68 | 0.23 | -0.89 |
| Mg | -0.13 | -0.34 | 0.58 | 0.70 |
| Al | 0.54 | -0.22 | 0.83 | 0.68 |
| P | 0.63 | 0.34 | -0.52 | -0.79 |
| K | -0.10 | 0.71 | 0.70 | -0.30 |
| Sc | 0.47 | -0.43 | 0.73 | 0.82 |
| Ti | 0.07 | 0.10 | 0.55 | 0.41 |
| V | 0.77 | 0.37 | -0.48 | -0.93 |
| Mn | -0.03 | 0.37 | 0.53 | -0.08 |
| Fe | 0.28 | 0.14 | 0.45 | 0.39 |
| Co | 0.56 | -0.11 | -0.66 | -0.50 |
| Ni | 0.51 | 0.31 | -0.53 | -0.91 |
| Zn | 0.99 | 0.37 | 0.01 | -0.91 |
| Cd | -0.34 | 0.66 | -0.86 | -0.90 |
| Cs | -0.07 | 0.49 | 0.66 | -0.03 |
| Nd | 0.28 | -0.19 | 0.83 | 0.57 |
| Eu | 0.10 | -0.41 | 0.52 | 0.97 |
| Dy | 0.39 | -0.41 | 0.71 | 0.80 |
| Ho | -0.09 | -0.59 | 0.64 | 0.81 |
| W | 0.77 | -0.03 | -0.44 | -0.49 |
| Crustal Material | 0.03 | -0.50 | 0.56 | 0.82 |

I. Summary and Conclusions

The mass closure of PMs during dust and non-dust episodes were successfully constructed with an unidentified percentage averaged at 0 and 30 % for fine and coarse fractions, respectively. The major aerosol speciation considered in this study included OM, EC, SS, SI, CM and TE. During dust episodes, both coarse and fine PM number and mass concentration increased with respect to non-dust episodes. Crustal material PM composition increased in both coarse (47 %) and fine (107 %) fractions while the secondary ions and sea salt contribution to PM mass decreased. Elemental carbon and trace element PM mass concentrations only change in the coarse PM. The corresponding ROS activity of size-segregated dust and non-dust PM samples, which was measured using the DTT and m-ROS assays, showed an increase in the activity for the coarse PM fraction and a decrease for the fine fraction during dust episodes. The relative variation in the redox activity in both fractions can be the result of changes in chemical composition, particularly in trace elements, crustal materials and organic matter. Correlation factors show that both assays are affected by different trace elements. However, when assessing the overall redox activity of PM₁₀ in dust and non-dust episodes, it is shown that PM₁₀ redox activity in Beirut mainly depends on the local sources with higher activities observed during non-dust episodes.

CHAPTER V

THE EFFECT OF METAL OXIDE NANOPARTICLES ON THE DTT ASSAY

A. Introduction

Nanoparticles are generally defined as particles with a diameter ranging between 100 nm and 1 nm¹⁸⁴. Their unique properties make them highly desired in different sectors¹⁸⁵ and therefore they are being engineered to the required size in large scales, with the nanotechnology industry expected to be a one trillion dollar enterprise by 2015^{186,187}. Many nanoparticles are used in countless products including toothpastes, cosmetics, electronics, food products and even used for drug delivery^{188,189}. Therefore, the common routes that one can be exposed to these nanoparticles are: oral, dermal, inhalation and injection¹⁹⁰. In many recent studies, the safety of nanoparticle exposure is being questioned^{186,191-199}. Depending on their nature, these nanoparticles can either cause oxidative stress on the cells, which can lead to unique inflammations, or have no effect^{186,191,194,197,200-205}. Cho et al.¹⁹⁴ show that CeO₂, NiO, ZnO and CuO nanoparticles can induce different inflammatory footprints both acutely and chronically. Hull et al.²⁰⁶ and Sano et al.²⁰⁷ show that chronic nanoparticle exposure can even cause pneumoconiosis. Other than the engineered nanoparticles, there are nanoparticles found in atmosphere from both anthropogenic (air pollutants) and biogenic (mineral dust), which one can be exposed to. Studies show that particulate matter (PM) of different sizes, coarse (2.5 µm – 10 µm in diameter), fine (0.25 µm – 2.5 µm) and quasi-ultrafine (0.25 µm and below), can induce oxidative stress, with quasi-ultrafine PM having the greatest effect^{10,11,175,176,208}

Since the amount of nanoparticles in general is huge, Nel et al.¹⁸⁶ suggest that it is important to establish a toxicity screening method. For such purpose, Oberdorster et al.¹⁹⁰ propose three key elements: Physicochemical characterization, *in vivo* assays and cellular and acellular *in vitro assays*. Concerning the physicochemical characterization, what little information is available suggest that there is a relationship between the toxicity of the nanoparticle and their physicochemical parameters (size distribution, surface area, porosity, shape, agglomeration state, chemical composition...). *In vivo* assays, on the other hand, can provide a complete characterization of the nanoparticles tested, and a complete risk assessment. While *In vitro* assays, whether cellular or acellular, allow the isolation of specific pathways to be tested under controlled conditions, they do have some drawbacks, like dosimetry mismatch and non-involvement of the complete inflammatory response¹⁹⁰. When assessing the toxicity of nanoparticles and their biological activities, many agree that the parameter to rely on is the ability of these particles to generate oxidative stress, whether directly or indirectly^{202,209-211}. Many methods have been suggested for assessing the redox ability of different nanoparticles (ambient particulate matter and engineered nanoparticles). While some of these methods are cellular assays like MTT method, LDH leakage, respiratory burst^{191,195,201,212}, others are predictive and need to be accompanied with a cytotoxic assay to validate the results. The analysis of the conduction band energy levels of the nanoparticles in relation to the cellular redox potential is one of these methods, if the conduction band overlaps with the cellular redox potential, then this nanoparticle can induce oxidative stress. Yet this method failed when it comes to some nanoparticle metal oxides like CuO and ZnO, where although their conduction bands don't overlap with the cellular redox potential, they can still induce oxidative stress^{192,193,199}. Another

type is the acellular assays, like the electron spin resonance^{213,214} or the more common assays dithiothreitol (DTT) and dichlorofluorescin (DCFH)^{10,11,15,113,115,127,129,134,139,154,177,179,208,215}. This study will focus on the DTT assay, a colorimetric assay that relies on the depletion of DTT. DTT shares a similar structure to glutathione, an anti-oxidant present in the cells¹²⁸ and can thus mimic cell-like activity towards certain ROS²¹⁶. This assay depends on the oxidation of DTT to its disulfide form by the redox-active material present in the PM sample. These redox-active species can then donate an electron to the dissolved molecular oxygen, to form superoxide¹⁵⁶ which can later form other reactive oxygen species. The rate of electron transfer is proportional to the concentration of the catalytically redox-active species in the PM samples and can be monitored by the rate at which DTT is consumed. The rate loss of DTT is, therefore, an indication of the amount of ROS present in a sample (the greater the loss, the higher the ROS levels). In this study the redox activity of different metal oxide nanoparticles is measured using the DTT assay. The DTT rate loss obtained are normalized to the size and surface area of the individual nanoparticles, in order to assess the effect of different physicochemical parameters on the redox activity. The size of the particles was obtained by using the dynamic light scattering (DLS), and the required calculations were done to obtain the surface area. Additionally, Scanning Electron Microscope (SEM) was used to assess whether the morphology of the particles was playing a role on the redox activity.

B. Methodology

1. *Solution Preparation*

For this study, six metal oxide nanoparticles (MO) are chosen, Chromium

Oxide (Cr₂O₃), Copper II Oxide (CuO), Manganese Dioxide (MnO₂), Lead Oxide Yellow (PbO), Lead Oxide Red (Pb₂O₃) and Zinc Oxide (ZnO). The MO solutions were prepared by dissolving the required mass in 20 mL methanol. In addition a 25 μM Copper II Chloride (CuCl₂) methanolic solution was prepared as a positive control for the DTT assay.

For size assessment and SEM imaging, three of the oxides mentioned above; CuO, Cr₂O₃ and MnO₂ were prepared by weighing 0.1 g of each MO and suspending them in 25 mL methanol.

2. DTT Assay

The DTT assay used in this study is the procedure optimized by Li et al. ¹²⁶, with a few adjustments. The original assay dictates taking a small aliquot of the samples or MO suspended solutions to run the assay on. Since the MO are insoluble, the aliquots taken were not homogenous and the results were not reproducible. For this reason the experiment had to be done on the original solution without the need to take out aliquots. Therefore, the volumes and concentrations of the DTT, 5,5'-dithiobis-(2-nitrobenzoic acid) (DTNB) and phosphate buffer had to be increased to account for the large volume samples. For optimization purposes, the new DTT assay method was run in parallel against the original method. CuCl₂, which is known to have DTT activity ¹³⁹, was run on both assays in triplicates. Figure 5.1 shows that both assays showed similar results, with the old method giving 53.73 ± 4.88 nmol DTT/min and the new method giving 64.05 ± 2.23 nmol DTT/min.

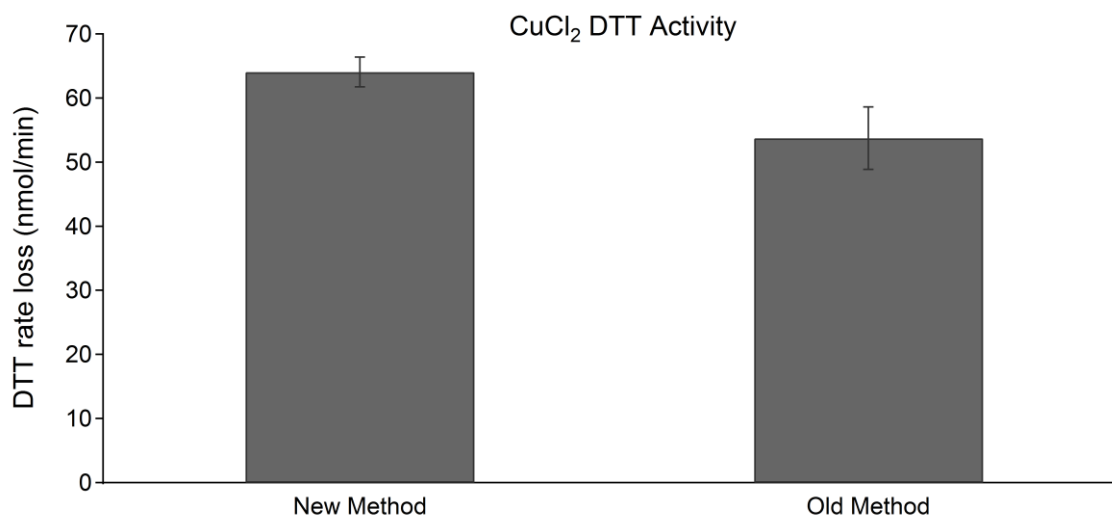


Figure 5.1. Controlled experiment, DTT rate loss for CuCl₂ on the New and Old DTT assay

Mineral Oxide suspended solutions were sonicated for 30 minutes, prior to the experiment. The solution was then mixed with 100 ml 0.1 M phosphate buffer, followed by the addition of 5 ml of 1 mM DTT. The mixture was placed in a water bath incubator/shaker (37°C, 180 rpm) throughout the experiment to insure homogeneity. At the optimized designated times, 1 ml of the mixture was taken out and added to 1 ml, 1.5 mM DTNB. The yellow 2-nitro-5-thiobenzoate (TNB) solution was measured within 1 hour of the experiment's completion using a UV/Vis spectrophotometer. All MO samples were run in triplicates.

3. DLS Experiment

The DLS (90Plus/BI-MAS) was used to assess the size of the MO. As with the DTT assay, the solutions were sonicated for 30 minutes before the experiment. 3 mL of each suspension was then placed in a glass cuvette and run on the machine. Each run lasted for 6 minutes and was repeated in triplicates.

4. SEM Imaging

The SEM (Tescan Model 51-XXM0010) was used for particle imaging. 10 μL of the MO solutions were placed on a carbon coated Aluminum stub, and placed in a vacuum oven overnight. Voltage set at 20-30 KeV with 60 μA beam current allowed the detection of good quality images without damaging the sample.

C. Results and Discussion

1. DTT Response for Metal Oxide Nanoparticles

In addition to the mineral oxides chosen, CuCl_2 was chosen as a positive control, since it was shown to have an effect on the DTT assay¹³⁹(Charrier et al. 2012). For the MO, as shown in Figure 5.2.

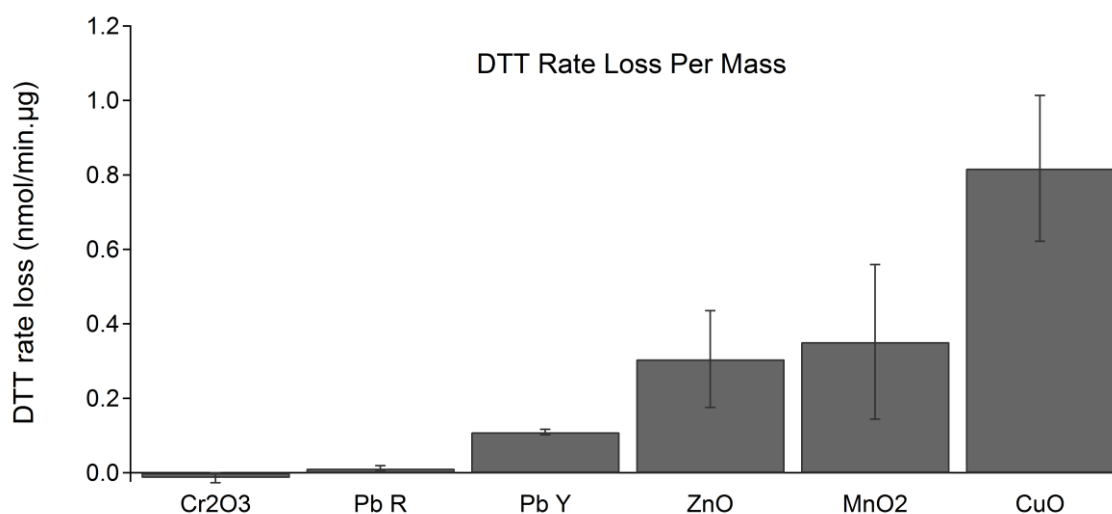


Figure 5.2. DTT rate loss for metal oxide nanoparticles (normalized to mass).

CuO showed the highest redox activity ($0.818 \text{ nmol DTT/ min} \times \mu\text{g} \pm 0.196$) followed by MnO_2 and ZnO (0.352 ± 0.208 and $0.305 \pm 0.130 \text{ nmol DTT/ min} \times \mu\text{g}$, respectively). PbO , Pb_2O_3 also showed DTT activity (0.110 ± 0.007 and 0.012 ± 0.007

nmol DTT/ min x μg , respectively). On the other hand both Cr_2O_3 showed no reactivity (-0.013 ± 0.013 nmol DTT/ min x μg).

Up to the author's knowledge, apart from lead oxide²¹⁷, there are no literature values for the reactivity of DTT and MO chosen. Yet there are studies about MO and their abilities to form ROS. In these studies the ability of these MO to produce ROS is tested on different cellular assays (MTT assay, LDH Leakage...) ^{191,195,201,212}. Although the DTT assay and other cellular assays have different mode of actions ¹¹⁵, many studies have shown that DTT can mimic cell-like response when it comes to redox activity^{11,129,154,179}. This comes from the structural similarities between DTT and glutathione, an antioxidant found in the cells ¹²⁸.

As for the ability of MO to produce ROS, each oxide is thought to have its own mode of action ¹⁹⁴. Concerning CuO and ZnO¹⁹⁸, it is stated that their ability to generate ROS is due to their slight solubility. Both CuO and ZnO are able to release Cu and Zn ions respectively through particle dissolution, which could increase their redox activity ^{194,198,199,217}. ICP-MS data done by Zhang et al. ¹⁹⁹ show that both ions dissolved by around 10%. Both ions are known to have an effect on the DTT assay ¹³⁹. In a separate study by Zhao et al. ²¹⁸, they propose a mechanism by which H_2O_2 can adsorb on MO surfaces and release free radicals when in solution. These free radicals can also play a role in the DTT assay ^{10,11,126,139,154,156}. Additionally Studies ^{217,219}, show that DTT can complex with oxides through its sulfur bonds, which would make the DTT unavailable to complete the assay (reaction with DTNB), which would lead to more DTT consumption. Uzu et al. ²¹⁷ show that DTT can also complex with solubilized ions released from the oxide when in solution (Figure 5.3). In their study they show that PbO can also dissolve to give Pb ions, which explains their activity in the DTT assay.

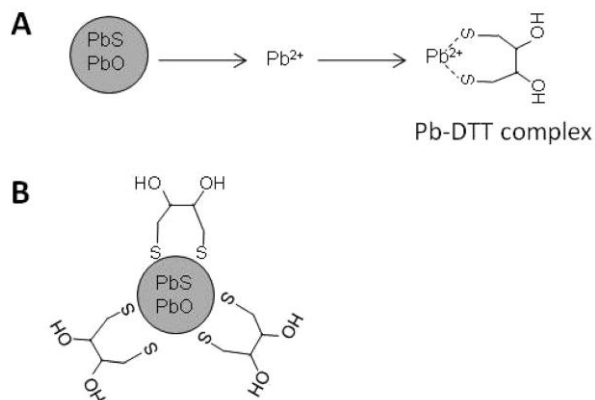


Figure 5.3. Potential mechanisms of DTT stabilization through complexation with solubilized lead (A) or PM surfaces (B) (Uzu et al. 2011)

As for MnO_2 , Lison et al.²²⁰, show that MnO_2 does have a redox activity and is able to induce oxidative stress when tested on LDH leakage test. Additionally, Burello and Worth^{192,193} showed that its band gap overlaps with the band gap of the cell. This study states that if the band gap of the MO overlaps with the band gap of the cell, then this MO is able to induce oxidative stress in the cells. This was further confirmed by Zhang et al²²¹, where they tested the redox potential of different MO that have a band gap overlapping with that of the cell using different cellular and cytotoxic assays. The theory of the band gap was proven to be good at predicting whether an MO can induce oxidative stress or not. Finally, concerning Cr_2O_3 , Burello and Worth^{192,193} and Zhang et al.²²¹ show that it has a band gap that overlaps with that of the cell and has the ability to cause oxidative stress in the cells, when tested using cytotoxic in vitro studies. Yet, it did not show any activity in the DTT assay. This discrepancy between the non-oxidative properties of Cr_2O_3 with the DTT assay and the in vitro cytotoxic assay could be due to cellular interactions with Cr_2O_3 and not its intrinsic oxidative properties.

D. Physicochemical Characteristics and Redox Activity

Since the MO are not soluble in methanol, any interaction between these MO and DTT should be to be heterogeneous. For this reason, the physicochemical properties of the MO might be a factor affecting their DTT redox reactivity. The physicochemical properties investigated in this study are the size (diameter), surface area and morphology. For the size and surface area, the DLS was used, whereas the SEM was used for morphology imaging. Three MOs of different DTT redox reactivity values were chosen for this test: CuO (high redox activity), MnO₂ (moderate redox activity) and Cr₂O₃ (no redox activity). The DTT rate loss values were normalized against particle diameter and particle surface area. The morphologies of the particles were studied to check whether there are any similarities between the morphologies of the particles that have similar DTT rate loss values.

a. Metal Oxide DTT Redox Activity with Respect to Particle Size

In order to assess whether, particle size is a controlling factor in the redox reactivity of the MO, the DTT rate loss values were normalized against the particle size obtained from the DLS. Table 5.1 shows the particle size in nm for the MO.

Table 5.1. MO Particle Size (nm)

| MO | Particle Diameter (nm) |
|--------------------------------|------------------------|
| CuO | 218.47 |
| MnO ₂ | 369.63 |
| Cr ₂ O ₃ | 376.89 |

Additionally, a strong negative correlation is observed between size and DTT redox activity ($R = -0.88$), CuO, which has the highest DTT redox activity, has the smallest size.

b. Metal Oxide DTT Redox Activity with Respect to Surface Area

When it comes to surface area and redox activity, many studies agree that the larger the surface area the higher the redox activity^{190,222-224}. Lison et al²²⁰ demonstrate that for MnO₂, particles with a 62 m²/g surface area had a higher response on the LDH leakage test than those with 17 m²/g. For surface area assessment, there are a number of analytical techniques that can be used. In this study, the DLS is used to calculate the surface areas of the mineral oxides based on particle mean diameter. A moderate correlation was observed between surface area and DTT redox activity ($R = 0.51$). This somewhat of a contradicting result could be due to a number of assumptions done when using the DLS, one being the assumption that the particles are solid spheres with no pores. Nonetheless, it is still good to show that there is some dependence of the DTT redox reactivity on the surface area.

i. Sample Calculation

The following is a sample for the calculations for the surface area for the different mineral oxides. In this example CuO is used.

Step One:

Density of CuO: 6.31 g/cm³ (Literature Value)

Mass: 0.001 g (Weighed)

Volume of Solution: 25 ml, Methanol

When this solution was run on the DLS, the average count rate was above the calibrated range (100 kcps), for this reason a fraction of the stock solution was taken.

Volume Taken: 0.25 ml

Assuming the sample is homogenous, the mass of the particles taken in the fraction was calculated:

$$\begin{aligned}
 0.001 \text{ g} &\rightarrow 25 \text{ ml} \\
 x &\rightarrow 2 \text{ ml} \\
 x &= \frac{(0.001)(2)(1000)}{25} = 0.01 \text{ mg}
 \end{aligned}$$

Then the volume of the mineral oxides was calculated:

$$d = \frac{m}{v} \rightarrow v = \frac{m}{d} = \frac{0.01 \times 10^{-3}}{6.31} = 1.58 \times 10^{-6} \text{ cm}^3 \text{ or } 1.58 \times 10^{-6} \text{ ml}$$

Step Two:

The DLS report gives the cumulative percentage for the size bins, from the cumulative percentage find the percentage of each size bin:

Cumulative Percentage = Percentage of Size Bin 1 + Percentage of Size Bin 2

Percentage of Size Bin 2 = Cumulative Percentage – Percentage of Size Bin 1

Example: The percentage of the size bin 308.1 nm would be the cumulative percentage minus the percentage of the size bin before it, which in this case is 278.3 nm.

$$\text{Percentage of 308.1} = \text{Cumulative Percentage} - \text{Percentage 278.3}$$

$$\text{Percentage of 308.1} = 37 - 13 = 24$$

The weighted volume of each size bin was then calculated from the diameter and the percentage. The particles are assumed to be spherical.

Example: The weighted volume of the size bin of diameter 308.1 nm is calculated as follows:

The radius was calculated in cm as a first step:

$$radius (cm) = \frac{diameter (nm)}{2} \times 10^{-7}$$

$$v = \left(\frac{4}{3}\pi r^3\right) \times Percentage$$

$$v = \left(\frac{4}{3}\pi \left(\frac{308.1}{2} \times 10^{-7}\right)^3\right) \times \left(\frac{24}{100}\right) = 3.68 \times 10^{-15} ml$$

The weighted volume for the remaining size bins was calculated similarly and then added to get the total volume of the particles in solution:

Total Weighted Volume

$$= \sum \text{Weighted Volume for Individual Size Bins}$$

$$= 2.17 \times 10^{-14} ml$$

To get the total particle count, the volume of the oxide was divided by the weighted volume:

$$Total Count = \frac{Oxide Volume}{Total Weighted Volume} = \frac{1.58 \times 10^{-6}}{2.17 \times 10^{-14}} = 7.30 \times 10^7 \text{ particles}$$

The particle count for each size bin was calculated from the total particle count and the percentage of each corresponding size bin

Example: To calculate the number the of particles with a diameter of 308.1 nm, the percentage of this size bin is multiplied by the total count

$$Particles \text{ with a diameter of } 308.1 \text{ nm} = Percentage \times Total Count$$

$$= \frac{24}{100} \times 7.30 \times 10^7 = 1.75 \times 10^7$$

Step Three:

The surface area for each size bin was calculated as follows:

The radius was calculated in cm:

$$radius (cm) = \frac{diameter (nm)}{2} \times 10^{-7}$$

$$Surface Area = 4\pi r^2$$

Examples: The surface area of particles with a diameter of 308.1 nm was calculated

$$Surface Area = 4\pi \left(\frac{308.1}{2} \times 10^{-7} \right)^2 = 2.98 \times 10^{-9} cm^2$$

The weighted surface area was then calculated by multiplying the surface area for each size bin by the number of particles for this size bin.

Example: The weighted surface area for particles with a diameter 308.1 nm was calculated by multiplying the surface area of this size bin with its number of particles:

$$\begin{aligned} Weighted Surface Area &= Surface Area_{308.1} \times Particle Count_{308.1} \\ &= 2.98 \times 10^{-9} \times 1.75 \times 10^7 = 0.052 cm^2 \end{aligned}$$

Finally the Total Weighted Surface Area is calculated by adding the Weighted Surface Areas for all size bins

$$Total Weighted Surface Area = \sum Individual Surface Areas = 0.27 cm^2$$

The Total Weighted Surface Area was then divided by the mass of the fraction taken to normalize against the mass:

$$\begin{aligned} Surface Area (cm^2/mg) &= \frac{Total Weighted Surface Area}{Mass of Fraction} = \frac{0.27}{0.01} \\ &= 27.07 cm^2/mg \end{aligned}$$

c. Metal Oxide DTT redox activity with respect to surface morphology:

For surface area imaging, the SEM was used. Figure 5.4 shows the different morphologies of the following oxides: CuO, MnO₂, ZnO and Cr₂O₃. Cr₂O₃ appears to have a smooth surface, while CuO appears to be extremely porous and sponge-like.

MnO₂ on the other hand seems to be needle shaped with a rough surface. Finally ZnO appears to be plate-like with rough edges forming clusters. The different reactivities of the MO cannot be explained by the morphology. MnO₂ and ZnO, which have similar redox reactivities, have different morphologies.

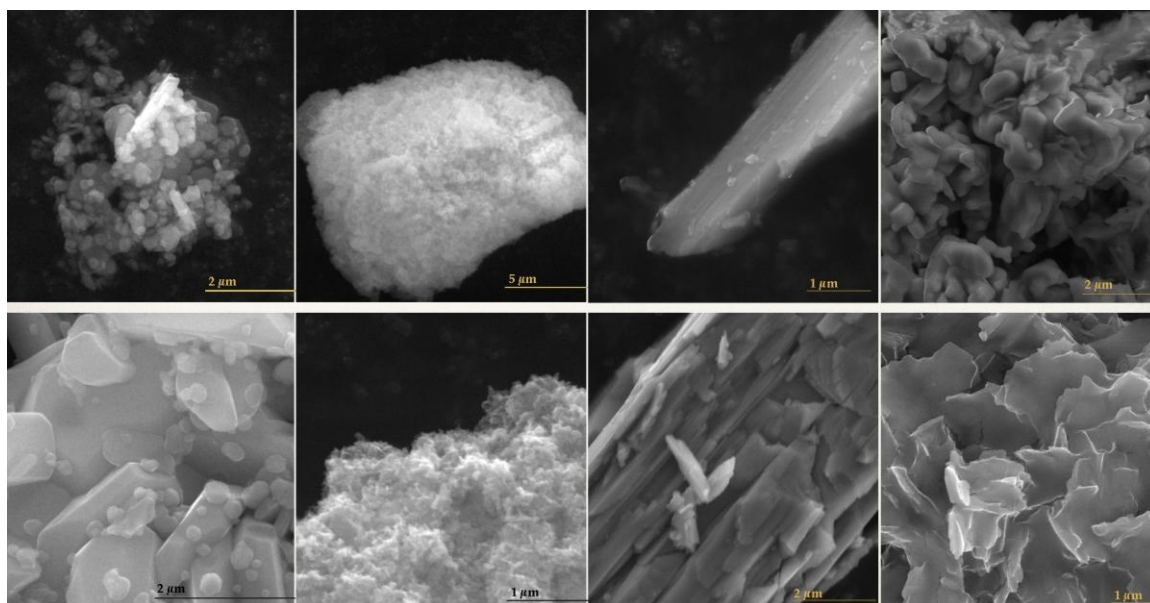


Figure 5.4. SEM images of different MO (Left to Right) Cr₂O₃, CuO, MnO₂, ZnO

E. Conclusion

Nanoparticles have countless uses, yet their toxicity has yet to be understood completely. For this reason, a screening method has to be adopted to test for their toxicity, this includes, their physicochemical properties, cytotoxicity and their ability to induce oxidative stress. In this study the redox activity with respect to DTT is tested for the six metal oxide nanoparticles, CuO, MnO₂, ZnO, PbO, Pb₂O₃ and Cr₂O₃. The order of their redox activities in decreasing order is: CuO > MnO₂ ~ ZnO > PbO > Pb₂O₃ > Cr₂O₃. In order to understand this difference in the redox reactivity, the physicochemical properties of some of these oxides are tested. The DLS was used to acquire the size and surface area, correlation between DTT redox activity and size was negative, indicating that the smaller the size, the higher the reactivity. While a moderate

correlation was observed between the redox reactivity and surface area, even though studies show a high dependence of surface area on the redox activity. This discrepancy could be explained by the assumptions that are taken when calculating the surface area using DLS. SEM imaging did show different morphologies but no relation was found between the morphology and redox activity; ZnO and MnO₂, which had similar reactivities, had different morphologies. When looking at the redox activity of the different nanoparticles, it is important to look at their chemical itself in addition to surface area and size. The key controlling factor in assessing the redox potential of the nanoparticles is the elemental composition of the nanoparticle itself, with a minor role for physicochemical characteristics. Future work of this study include using the BET for surface area calculations

CHAPTER VI

CONCLUSION

Particulate matter (PM) in Beirut have been assessed in terms of their 1) variation in PM-chemical composition and -redox activity with location, season and particle-size, 2) association between their toxico-chemical properties and identification of source tracers implicated in the induction of PM oxidative potential, 3) intrinsic ROS-activity and its variation across urban environments. Additionally, the effect of Metal oxide nanoparticles and their physicochemical characteristics on one of the redox potential assays; DTT assay, were studied.

Comparing, roadside to AUB, an urban background, size-resolved particle mass levels were 1.3-2.6 times greater, with enrichment in markers of traffic emissions like Sb, and certain PAHs (Chrysene and Benzo(ghi)perylene). The chemical mass closure showed that PM_{10-2.5} was mostly composed of crustal material, contributing to 12-23% of its mass across sites. On the other hand, in PM_{2.5-0.25} and PM_{0.25}, organic matter (46-56%) was dominant at the roadside location, while secondary ions (54-68%) were more abundant at the background site.

In both locations, Mn, Cu, Co, V, Ni and Zn were overall mostly distributed in PM_{2.5-0.25} and PM_{0.25}, with high water-solubility in these modes (> 60%). The increased water-solubility and presence of these metals, many of which are air toxics, in small size ranges constitute an added health risk. Of particular concern are water-soluble elements with strong correlations ($R \geq 0.70$) with ROS-activity. In

PM_{2.5-10}, Mn and Co, which are road dust components, were highly associated with ROS-activity. In PM_{2.5-0.25}, Cu (a tracer of vehicular abrasion) and Co (a road dust element) were highly correlated with ROS generation. In PM_{0.25}, V and Ni, originating from fuel oil combustion, had the highest correlations with ROS formation.

Additionally, size-segregated ROS-activity, expressed per m³ of air volume, was 1.5-2.8 times greater at the roadside than background location, indicating that exposure to redox-active PM species may be greatest near the freeway. Furthermore, ROS-activity (on per unit of PM mass) displayed a particle-size dependency, with lowest activity associated with PM_{10-2.5}.

Concerning dust episodes, both coarse and fine PM number and mass concentration increased with respect to non-dust episodes. Crustal material PM composition increased in both coarse (47 %) and fine (107 %) fractions while the secondary ions and sea salt contribution to PM mass decreased. The corresponding ROS activity of size-segregated dust and non-dust PM samples, which was measured using the DTT and m-ROS assays, showed an increase in the activity for the coarse PM fraction and a decrease for the fine fraction during dust episodes. The relative variation in the redox activity in both fractions can be the result of changes in chemical composition, particularly in trace elements, crustal material (CM) and organic matter. For this reason, the effect of CM on the DTT assay was assessed. The redox activity with respect to DTT was tested for the six metal oxide nanoparticles, CuO, MnO₂, ZnO, PbO, Pb₂O₃ and Cr₂O₃, with CuO having the highest DTT redox reactivity and Cr₂O₃ having no activity. The physicochemical characteristics, which include the surface area, size and morphology, were analyzed to check whether they are a key factor in

controlling the redox potential. Using the DLS to acquire the size and surface area, a negative correlation was obtained between DTT redox activity and diameter, indicating that the smaller the size, the higher the reactivity. While a moderate correlation was observed between the redox reactivity and surface area, even though studies show a high dependence of surface area on the redox activity. Taking SEM images in consideration, the different surface morphologies call for a more accurate method like the BET to calculate surface areas.

Despite this, when assessing the overall redox activity of PM₁₀ in dust and non-dust episodes, it is shown that PM₁₀ redox activity in Beirut mainly depends on the local sources with higher activities observed during non-dust episodes.

These results provide insight on commuter exposure to traffic-related PM in the Beirut area and push for policies to address air quality. The levels of toxic vehicular tracers, in Beirut are higher than a heavy-duty diesel-impacted freeway in southern California. This can be attributed to different fuel composition as well as the predominance of old vehicles. Additionally, during dust episodes, although a change in the redox potential is observed, the overall, PM redox potential is still higher during non-dust episodes. These findings call for pressing and stricter regulations on motor vehicles.

While this thesis contributes to the current state of scientific knowledge on size-segregated particle properties (chemical and oxidative), variability and sources, further steps are needed to advance our knowledge on PM characteristics and related health effects. Taking into account the PM complexity and variability, continuous air monitoring is needed since it could provide greater insight on the formation mechanisms, source strength, emissions and oxidative profile. Moreover, specifying

chemical markers, would help in source apportionment and tracking long range transported PM. Finally, understanding the mode of action of PM components on the redox assays, for better toxicity assessments.

BIBLIOGRAPHY

- (1) Robinson, A. L.; Donahue, N. M.; Shrivastava, M. K.; Weitkamp, E. A.; Sage, A. M.; Grieshop, A. P.; Lane, T. E.; Pierce, J. R.; Pandis, S. N. *Science* **2007**, *315*, 1259.
- (2) Anderson, H. R. *Philosophical Transactions of the Royal Society of London. Series A: Mathematical, Physical and Engineering Sciences* **2000**, *358*, 2771.
- (3) EPA U.S. Environmental Protection Agency, Washington, DC **2004**, EPA 600/P-99/002aF-bF, 2004.
- (4) Hinds, W. C. **1982**.
- (5) Nemmar, A.; Hoet, P. H. M.; Vanquickenborne, B.; Dinsdale, D.; Thomeer, M.; Hoylaerts, M. F.; Vanbilloen, H.; Mortelmans, L.; Nemery, B. *Circulation* **2002**, *105*, 411.
- (6) Oberdörster, G.; Sharp, Z.; Atudorei, V.; Elder, A.; Gelein, R.; Lunts, A.; Kreyling, W.; Cox, C. *Journal of Toxicology and Environmental Health Part A* **2002**, *65*, 1531.
- (7) Pope, C. A., 3rd, , Burnett, R.T., Thun, M.J., Calle, E.E., Krewski, D., Ito, K., Thurston, G.D. *Journal of the American Medical Association* **2002**, *287*, 1132.
- (8) Peters, A., Dockery, D.W., Muller, J.E., Mittleman, M.A. *Circulation* **2001**, *103*, 2810.
- (9) Pope III, C. A.; Dockery, D. W. *EM: Air and Waste Management Association's Magazine for Environmental Managers* **2006**.
- (10) Cho, A. K.; Sioutas, C.; Miguel, A. H.; Kumagai, Y.; Schmitz, D. A.; Singh, M.; Eiguren-Fernandez, A.; Froines, J. R. *Environmental Research* **2005**, *99*, 40.
- (11) Li, N.; Sioutas, C.; Cho, A.; Schmitz, D.; Misra, C.; Sempf, J.; Wang, M.; Oberley, T.; Froines, J.; Nel, A. *Environmental Health Perspectives* **2003**, *111*, 455.
- (12) Sheesley, R. J.; Schauer, J. J.; Chowdhury, Z.; Cass, G. R.; Simoneit, B. R. T. *Journal of Geophysical Research D: Atmospheres* **2003**, *108*, AAC 8.
- (13) Halliwell, B.; Cross, C. E. *Environmental Health Perspectives* **1994**, *102*, 5.
- (14) Bayr, H. *Critical Care Medicine* **2005**, *33*, S498.
- (15) Schäfer, M.; Schäfer, C.; Ewald, N.; Piper, H. M.; Noll, T. *Circulation Research* **2003**, *92*, 1010.
- (16) Sternbeck, J.; Sjödin, Å.; Andréasson, K. *Atmospheric Environment* **2002**, *36*, 4735.
- (17) Westerdahl, D.; Fruin, S.; Sax, T.; Fine, P. M.; Sioutas, C. *Atmospheric Environment* **2005**, *39*, 3597.
- (18) Tonne, C.; Melly, S.; Mittleman, M.; Coull, B.; Goldberg, R.; Schwartz, J. *Environmental Health Perspectives* **2007**, *115*, 53.
- (19) Phuleria, H. C.; Sheesley, R. J.; Schauer, J. J.; Fine, P. M.; Sioutas, C. *Atmospheric Environment* **2007**, *41*, 4653.
- (20) Ntziachristos, L.; Ning, Z.; Geller, M. D.; Sheesley, R. J.; Schauer, J. J.; Sioutas, C. *Atmospheric Environment* **2007**, *41*, 5684.
- (21) Hu, S.; Polidori, A.; Arhami, M.; Shafer, M. M.; Schauer, J. J.; Cho, A.; Sioutas, C. *Atmospheric Chemistry and Physics Discussions* **2008**, *8*, 11643.

- (22) See, S. W.; Wang, Y. H.; Balasubramanian, R. *Environmental Research* **2007**, *103*, 317.
- (23) Seagrave, J.; Gigliotti, A.; McDonald, J. D.; Seilkop, S. K.; Whitney, K. A.; Zielinska, B.; Mauderly, J. L. *Toxicological Sciences* **2005**, *87*, 232.
- (24) Morawska, L.; Thomas, S.; Bofinger, N.; Wainwright, D.; Neale, D. *Atmospheric Environment* **1998**, *32*, 2467.
- (25) Hughes, L. S.; Cass, G. R.; Gone, J.; Ames, M.; Olmez, I. *Environmental Science & Technology* **1998**, *32*, 1153.
- (26) Saliba, N. A.; El Jam, F.; El Tayar, G.; Obeid, W.; Roumie, M. *Atmospheric Research* **2010**, *97*, 106.
- (27) MoE/URC/GEF *Lebanon Technology Needs Assessment Report for Climate Change. Chapter 5.*, 2012.
- (28) Massoud, R.; Shihadeh, A. L.; Roumié, M.; Youness, M.; Gerard, J.; Saliba, N.; Zaarour, R.; Abboud, M.; Farah, W.; Saliba, N. A. *Atmospheric Research* **2011**, *101*, 893.
- (29) Kouyoumdjian, H.; Saliba, N. A. *Atmospheric Chemistry and Physics Discussions* **2005**, *5*, 13053.
- (30) Shaka, H.; Saliba, N. A. *Atmospheric Environment* **2004**, *38*, 523.
- (31) Misra, C.; Singh, M.; Shen, S.; Sioutas, C.; Hall, P. M. *Journal of Aerosol Science* **2002**, *33*, 1027.
- (32) Birch, M. E.; Cary, R. A. *The Analyst* **1996**, *121*, 1183.
- (33) Sullivan, A. P.; Weber, R. J.; Clements, A. L.; Turner, J. R.; Bae, M. S.; Schauer, J. J. *Geophysical Research Letters* **2004**, *31*, n/a.
- (34) Herner, J. D.; Green, P. G.; Kleeman, M. J. *Environmental Science & Technology* **2006**, *40*, 1925.
- (35) Sheesley, R. J.; Schauer, J. J.; Bean, E.; Kenski, D. *Environmental Science & Technology* **2004**, *38*, 6491.
- (36) Sillanpää, M.; Frey, A.; Hillamo, R.; Pennanen, A. S.; Salonen, R. O. *Atmos. Chem. Phys.* **2005**, *5*, 2869.
- (37) Ntziachristos, L.; Ning, Z.; Geller, M. D.; Sioutas, C. *Environmental Science & Technology* **2007**, *41*, 2223.
- (38) Turpin, B. J.; Lim, H.-J. *Aerosol Science and Technology* **2001**, *35*, 602.
- (39) Seinfeld, J. H.; Pandis, S. N. *Atmospheric Chemistry and Physics: From Air Pollution to Climate Change*; John Wiley & Sons, 2006.
- (40) Chow, J. C.; Watson, J. G.; Fujita, E. M.; Lu, Z.; Lawson, D. R.; Ashbaugh, L. L. *Atmospheric Environment* **1994**, *28*, 2061.
- (41) Hueglin, C.; Gehrig, R.; Baltensperger, U.; Gysel, M.; Monn, C.; Vonmont, H. *Atmospheric Environment* **2005**, *39*, 637.
- (42) Marcazzan, G. M.; Vaccaro, S.; Valli, G.; Vecchi, R. *Atmospheric Environment* **2001**, *35*, 4639.
- (43) Putaud, J.-P.; Raes, F.; Van Dingenen, R.; Brüggemann, E.; Facchini, M. C.; Decesari, S.; Fuzzi, S.; Gehrig, R.; Hüglin, C.; Laj, P.; Lorbeer, G.; Maenhaut, W.; Mihalopoulos, N.; Müller, K.; Querol, X.; Rodriguez, S.; Schneider, J.; Spindler, G.; Brink, H. t.; Tørseth, K.; Wiedensohler, A. *Atmospheric Environment* **2004**, *38*, 2579.
- (44) Bauer, H.; Schueller, E.; Weinke, G.; Berger, A.; Hitztenberger, R.; Marr, I. L.; Puxbaum, H. *Atmospheric Environment* **2008**, *42*, 5542.

- (45) Weber, R. J.; Sullivan, A. P.; Peltier, R. E.; Russell, A.; Yan, B.; Zheng, M.; de Gouw, J.; Warneke, C.; Brock, C.; Holloway, J. S.; Atlas, E. L.; Edgerton, E. *Journal of Geophysical Research: Atmospheres* **2007**, *112*, n/a.
- (46) Kam, W.; Liacos, J. W.; Schauer, J. J.; Delfino, R. J.; Sioutas, C. *Atmospheric Environment* **2012**, *55*, 90.
- (47) Schauer, J. J. *Journal of Exposure Analysis and Environmental Epidemiology* **2003**, *13*, 443.
- (48) MoE/UNDP/GEF *Lebanon's Second National Communication Report to the UNFCCC*, 2011.
- (49) Karageorgos, E. T.; Rapsomanikis, S. *Atmos. Chem. Phys.* **2007**, *7*, 3015.
- (50) Sillanpää, M.; Hillamo, R.; Saarikoski, S.; Frey, A.; Pennanen, A.; Makkonen, U.; Spolnik, Z.; Van Grieken, R.; Braniš, M.; Brunekreef, B.; Chalbot, M.-C.; Kuhlbusch, T.; Sunyer, J.; Kerminen, V.-M.; Kulmala, M.; Salonen, R. O. *Atmospheric Environment* **2006**, *40*, Supplement 2, 212.
- (51) Noble, C. A.; Prather, K. A. *Environmental Science & Technology* **1996**, *30*, 2667.
- (52) Zhuang, H.; Chan, C. K.; Fang, M.; Wexler, A. S. *Atmospheric Environment* **1999**, *33*, 4223.
- (53) Kouyoumdjian, H.; Saliba, N. A. *Atmospheric Chemistry and Physics* **2006**, *6*, 1865.
- (54) Robarge, W. P.; Walker, J. T.; McCulloch, R. B.; Murray, G. *Atmospheric Environment* **2002**, *36*, 1661.
- (55) Saliba, N. A.; Kouyoumdjian, H.; Roumié, M. *Atmospheric Environment* **2007**, *41*, 6497.
- (56) Sciare, J.; Bardouki, H.; Moulin, C.; Mihalopoulos, N. *Atmos. Chem. Phys.* **2003**, *3*, 291.
- (57) Draxler, R. L.; Rolph, G. D.; NOAA Air Resources Laboratory, Silver Spring, MD: 2003.
- (58) Arhami, M.; Sillanpää, M.; Hu, S.; Olson, M. R.; Schauer, J. J.; Sioutas, C. *Aerosol Science and Technology* **2009**, *43*, 145.
- (59) A.-F. M. Abdel-Rahman; Nader, F. H. *Geological Journal* **2002**, *37*, 69.
- (60) Andrews, E.; Saxena, P.; Musarra, S.; Hildemann, L. M.; Koutrakis, P.; McMurry, P. H.; Olmez, I.; White, W. H. *Journal of the Air & Waste Management Association (1995)* **2000**, *50*, 648.
- (61) IARC **1987**.
- (62) Manchester-Neesvig, J. B.; Schauer, J. J.; Cass, G. R. *Journal of the Air & Waste Management Association (1995)* **2003**, *53*, 1065.
- (63) Zielinska, B.; Samy, S.; McDonald, J. D.; Seagrave, J. *Research report (Health Effects Institute)* **2010**, 5.
- (64) Mader, B. T.; Pankow, J. F. *Environmental Science & Technology* **2002**, *36*, 5218.
- (65) Schauer, J. J.; Kleeman, M. J.; Cass, G. R.; Simoneit, B. R. T. *Environmental Science & Technology* **2002**, *36*, 1169.
- (66) Ning, Z.; Polidori, A.; Schauer, J. J.; Sioutas, C. *Atmospheric Environment* **2008**, *42*, 3099.

- (67) Menichini, E.; Monfredini, F.; Merli, F. *Atmospheric Environment* **1999**, *33*, 3739.
- (68) Liacos, J. W.; Kam, W.; Delfino, R. J.; Schauer, J. J.; Sioutas, C. *The Science of the total environment* **2012**, *435-436*, 159.
- (69) Rogge, W. F.; Hildemann, L. M.; Mazurek, M. A.; Cass, G. R.; Simoneit, B. R. T. *Environmental Science & Technology* **1993**, *27*, 636.
- (70) Waked, A.; Afif, C. *Atmospheric Environment* **2012**, *61*, 446.
- (71) Zielinska, B.; Sagebiel, J.; McDonald, J. D.; Whitney, K.; Lawson, D. R. *Journal of the Air & Waste Management Association (1995)* **2004**, *54*, 1138.
- (72) Peters, K. E.; Scheuerman, G. L.; Lee, C. Y.; Moldowan, J. M.; Reynolds, R. N.; Pena, M. M. *Energy & Fuels* **1992**, *6*, 560.
- (73) Simoneit, B. R. T. *Journal of Atmospheric Chemistry* **1989**, *8*, 251.
- (74) Arhami, M.; Minguillón, M. C.; Polidori, A.; Schauer, J. J.; Delfino, R. J.; Sioutas, C. *Indoor Air* **2009**, *20*, 17.
- (75) Rogge, W. F.; Hildemann, L. M.; Mazurek, M. A.; Cass, G. R.; Simoneit, B. R. T. *Environ. Sci. Technol.* **1993**, *27* 2700.
- (76) Rogge, W. F.; Hildemann, L. M.; Mazurek, M. A.; Cass, G. R.; Simoneit, B. R. T. *Environmental Science & Technology* **1993**, *27*, 1892.
- (77) Nel, A. *Science* **2005**, *308*, 804.
- (78) NRC National Research Council. *Committee on Research Priorities for Airborne Particulate Matter. Research Priorities for Airborne Particulate Matter: IV.*, 2004.
- (79) Nel, A. E.; Diaz-Sanchez, D.; Li, N. *Current opinion in pulmonary medicine* **2001**, *7*, 20.
- (80) Squadrito, G. L.; Cueto, R.; Dellinger, B.; Pryor, W. A. *Free Radical Biology and Medicine* **2001**, *31*, 1132.
- (81) Goldsmith, C. A.; Imrich, A.; Danaee, H.; Ning, Y. Y.; Kobzik, L. *Journal of toxicology and environmental health. Part A* **1998**, *54*, 529.
- (82) Prophete, C.; Maciejczyk, P.; Salnikow, K.; Gould, T.; Larson, T.; Koenig, J.; Jaques, P.; Sioutas, C.; Lippmann, M.; Cohen, M. *Journal of toxicology and environmental health. Part A* **2006**, *69*, 935.
- (83) Fantel, A. G. *Teratology* **1996**, *53*, 196.
- (84) Valko, M.; Morris, H.; Cronin, M. T. D. *Current medicinal chemistry* **2005**, *12*, 1161.
- (85) Chalupa, D. C.; Morrow, P. E.; Oberdorster, G.; Utell, M. J.; Frampton, M. W. *Environmental Health Perspectives* **2004**, *112*, 879.
- (86) Morawska, L.; Bofinger, N. D.; Kocis, L.; Nwankwoala, A. *Environmental Science & Technology* **1998**, *32*, 2033.
- (87) Hughes, L. S.; Cass, G. R.; Gone, J.; Ames, M.; Olmez, I., 1998. *Environmental Science & Technology* **1998**, *32*, 1153.
- (88) Ntziachristos, L.; Froines, J. R.; Cho, A. K.; Sioutas, C. *Particle fibre and toxicology* **2007**, *4*.
- (89) MoE/URC/GEF *Lebanon Technology Needs Assessment Report for Climate Change. Chapter 5., Beirut, Lebanon.*, 2012.
- (90) Saliba, N. A.; Kouyoumdjian, H.; Kadamany, G. A.; Roumie, M.; Mellouki, A.; Ravishankara, A. R. In *Regional Climate Variability and its Impacts in The Mediterranean Area*; Springer Netherlands: 2007, p 129.

- (91) Schauer, J. J.; Rodger, B.; Kerr, S. C. *Journal of Environmental Engineering and Science* **2004**, *3*, 213.
- (92) Sullivan, A. P.; Weber, R. J.; Clements, A. L.; Turner, J. R.; Bae, M. S.; Schauer, J. J. *Geophysical Research Letters* **2004**, *31*, L13105.
- (93) Landreman, A. P.; Shafer, M. M.; Hemming, J. C.; Hannigan, M. P.; Schauer, J. J. *Aerosol Science and Technology* **2008**, *42*, 946.
- (94) EPA; Vol. May 2013.
- (95) Taylor, S. R.; McLennan, S. M. *The continental crust: Its composition and evolution*; Blackwell Scientific, Boston, Mass., 1985.
- (96) Birmili, W.; Allen, A. G.; Bary, F.; Harrison, R. M. *Environmental Science & Technology* **2006**, *40*, 1144.
- (97) Sternbeck, J.; Sjödin, Å.; Andréasson, K. *Atmospheric Environment* **2002**, *36*, 4735.
- (98) Lin, C.-C.; Chen, S.-J.; Huang, K.-L.; Hwang, W.-I.; Chang-Chien, G.-P.; Lin, W.-Y. *Environmental Science & Technology* **2005**, *39*, 8113.
- (99) Thorpe, A.; Harrison, R. M. *The Science of the total environment* **2008**, *400*, 270.
- (100) Sanders, P. G.; Xu, N.; Dalka, T. M.; Maricq, M. M. *Environmental Science & Technology* **2003**, *37*, 4060.
- (101) Hays, M. D.; Cho, S.-H.; Baldauf, R.; Schauer, J. J.; Shafer, M. *Atmospheric Environment*, *45*, 925.
- (102) Manoli, E.; Voutsas, D.; Samara, C. *Atmospheric Environment* **2002**, *36*, 949.
- (103) Isakson, J.; Persson, T. A.; Selin Lindgren, E. *Atmospheric Environment* **2001**, *35*, 3659.
- (104) Lu, G.; Brook, J. R.; Rami Alfarra, M.; Anlauf, K.; Richard Leaitch, W.; Sharma, S.; Wang, D.; Worsnop, D. R.; Phinney, L. *Atmospheric Environment* **2006**, *40*, 2767.
- (105) Song, F.; Gao, Y. *Atmospheric Environment* **2011**, *45*, 6714.
- (106) Wang, Y.-F.; Huang, K.-L.; Li, C.-T.; Mi, H.-H.; Luo, J.-H.; Tsai, P.-J. *Atmospheric Environment* **2003**, *37*, 4637.
- (107) Allen, A. G.; Nemitz, E.; Shi, J. P.; Harrison, R. M.; Greenwood, J. C. *Atmospheric Environment* **2001**, *35*, 4581.
- (108) Costa, D. L.; Dreher, K. L. *Environmental Health Perspectives* **1997**, *105*.
- (109) Ciapetti, G.; Granchi, D.; Verri, E.; Savarino, L.; Cenni, E.; Savioli, F.; Pizzoferrato, A. *Journal of Biomedical Materials Research* **1998**, *41*, 455.
- (110) Noble, C. A.; Prather, K. A. *Environmental Science & Technology* **1996**, *30*, 2667.
- (111) Cheung, K.; Shafer, M. M.; Schauer, J. J.; Sioutas, C. *Environmental science & technology* **2012**, *46*, 3779.
- (112) S. Hu; A. Polidori ; M. Arhami.; M. M. Shafer; J.J. Schauer; A. Cho; Sioutas., C. *Atmospheric Chemistry and Physics* **2008**, *8*, 6439.
- (113) Shafer, M. M.; Perkins, D. A.; Antkiewicz, D. S.; Stone, E. A.; Quraishi, T. A.; Schauer, J. J. *Journal of Environmental Monitoring* **2010**, *12*, 704.

- (114) Daher, N.; Ruprecht, A.; Invernizzi, G.; De Marco, C.; Miller-Schulze, J.; Heo, J. B.; Shafer, M. M.; Shelton, B. R.; Schauer, J. J.; Sioutas, C. *Atmospheric Environment* **2012**, *49*, 130.
- (115) Verma, V.; Ning, Z.; Cho, A. K.; Schauer, J. J.; Shafer, M. M.; Sioutas, C. *Atmospheric Environment* **2009**, *43*, 6360.
- (116) Verma, V.; Polidori, A.; Schauer, J. J.; Shafer, M. M.; Cassee, F. R.; Sioutas, C. *Environmental Science & Technology* **2009**, *43*, 954.
- (117) Saffari, A.; Daher, N.; Shafer, M. M.; Schauer, J. J.; Sioutas, C. *Under review* **2013**.
- (118) Zhang, Y.; Schauer, J. J.; Shafer, M. M.; Hannigan, P. M.; Dutton, J. S. *Environmental Science & Technology* **2008**, *42*, 7502.
- (119) Ayres, J. G.; Borm, P.; Cassee, F. R.; Castranova, V.; Donaldson, K.; Ghio, A.; Harrison, R. M.; Hider, R.; Kelly, F.; Kooter, I. M.; Marano, F.; Maynard, R. L.; Mudway, I.; Nel, A.; Sioutas, C.; Smith, S.; Baeza-Squiban, A.; Cho, A.; Duggan, S.; Froines, J. *Inhalation toxicology* **2008**, *20*, 75.
- (120) Von Schneidmesser, E.; Stone, E. A.; Quraishi, T. A.; Shafer, M. M.; Schauer, J. J. *Science of The Total Environment* **2010**, *408*, 1640.
- (121) Pope III, C. A.; Thun, M. J.; Namboodiri, M. M.; Dockery, D. W.; Evans, J. S.; Speizer, F. E.; Heath Jr, C. W. *American Journal of Respiratory and Critical Care Medicine* **1995**, *151*, 669.
- (122) Laden, F.; Schwartz, J.; Speizer, F. E.; Dockery, D. W. *American Journal of Respiratory and Critical Care Medicine* **2006**, *173*, 667.
- (123) Lepeule, J.; Laden, F.; Dockery, D.; Schwartz, J. *Environmental Health Perspectives* **2012**, *120*, 965.
- (124) Donaldson, K.; Stone, V.; Seaton, A.; MacNee, W. *Environmental Health Perspectives* **2001**, *109*, 523.
- (125) Halliwell, B.; Gutteridge, J. *Free Radicals in Biology and Medicine*; Oxford University Press: New York, 1989.
- (126) Li, Q.; Wyatt, A.; Kamens, R. M. *Atmospheric Environment* **2009**, *43*, 1037.
- (127) Verma, V.; Pakbin, P.; Cheung, K. L.; Cho, A. K.; Schauer, J. J.; Shafer, M. M.; Kleinman, M. T.; Sioutas, C. *Atmospheric Environment* **2011**, *45*, 1025.
- (128) Held, K. D.; Sylvester, K. C.; Hopcia, K. L.; Biaglow, J. E. *Radiation Research* **1996**, *145*, 542.
- (129) Sauvain, J. J.; M.J., R.; Riediker, M. *Aerosol Science and Technology* **2013**, *47*, 218.
- (130) Goudie, A. S.; Middleton, N. J. *Desert Dust in the Global System*; Springer Berlin Heidelberg: New York, 2006; Vol. 2013.
- (131) Kyung, S. Y.; Yoon, J. Y.; Kim, Y. J.; Lee, S. P.; Park, J.-W.; Jeong, S. H. *Tuberculosis and Respiratory Diseases* **2012**, *73*, 84.
- (132) Hnizdo, E.; Vallyathan, V. *Occupational Environmental Medicine* **2003**, *60*, 237.
- (133) Halatek, T.; Opalska, B.; Lao, I.; Stetkiewicz, J.; Rydzunski, K. *International Journal of Occupational Medicine and Environmental Health* **2005**, *18*, 59.
- (134) Cheung, K.; Shafer, M. M.; Schauer, J. J.; Sioutas, C. *Environment Science and Technology* **2012**, *46*, 3779–3787.

- (135) Perez, L.; Tobías, A.; Querol, X.; Pey, J.; Alastuey, A.; Díaz, J.; Sunyer, J. *Environment International* **2012**, *48*, 150.
- (136) Tobías, A.; Caylà, J. A.; Pey, J.; Alastuey, A.; Querol, X. *International Journal of Infectious Diseases* **2011**, *15*, e503.
- (137) Massoud, R.; Shihadeh, A.; Roumié, M.; Youness, M.; Gerard, J.; Saliba, N.; Zaarour, R.; Abboud, M.; Farah, W.; Saliba, N. A. *Atmospheric Research* **2011**, *101*, 893.
- (138) Saliba, N. A.; Kouyoumdjian, H.; Roumié, M. *Atmospheric Environment* **2007**, *41*, 6497.
- (139) Charrier, J. G.; Anastasio, C. *Atmospheric Chemistry and Physics* **2012**, *12*, 9321.
- (140) Prophete, C.; Maciejczyk, P.; Salnikow, K.; Gould, T.; Larson, T.; Koenig, J.; Jaques, P.; Sioutas, C.; Lippmann, M.; Cohen, M. *Journal of Toxicology and Environmental Health - Part A: Current Issues* **2006**, *69*, 935.
- (141) Lindbom, J.; Gustafsson, M.; Blomqvist, G.; Dahl, A.; Gudmundsson, A.; Swietlicki, E.; Ljungman, A. G. *Chemical Research and Toxicology* **2007**, *20*, 937.
- (142) Fubini, B.; Hubbard, A. *Free Radical Biology and Medicine* **2003**, *34*, 1507.
- (143) Daher, N.; Saliba, N. A.; Shihadeh, A. L.; Jaafar, M.; Baalbaki, R.; Sioutas, C. *Science of the total environment* **2014**, *Under review*.
- (144) Nawrot, T. S.; Kuenzli, N.; Sunyer, J.; Shi, T.; Moreno, T.; Viana, M.; Heinrich, J.; Forsberg, B.; Kelly, F. J.; Sughis, M.; Nemery, B.; Borm, P. *Atmospheric Environment* **2009**, *43*, 4595.
- (145) Dada, L.; Mrad, R.; Sifferet, S.; Saliba, N. A. *Journal of Aerosol Science* **2013**, *Under review*.
- (146) Baalbaki, R.; Al-Assaad, K.; Mehanna, C. J.; Saliba, N. A.; Katurji, M.; Roumié, M. *Journal of the Air and Waste Management Association* **2013**, *63*, 327.
- (147) Draxler, R. R.; Rolph, G. D., 2013. ; NOAA Air Resources Laboratory, Silver Spring, MD.: 2013.
- (148) Kubilay, N.; Nickovic, S.; Moulin, C.; Dulac, F. *Atmospheric Environment* **2000**, *34*, 1293.
- (149) Papayannis, A.; Amiridis, V.; Mona, L.; Tsaknakis, G.; Balis, D.; Bösenberg, J.; Chaikovski, A.; De Tomasi, F.; Grigorov, I.; Mattis, I.; Mitev, V.; Müller, D.; Nickovic, S.; Pérez, C.; Pietruczuk, A.; Pisani, G.; Ravetta, F.; Rizi, V.; Sicard, M.; Trickl, T.; Wiegner, M.; Gerding, M.; Mamouri, R. E.; D'Amico, G.; Pappalardo, G. *Journal of Geophysical Research: Atmospheres* **2008**, *113*, D10204.
- (150) EU In *Establishing guidelines for demonstration and subtraction of exceedances attributable to natural sources under the Directive 2008/50/EC on ambient air quality and cleaner air for Europe* Brussels, SEC(2011) 208 final, 2011.
- (151) Herner, J. D.; Green, P. G.; Kleeman, M. J. *Environmental Science and Technology* **2006**, *40*, 1925.
- (152) Birch, M. E.; Cary, R. A. *The Analyst* **1996**, *121*, 1183.
- (153) Sullivan, A. P.; Weber, R. J.; Clements, A. L.; Turner, J. R.; Bae, M. S.; Schauer, J. J. *Geophysical Research Letters* **2004**, *31*, L13105 1.
- (154) Rattanavaraha, W.; Rosen, E.; Zhang, H.; Li, Q.; Pantong, K.; Richard M. Kamens, R. M. *Atmospheric Environment* **2011**, *45*, 3848.

- (155) Verma, V.; Rico-Martinez, R.; Kotra, N.; King, L.; Liu, J.; Snell, T. W.; Weber, R. J. *Environment Science and Technology* **2012**, *46*, 11384–11392.
- (156) Kumagai, Y.; Koide, S.; Taguchi, K.; Endo, A.; Nakai, Y.; Yoshikawa, T.; Shimojo, N. *Chemical Research in Toxicology* **2002**, *15*, 483.
- (157) Gnauk, T.; Brüggemann, E.; Müller, K.; Chemnitzer, R.; Rüd, C.; Galgon, D.; Wiedensohler, A.; Acker, K.; Auel, R.; Wieprecht, W.; Möller, D.; Jaeschke, W.; Herrmann, H. *Atmospheric Environment* **2005**, *39*, 4209.
- (158) Sciare, J.; Oikonomou, K.; Cachier, H.; Mihalopoulos, N.; Andreae, M. O.; Maenhaut, W.; Sarda-Estève, R. *Atmos. Chem. Phys.* **2005**, *5*, 2253.
- (159) Takahashi, K.; Minoura, H.; Sakamoto, K. *Atmospheric Environment* **2008**, *42*, 113.
- (160) Terzi, E.; Argyropoulos, G.; Bougatioti, A.; Mihalopoulos, N.; Nikolaou, K.; Samara, C. *Atmospheric Environment* **2010**, *44*, 2231.
- (161) Seinfeld, J. H.; Pandis, S. N. *Atmospheric Chemistry and Physics: From Air Pollution to Climate Change, 2nd Edition*; John Wiley and Sons: New Jersey, 2006.
- (162) Remoundaki, E.; Kassomenos, P.; Mantas, E.; Mihalopoulos, N.; Tsezos, M. *Aerosol and Air Quality Research* **2013**, *13*, 72.
- (163) Daher, N.; Saliba, N. A.; Shihadeh, A. L.; Jaafar, M.; Baalbaki, R.; Sioutas, C. *Atmospheric Environment* **2013**, *80*, 96.
- (164) Querol, X.; Alastuey, A.; Rodriguez, S.; Plana, F.; Ruiz, C. R.; Cots, N.; Massagué, G.; Puig, O. *Atmospheric Environment* **2001**, *35*, 6407.
- (165) Lazaridis, M.; Dzumbova, L.; Kopanakis, I.; Ondracek, J.; Glytsos, T.; Aleksandropoulou, V.; Voulgarakis, A.; Katsivela, E.; Mihalopoulos, N.; Eleftheriadis, K. *Water Air Soil Pollut* **2008**, *189*, 85.
- (166) Pérez, N.; Pey, J.; Castillo, S.; Viana, M.; Alastuey, A.; Querol, X. *Science of The Total Environment* **2008**, *407*, 527.
- (167) Tsyro, S. G. *Atmos. Chem. Phys.* **2005**, *5*, 515.
- (168) Perrino, C.; Canepari, S.; Catrambone, M. *Aerosol and Air Quality Research* **2013**, *13*, 137.
- (169) Shi, Z.; Zhang, D.; Hayashi, M.; Ogata, H.; Ji, H.; Fujiie, W. *Atmospheric Environment* **2008**, *42*, 822.
- (170) Bozlaker, A.; Prospero, J. M.; Fraser, M. P.; Chellam, S. *Environmental Science & Technology* **2013**, *47*, 10179.
- (171) Rodríguez, S.; Querol, X.; Alastuey, A.; Kallos, G.; Kakaliagou, O. *Atmospheric Environment* **2001**, *35*, 2433.
- (172) Dada, L.; Mrad, R.; Siffert, S.; Saliba, N. A. *Journal of Aerosol Science* **2013**, *66*, 187.
- (173) Herut, B.; Nimmo, M.; Medway, A.; Chester, R.; Krom, M. D. *Atmospheric Environment* **2001**, *35*, 803.
- (174) Zhang, R.; Jing, J.; Tao, J.; Hsu, S.-C.; Wang, G.; Cao, J.; Lee, C. S. L.; Zhu, L.; Chen, Z.; Zhao, Y.; Shen, Z. *Atmospheric Chemistry and Physics* **2013**, *13*, 7053.
- (175) Hu, S.; Polidori, A.; Arhami, M.; Shafer, M. M.; Schauer, J. J.; Cho, A.; Sioutas, C. *Atmos. Chem. Phys.* **2008**, *8*, 6439.
- (176) Mugica, V.; Ortiz, E.; Molina, L.; De Vizcaya-Ruiz, A.; Nebot, A.; Quintana, R.; Aguilar, J.; Alcántara, E. *Atmospheric Environment* **2009**, *43*, 5068.

- (177) Reche, C.; Moreno, T.; Amato, F.; Viana, M.; van Drooge, B. L.; Chuang, H.-C.; Bérubé, K.; Jones, T.; Alastuey, A.; Querol, X. *Ecotoxicology and Environmental Safety* **2012**, *78*, 327.
- (178) Saffari, A.; Daher, N.; Shafer, M. M.; Schauer, J. J.; Sioutas, C. *Atmospheric Environment* **2013**, *79*, 566.
- (179) Verma, V.; Polidori, A.; Schauer, J. J.; Shafer, M. M.; Cassee, F. R.; Sioutas, C. *Environmental Science & Technology* **2009**, *43*, 954.
- (180) Schoonen, M. A. A.; Cohn, C. A.; Roemer, E.; Laffers, R.; Simon, S. R.; O'Riordan, T. *Medical Mineralogy and Geochemistry* **2006**, *64*, 179.
- (181) Daher, N.; Ruprecht, A.; Invernizzi, G.; De Marco, C.; Miller-Schulze, J.; Heo, J. B.; Shafer, M. M.; Shelton, B. R.; Schauer, J. J.; Sioutas, C. *Atmospheric Environment* **2012**, *49*, 130.
- (182) Biswas, S.; Verma, V.; Schauer, J. J.; Cassee, F. R.; Cho, A. K.; Sioutas, C. *Environmental Science & Technology*. **2009**.
- (183) Finger, E.; Helmy, H. M. *Mineralogy and Petrology* **1998**, *62*, 269.
- (184) International, A.
- (185) Council, N. R. *A Review of the National Nanotechnology Initiative 2002*, Washinton, DC, National Academy Press.
- (186) Nel, A.; Xia, T.; Mädler, L.; Li, N. *Science* **2006**, *311*, 622.
- (187) Roco, M. C. *Environmental science & technology* **2005**, *39*, 106A.
- (188) Buzea, C.; Pacheco, I. I.; Robbie, K. *Biointerphases* **2007**, *2*, MR17.
- (189) Nanotechnology, T. P. O. E. **2008**.
- (190) Oberdörster, G.; Maynard, A.; Donaldson, K.; Castranova, V.; Fitzpatrick, J.; Ausman, K.; Carter, J.; Karn, B.; Kreyling, W.; Lai, D. *Particle and Fibre Toxicology* **2005**, *2*, 8.
- (191) Breznan, D.; Goegan, P.; Chauhan, V.; Karthikeyan, S.; Kumarathasan, P.; Cakmak, S.; Nadeau, D.; Brook, J. R.; Vincent, R. *Toxicology in Vitro* **2013**, *27*, 1287.
- (192) Burello, E.; Worth, A. P. *Nanotoxicology* **2011**, *5*, 228.
- (193) Burello, E.; Worth, A. P. *Wiley Interdisciplinary Reviews: Nanomedicine and Nanobiotechnology* **2011**, *3*, 298.
- (194) Cho, W.-S.; Duffin, R.; Poland, C. A.; Howie, S. E. M.; MacNee, W.; Bradley, M.; Megson, I. L.; Donaldson, K. *Environmental health perspectives* **2010**, *118*, 1699.
- (195) Jeng, H. A.; Swanson, J. *Journal of Environmental Science and Health Part A* **2006**, *41*, 2699.
- (196) Maynard, A.; Aitken, R. J.; Butz, T.; Colvin, V.; Donaldson, K.; Oberdörster, G.; Philbert, M. A.; Ryan, J.; Seaton, A.; Stone, V. *Nature-london-* **2006**, *444*, 267.
- (197) Xia, T.; Kovochich, M.; Brant, J.; Hotze, M.; Sempf, J.; Oberley, T.; Sioutas, C.; Yeh, J. I.; Wiesner, M. R.; Nel, A. E. *Nano letters* **2006**, *6*, 1794.
- (198) Xia, T.; Kovochich, M.; Liong, M.; Mädler, L.; Gilbert, B.; Shi, H.; Yeh, J. I.; Zink, J. I.; Nel, A. E. *ACS nano* **2008**, *2*, 2121.
- (199) Zhou, T.; Rong, Y.; Liu, Y.; Zhou, Y.; Guo, J.; Cheng, W.; Wang, H.; Chen, W. *Journal of Occupational and Environmental Medicine* **2012**, *54*, 459.
- (200) Antonini, J. M.; Murthy, G. G.; Rogers, R. A.; Albert, R.; Ulrich, G. D.; Brain, J. D. *Toxicology and applied pharmacology* **1996**, *140*, 188.

- (201) Becker, S.; Soukup, J. M.; Gallagher, J. E. *Toxicology in vitro* **2002**, *16*, 209.
- (202) Borm, P. J. A.; Kelly, F.; Künzli, N.; Schins, R. P. F.; Donaldson, K. *Occupational and environmental medicine* **2007**, *64*, 73.
- (203) Goldsmith, C.-A.; Frevert, C.; Imrich, A.; Sioutas, C.; Kobzik, L. *Environmental health perspectives* **1997**, *105*, 1191.
- (204) McNeilly, J. D.; Heal, M. R.; Beverland, I. J.; Howe, A.; Gibson, M. D.; Hibbs, L. R.; MacNee, W.; Donaldson, K. *Toxicology and applied pharmacology* **2004**, *196*, 95.
- (205) Nel, A. E.; Mädler, L.; Velegol, D.; Xia, T.; Hoek, E. M. V.; Somasundaran, P.; Klaessig, F.; Castranova, V.; Thompson, M. *Nature materials* **2009**, *8*, 543.
- (206) Hull, M. J.; Abraham, J. L. *Human pathology* **2002**, *33*, 819.
- (207) Sano, T. *Pathology International* **1963**, *13*, 77.
- (208) Daher, N.; Saliba, N. A.; Shihadeh, A. L.; Jaafar, M.; Baalbaki, R.; Shafer, M. M.; Schauer, J. J.; Sioutas, C. *The Science of the total environment* **2014**, *470-471*, 417.
- (209) Donaldson, K.; Beswick, P. H.; Gilmour, P. S. *Toxicology letters* **1996**, *88*, 293.
- (210) Gilliland, F. D.; McConnell, R.; Peters, J.; Gong Jr, H. *Environmental health perspectives* **1999**, *107*, 403.
- (211) Kelly, F. J. *Occupational and environmental medicine* **2003**, *60*, 612.
- (212) Gwinn, M. R.; Vallyathan, V. *Environmental health perspectives* **2006**, *114*, 1818.
- (213) Briedé, J. J.; de Kok, T. M. C. M.; Hogervorst, J. G. F.; Moonen, E. J. C.; op den Camp, C. L. B.; Kleinjans, J. C. S. *Environmental science & technology* **2005**, *39*, 8420.
- (214) Shi, T.; Schins, R. P. F.; Knaapen, A. M.; Kuhlbusch, T.; Pitz, M.; Heinrich, J.; Borm, P. J. A. *Journal of Environmental Monitoring* **2003**, *5*, 550.
- (215) Verma, V.; Shafer, M. M.; Schauer, J. J.; Sioutas, C. *Atmospheric Environment* **2010**, *44*, 5165.
- (216) Sauvain, J. J.; M.J., R.; Riediker, M. *Aerosol Science and Technology* **2013**, *47*, 218.
- (217) Uzu, G.; Sauvain, J.-J.; Baeza-Squiban, A.; Riediker, M.; Sánchez Sandoval Hohl, M.; Val, S. p.; Tack, K.; Denys, S.; Pradère, P.; Dumat, C. *Environmental science & technology* **2011**, *45*, 7888.
- (218) Zhao, Y.; Chen, Z.; Shen, X.; Zhang, X. *Environmental science & technology* **2011**, *45*, 3317.
- (219) Kachur, A. V.; Held, K. D.; Koch, C. J.; Biaglow, J. E. *Radiation research* **1997**, *147*, 409.
- (220) Lison, D.; Lardot, C.; Huaux, F.; Zanetti, G.; Fubini, B. *Archives of toxicology* **1997**, *71*, 725.
- (221) Zhang, Z.; Shang, J.; Zhu, T.; Li, H.; Zhao, D.; Liu, Y.; Ye, C. *Journal of Environmental Sciences* **2012**, *24*, 1753.
- (222) Dalal, N. S.; Shi, X.; Vallyathan, V. *Journal of Toxicology and Environmental Health, Part A Current Issues* **1990**, *29*, 307.

(223) Fubini, B.; Giamello, E.; Volante, M.; Bolis, V. *Toxicology and industrial health* **1990**, *6*, 571.

(224) Vallyathan, V.; Castranova, V.; Pack, D.; Leonard, S.; Shumaker, J.; Hubbs, A. F.; Shoemaker, D. A.; Ramsey, D. M.; Pretty, J. R.; McLaurin, J. L. *American journal of respiratory and critical care medicine* **1995**, *152*, 1003.